

Comparison between the turbulence parameter in the Cumulative Overload Method and the turbulence predictions of an OpenFOAM model for wave overtopping flow over a simple dike profile

MSc. Thesis report



MSc. Thesis report

Comparison between the turbulence parameter in the Cumulative Overload Method and the turbulence predictions of an OpenFOAM model for wave overtopping flow over a simple dike profile

Ing. L. (Lydia) Heida

Master of Science

Water Engineering and Management
Marine and Fluvial Systems

November 2021

Graduation committee:

dr. J.J. Warmink	University of Twente, <i>Faculty of Engineering Technology</i>
dr. ir. E.M. Horstman	University of Twente, <i>Faculty of Engineering Technology</i>
V.M. Bergeijk, MSc	University of Twente, <i>Faculty of Engineering Technology</i>
ir. G.J. Steendam	Infram-Hydren, <i>Manager Infram-Hydren</i>
ir. R. Mom	Infram-Hydren, <i>Senior advisor</i>
ir. K.A. Maroudi	Infram-Hydren, <i>Advisor</i>

University of Twente

Faculty of Engineering Technology
Drienerlolaan 5
7522 NB Enschede
+31 53 - 489 9111

Infram-Hydren

Waterbouw, Innovatie en Onderzoek
Amersfoortseweg 9
3951 LA Maarn
+31 343 - 745 600

Preface

The presented thesis provides the final piece to fulfill my master study in Water Engineering and Management at the University of Twente. This research was a collaboration between Infram Hydren and UTwente, and was partly carried at home due to Corona, and partly at the office of Infram.

This research would not be possible without the support of many individuals during this research process. Therefore, I would like to express my appreciation. Firstly, I would like to thank my kind and diverse thesis commission, who helped me throughout this thesis project. I sincerely enjoyed the process of getting to know each other and the contrast we had between professionalism and fun during our meetings. I would specially like to thank my daily supervisor, Erik Horstman, for his full and kind support and his keen overarching view during my thesis. I enjoyed our discussions and even our shared frustrations. I would also like to thank Vera van Bergeijk, as she always took the time to help me with the OpenFOAM model and other questions, even in between her own PHD research work. I really appreciate your help and supportive way of talking, as it made me feel more ensured. My gratitude also goes to Teni Maroudi, Roy Mom and Gosse-Jan Steendam, who provided a very work-friendly environment and a lot of practical insights during my research. I truly enjoyed meeting you at the Vecht dike and during the Infram-days. During my thesis, I felt very encouraged by your way of thinking and thoughtfulness, as this research was sometimes very challenging. In addition to my daily commission members, I would also like to express my gratitude to Jord Warmink, the chairman of my commission, as this research would not have existed without your interest in the field of flood defences and desire for new challenging research.

I would like to express sincere gratitude to the Infram (Hydren) team for their warm welcome, wherein I enjoyed doing the various fun activities. I would also like to express my appreciation to Gijs Hoffmans, who helped me with some theoretical questions to gain more insights on turbulence.

My gratitude also goes out to my family, friends and Palette, for the fun distractions and ideas they have given me during my research period.

Lastly, I would like to give my special thanks to my boyfriend, Bert Eekman. Without his love, aid and sympathy, I would not have been able to present this quality of work. He helped me with the grammar and even gave me food and drinks, while I was busy working on my thesis. He helped me physically and mentally through this process and I sincerely and truly thank him for all his work. Now with my thesis behind me, I am looking forward to our upcoming challenges and to my future as an Engineer!

Lydia Heida,

Enschede, 23 November 2021

Abstract

In the Netherlands dikes are often used as flood defences along rivers and coasts to protect the hinterland from floods. One of the main reasons that dikes are damaged or breach is due to wave overtopping. Wave overtopping occurs when high waves approach a flood defence, run up the waterside slope and run over the crest onto the landward slope of the dike. Wave overtopping causes damage to the crest and the landward slope of the dike, as these parts typically consist of a grass cover, which is more vulnerable to erosion than the cover types on the outer slope of dikes, such as stones or asphalt. To reduce the hazard of dike failure due to wave overtopping, a lot of research is performed in order to accurately predict wave overtopping damage and better understand the failure mechanisms involved. An important, yet less understood, mechanism known to contribute to wave overtopping failure is turbulence. Wave overtopping turbulence is an important parameter, as it impacts the onset of erosion, the erosion location and the amount of erosion. Therefore, wave overtopping turbulence has a critical effect on the failure process of a dike. Currently, the relative depth-averaged turbulence intensity (r_0) is used within empirical equations of the critical flow velocity (U_c) and indirectly within cumulative overload method (COM), used to predict dike erosion under wave overtopping, to account for the processes related to wave overtopping turbulence. However, due to the knowledge gap on the topic of wave overtopping turbulence, the turbulence intensity can take a range of possible values, without the ability to determine the correctness of the applied values. Therefore, the turbulence intensity is often used as a way to correct the resulting critical flow velocity (U_c), to better fit the field measurements, instead of calculated using the available empirical equations. Thus, the turbulence intensity and critical flow velocity are obtained by reverse engineering.

The aim of this research is to gain more insights into the topic of wave overtopping turbulence using a numerical wave overtopping model in OpenFOAM. The OpenFOAM model was used to simulate different wave overtopping volume (V) and roughness height (k_s) scenarios. Thereafter, the resulting depth-averaged turbulent kinetic energy or TKE (k_0) is plotted to analyse the sensitivity of the modelled TKE for changes in wave overtopping volumes and roughness heights. In addition, the sensitivity of the relative depth-averaged turbulence intensity (r_0) was analysed by computing the turbulence intensity with two different empirical equation approaches, using the modelled velocity (u), waver layer thickness (h) and TKE (k_0), for the same wave overtopping volume and roughness height scenarios as used for the sensitivity analysis in OpenFOAM. This was done to analyse the overall range and sensitivity of the turbulence intensity and the differences in result between the two empirical approaches. Finally, the found trends of the modelled TKE and the calculated relative turbulence intensities are compared, to find if both turbulence parameters present similarities and analyse whether the current approach of wave overtopping turbulence within the COM method is appropriate. During this research the main question was:

'To what extent does the wave overtopping turbulence predicted with an OpenFOAM model for a simple dike profile, with a single slope angle and cover type, vary with the cover roughness and wave overtopping volume and is this variability represented in the turbulence parameter that is used in the empirical models to predict wave overtopping damage on landward dike slopes?'

Using the OpenFOAM model it was found that the TKE during wave overtopping increases linearly when the wave overtopping volume increases and non-linearly when the roughness height increases. When large roughness heights (4.0 cm) are applied, the TKE maxima (maximum TKE, maximum significant (highest 33%) TKE and maximum mean TKE) will all occur at the same location on the dike profile, which is caused by the significant increase of the maximum TKE. Furthermore, it was also found that the TKE maxima all shift towards the toe of the dike for increasing wave overtopping volumes, while the TKE maxima shift towards the dike crest when the roughness height is increased. The deviation between the position of each TKE maxima depends on the applied roughness height. To conclude whether one turbulence maxima or the combined effort of all three turbulence maxima contribute the most to wave overtopping damage, it is recommended to validate whether the predicted locations of the turbulence maxima correlates with the observed positioning of damage in the field. When the relative turbulence intensity (r_0) was compared, using two different calculation methods, it was found that both turbulence intensities decrease with an increasing wave overtopping volume and a decreasing roughness height. Although, both calculation methods present similar trends, it can be stated that the range, magnitude and sensitivity of each method still presents a relatively large difference. One method presents a high range of intensities ($r_0 = 0.25 - 0.6$), while the other method presents a lower range ($r_0 = 0.05 - 0.4$). As a slight difference of 1% for the relative turbulence intensity will affect the resulting critical flow velocity, which represents the grass erosion threshold, by approximately 8% (Bijlard, 2015), this difference in turbulence intensity can result in significantly different critical flow velocities.

This study revealed that the trends of the modelled TKE (k_0) and the empirically calculated relative turbulence intensities (r_0) are similar for an increasing roughness height, but present opposing trends for an increasing wave overtopping volume. Although, both parameters are often used in studies to represent the amount of turbulence within a flow, it is known that both turbulence parameters represent a different (type of) turbulence quantity. This difference in trend between the turbulence maxima and the relative turbulence intensity is caused by the fact that both turbulence parameters represent different turbulence quantities. However, because both parameters represent the amount of turbulence within a flow, it is important to validate whether the relative turbulence intensity is a correct representation of wave overtopping turbulence. As often reverse engineering is used to obtain the r_0 , it is possible that another turbulence parameter, such as the depth-averaged TKE (k_0) or the root mean square (RMS) turbulent intensity in multiple flow directions (r_u, r_w), would provide a more appropriate representation of wave overtopping turbulence. Furthermore, the turbulence intensity parameter is currently often used to help calibrate the critical flow velocity in order to fit the field measurements. This could, however, easily lead to misrepresentations of the processes that occur in reality. Therefore, it is pointed out in this research that the relative depth-average turbulence intensity is probably used incorrectly and that it would be more appropriate to separate the turbulence intensity from the critical flow velocity (U_c) equation. This separation can be done by introducing a 'new' load-term, in which the transition and obstacle factor (α_m), the gravitational acceleration factor (α_a) and a turbulence parameter are combined. This 'new' load-term can then be directly used within the COM to increase or decrease the critical flow velocity (U_c), which represents the strength of the grass cover (strength-term), or the front velocity of the overtopping wave (U_i), which represents the load on the grass cover (load-term). Herein, the latter (increase or decrease the U_i) would be more appropriate.

Keywords: Wave overtopping, Turbulence, Critical flow velocity, Cumulative Overload Method (COM), OpenFOAM, Numerical modelling

List of abbreviations

Abbreviation	Description	First page
<i>2DV</i>	Two-dimensional (2D) Vertical	5
<i>3D</i>	Three-dimensional	53
<i>CFD</i>	Computational Fluid Dynamics	16
<i>COM</i>	Cumulative Overload Method	4
<i>DES</i>	Direct Eddy Simulation	23
<i>DNS</i>	Direct Numerical Simulation	23
<i>HWBP</i>	High Water Defence Program (Dutch program)	19
<i>LES</i>	Large Eddy Simulation	23
<i>RANS</i>	Reynolds-Averaged Navier-Stokes	17
<i>RMS</i>	Root-Mean-Square	52
<i>SST</i>	Shear Stress Transport	18
<i>TKE</i>	Turbulent Kinetic Energy	8

List of symbols

Symbols		Description	Units
a		Scale factor to normalize Weibull distribution	[-]
b		Shape factor for the extreme tail in Weibull distribution	[-]
C		Chézy coefficient	$[m^{1/2}/s]$
C_s		Roughness constant	[-]
d		Particle diameter	$[m]$
D		Damage number in Cumulative Overload Method	$[m^2/s^2]$
f		External forces	$[N]$
g		Gravitational acceleration	$[m/s^2]$
h		Water layer thickness	$[m]$
\bar{h}		Mean water layer thickness	$[m]$
h_{max}		Maximum water layer thickness	$[m]$
Hz		Hertz	$[s^{-1}]$
I		Turbulent intensity	[-]
k	<i>TKE</i>	Turbulent kinetic energy	$[m^2/s^2]$
k_0		Depth-averaged turbulent kinetic energy	$[m^2/s^2]$
k_s		Nikuradse roughness height	$[m]$
m		Discharge shape constant ($m = a + b$)	[-]
n		Manning coefficient	[-]
N		Number of overtopping waves that exceed U_c	[-]
nu_t	<i>Nut</i>	Kinematic turbulent viscosity	$[m^2/s]$
p		Pressure	$[N/m^2]$
q		Wave overtopping discharge	$[l/s] [m^3/s]$
r		Relative turbulent intensity	[-]
r_0		Relative depth-averaged turbulent intensity	[-]
Re		Reynold's number	[-]
R_h		Hydraulic radius	$[m]$
S_b		Mean dike slope	$[^\circ]$
T_0		Overtopping period	$[s]$
u		Flow velocity	$[m/s]$
\bar{u}		Mean flow velocity (Reynolds decomposition)	$[m/s]$
u'		Fluctuations in flow velocity (Reynolds decomposition)	$[m/s]$
u_*		Bed shear velocity	$[m/s]$
U_0		Depth-averaged flow velocity	$[m/s]$
U_c		Critical flow velocity	$[m/s]$
U_i		Front velocity of i^{th} overtopping wave	$[m/s]$

U_{max}		Maximum flow velocity	[m/s]
V		Wave overtopping Volume	[l/m] [m ³ /m]
x		Cross-dike coordinate	[m]
α		Water fraction	[-]
α_0		Dimensionless constant of 1.21	[-]
α_a		Gravitational acceleration factor	[-]
$\alpha_{grass,U}$		Dimensionless constant of 2.0	[-]
α_m		Transitions and obstacle factor	[-]
α_s		Grass strength factor	[-]
Δx		Spatial difference	[m]
Δt		Time difference	[s]
δ		Kronecker delta	[-]
δ_v		Laminar boundary layer thickness	[m]
ε	<i>Epsilon</i>	Turbulent dissipation rate	[m ² /s ³]
φ		Slope steepness	[°]
ψ_c		Critical shields parameter	[-]
ρ		Water density	[kg/m ³]
ρw		Pore water pressure	[N/m ²]
$\sigma_{grass,c}(0)$		Critical mean grass normal stress at the ground level	[N/m ²]
σ		1. Friction coefficient	[kg/s ²]
		2. Normal stress	[N/m ²]
τ		Shear stress	[N/m ²]
ν		Viscosity	[m ² /s]
ω	<i>Omega</i>	Specific turbulent dissipation rate	[s ⁻¹]

Important subscripts and notations

Subscript	Description
0	1. Initial value 2. Depth-averaged
c	Critical value
$grass$	For grass
U	Velocity related
x or u	In x-direction (longitude)
y or v	In y-direction (transverse)
z or w	In z-direction (vertical)
i	In i-direction (longitude)
j	In j-direction (vertical)
Notation	Description
(0)	Surface level

Content

Preface	i
Abstract	iii
List of abbreviations	v
List of symbols	vii
Content	ix
1 Introduction	1
1.1. <i>Problem definition</i>	2
1.2. <i>Research objective</i>	4
1.3. <i>Research questions</i>	4
1.4. <i>Research method</i>	4
1.5. <i>Research scope</i>	6
1.6. <i>Report outline</i>	6
2 Current knowledge	7
2.1. <i>Turbulence</i>	7
2.2. <i>Turbulent boundary layer</i>	8
2.2.1. <i>Hydraulically smooth and rough flows</i>	9
2.2.2. <i>The effect of acceleration and deceleration</i>	9
2.3. <i>Wave overtopping turbulence</i>	10
2.4. <i>Wave overtopping erosion</i>	10
2.5. <i>The empirical equations</i>	11
2.5.1. <i>Cumulative Overload Method</i>	11
2.5.2. <i>Critical flow velocity</i>	13
2.5.3. <i>Relative (depth-averaged) turbulence intensity</i>	15
2.6. <i>The numerical wave overtopping model</i>	16
2.6.1. <i>Model Input</i>	16
2.6.2. <i>Model Output</i>	18
3 Study area	19
3.1. <i>Performed wave overtopping tests</i>	20
3.1.1. <i>Simulated wave overtopping volumes</i>	20
3.1.2. <i>Front velocity field measurements</i>	20
3.2. <i>The selected test section</i>	21

3.2.1.	Experiment results	21
4	CFD model set-up in OpenFOAM.....	23
4.1.	<i>Turbulence model</i>	23
4.1.1.	The selected turbulence model	23
4.1.2.	The turbulent kinetic energy.....	24
4.1.3.	The specific turbulent dissipation	24
4.1.4.	The kinematic turbulent viscosity	25
4.2.	<i>Numerical mesh</i>	25
4.3.	<i>Time settings</i>	26
4.4.	<i>Constants</i>	26
4.5.	<i>Initial and boundary conditions</i>	26
4.5.1.	Initial turbulence.....	26
4.5.2.	Velocity	26
4.5.3.	Water layer thickness	27
4.6.	<i>Model calibration and validation</i>	28
4.7.	<i>Scenarios for the sensitivity analysis</i>	29
4.7.1.	Volume scenarios.....	29
4.7.2.	Roughness scenarios.....	30
4.7.3.	Combination scenarios	31
5	Data processing.....	33
5.1.	<i>Data sampling</i>	33
5.2.	<i>Overtopping front velocity and maximum velocity</i>	33
5.3.	<i>Modelled wave overtopping turbulence</i>	34
5.4.	<i>Empirical relative turbulence intensity</i>	35
6	Model validation.....	37
7	Wave overtopping turbulence	39
7.1.	<i>The sensitivity towards the volume</i>	39
7.2.	<i>The sensitivity towards the roughness height</i>	42
7.3.	<i>The sensitivity towards the volume and roughness height</i>	45
8	Comparison of the turbulence intensity calculations	47
8.1.	<i>Comparison per wave overtopping volumes</i>	47
8.2.	<i>Comparison per roughness height</i>	48
8.3.	<i>Differences between modelled and empirical predictions</i>	49
9	Discussion	51
9.1.	<i>Relevance of this research</i>	51
9.2.	<i>Applicability of this research</i>	53

9.3.	<i>Research limitations</i>	55
10	Conclusion	59
10.1.	<i>Validation of the wave overtopping model</i>	59
10.2.	<i>Sensitivity of turbulence towards volume and roughness</i>	60
10.3.	<i>Similarities and differences in turbulence predictions</i>	61
10.4.	<i>Comparison of the modelled and calculated turbulence</i>	62
11	Further recommendations	63
11.1.	<i>Recommendations for the empirical equations in the COM</i>	63
11.2.	<i>Recommendations for further model research</i>	64
	References	65
Appendix A	Explanation of the turbulence models	69
Appendix B	Limitations of the turbulence models	79
Appendix C	The validation of the OpenFOAM model	81
Appendix D	The modelled turbulence results	85
	Appendix references	91

1

| Introduction

Many cities around the world are located near seas, rivers or lakes, as water was, and still is an important source of food and method for transportation. To keep these cities and the hinterland safe from flooding, many different types of flood defences, such as dikes, levees and sea walls, have been constructed over the past decades. These flood defences have been constructed to withstand most high-water, waves and weather conditions. However, flood defences are not indestructible. Therefore, when a flood defence does breach, cities and the hinterland can get flooded causing a lot of damage and potentially also many casualties. Figure 1 presents an example of the hinterland flooding after a dike breach. To prevent these events from happening, research is performed to better understand how these breaches occur and what factors contribute the most.

In the Netherlands, the dike one of the most used flood defence types. Dikes can come in many varieties, but mostly consist of strong revetments on the outer slope, such as stones and asphalt, and consist of a softer revetment at the crest and the landward side, often grass (Hoffmans et al., 2018). In addition, dikes usually consist of a sand core with a clay cover layer and in some cases the whole dike consists of sand. The dikes in the Netherlands are very important due to the low elevation of the land. For this reason, much investments are made and research is done to prevent the dikes from failing. When a flood defence, such as a dike, breaches it is called a 'dike failure'. However, failure of a flood defence does not necessarily mean a total collapse of the structure. Failure can also mean that a part of the flood defence has been weakened, causing the whole flood defence system to become fragile. This damaged part of the flood defence can be repaired in order to regain functionality and to again comply with the Dutch flood protection guidelines. However, when the damage is not repaired in time, the dike will eventually not be able to cope with the forces and loads exerted on that part of the structure and could collapse (Valk, 2009). In some cases, failure can also mean that an overtopping threshold is exceeded. For example for dikes with a so-called 'zero overtopping policy', the occurrence of overtopping already means that the dike has failed. However, very small discharges are still allowed.



Figure 1 – The flooding of the hinterland caused by a dike breach. Note: reprinted from Jüpner (2018).

In recent research it was concluded that wave overtopping is one of the main reasons that dikes fail (Yuan et al., 2014; Van Bergeijk et al., 2019b). Wave overtopping can occur when high waves approach a flood defence and run up the outer slope of the dike during a wave attack. While part of the wave run-up will run back down the outer dike slope into the water, a part of the wave run-up can also flow over the dike crest. The water that overtops the crest will then run down the landward slope under gravitational acceleration (Figure 2). The part of the attacking waves that flows over the crest is considered wave overtopping (Li et al., 2004; Aguilar-López et al., 2018; Van Bergeijk et al., 2019b).

Most dikes are designed to withstand a certain amount of wave overtopping. During normal circumstances almost no wave overtopping occurs, as the wave run-up will less likely exceed the design conditions for the maximum run-up (Li et al., 2004). The run-up during these normal circumstances is limited, because most of the wave energy gets dissipated during the breaking of the wave. An approaching wave will in most cases only overtop the crest of the dike when the design conditions are exceeded due to extreme circumstances, such as strong winds or high water levels. Nonetheless, an overtopping wave does not necessarily result in damage to the landward dike slope. This is because a single wave overtopping discharge, in most cases, does not exert loads that exceed the cover strength on the dike. During extreme circumstances, however, higher waves can reach the dike, as more wave energy and usually higher water levels are presented. This results in successive high waves breaking at the dike, which increase the wave run-up on the waterside and cause waves to overtop the crest successively (Aguilar-López et al., 2018; Van Bergeijk et al., 2019b). Thus, increasing the risk of erosion.

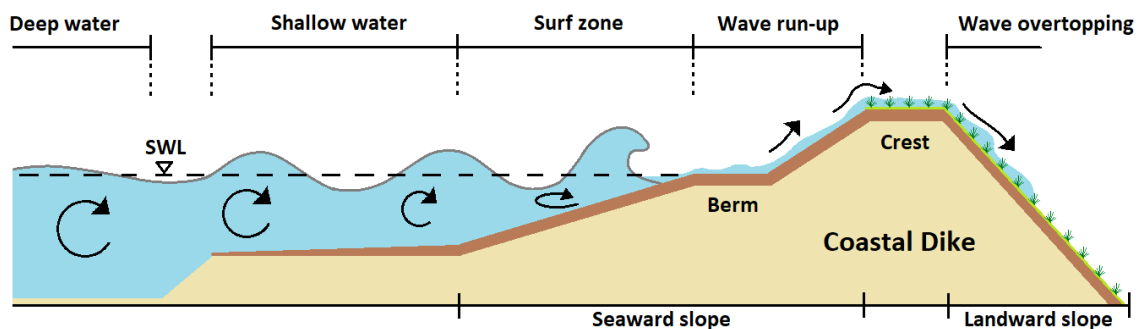


Figure 2 – The wave transformation during wave overtopping at a coastal dike. In deep water, incident waves are generated. These generated waves increase in height after entering shallow water. In the surf zone the waves start shoaling (deforming) and breaking. On the seaward slope of the dike wave run-up and run-down will occur. When this wave run-up exceeds the dike height, water will overtop the crest. The water that flows onto the landward slope is considered wave overtopping.

1.1. Problem definition

Wave overtopping mainly causes damage to the crest and the landward slope of the dike. The landward side is more vulnerable to wave overtopping due to the use of softer revetment (grass cover), which is more erodible than the stronger revetments, such as stone or asphalt. These stronger revetments are typically used on the outer slope of dikes (Yuan et al., 2014; Bomers et al., 2018; Hoffmans et al., 2018; Van Bergeijk et al., 2019a; Van Bergeijk et al., 2019b). This vulnerability of the grass cover is caused by the high velocities and turbulence within the overtopping flow (Hoffmans et al., 2018). Furthermore, additional turbulence can be produced during the wave overtopping due to the cover quality, obstacles and transitions in cover type. This additional turbulence enhances the onset of erosion, due to additional vortices, pressure fluctuations and shear stresses on the cover (Bijlard, 2015; Bomers et al., 2018). These dynamic processes between the turbulent wave overtopping and erodible crest and landward slope can result in local scour holes along the dike slope and will only end when either the wave overtopping ends or when the embankment breaches (Figure 3) (Zhang et al., 2010; Hoffmans et al., 2018). Nevertheless, dike erosion will only occur when the hydraulic load on the dike exceeds the strength of the grass cover (Van der Meer et al., 2010; Van Bergeijk et al., 2020).



Figure 3 – An example of dike damage due to wave overtopping simulated by the wave overtopping simulator. Note: reprinted from Van der Meer et al. (2010).

To reduce the hazard of dike failure due to wave overtopping, research needs to be performed to more accurately predict dike damage due to wave overtopping and to better understand the failure mechanisms involved (Hoffmans et al., 2018; Van Bergeijk et al., 2019a; Van Bergeijk et al., 2019b). Currently, wave overtopping research is mainly performed by using wave overtopping models, empirical equations and field experiments. These equations and models are often used to determine when and how much erosion will occur on the landward slope of the dike. An important, yet less understood, mechanism known to contribute to wave overtopping failure is turbulence. Wave overtopping turbulence is important, because it affects the onset of erosion, the location of erosion and the amount of erosion, therefore critically influencing the failure of a dike (Bijlard, 2015; Bomers et al., 2018; Hoffmans et al., 2018). However, despite the importance of turbulence in wave overtopping, the definition and processes involved are not yet fully comprehended, quantified or defined (Stewart, 1969; Kantha & Clayson, 2000; Loper, 2007). This knowledge gap on wave overtopping turbulence is partly caused by the fact that wave overtopping turbulence cannot yet be directly measured in the field and is also not fully understood. For these reasons, it remains difficult to quantify the turbulence intensity of the wave overtopping flow on the dike and to determine the influence of turbulence on dike erosion. This knowledge gap on the topic of wave overtopping turbulence causes the turbulence parameter, used within empirical equations to predict dike erosion under wave overtopping, to take on a range of possible constant values for different overtopping situations, without the ability to determine the correctness of the values (Bijlard, 2015).

Much research on the processes of wave overtopping is performed using numerical models. Numerical simulations can provide insights into the sensitivity of the wave overtopping turbulence for a number of conditions. Although the turbulence predictions of the model cannot be validated, as wave overtopping turbulence cannot be measured in the field yet, other parameters, such as the pressure, water layer thickness and flow velocity, can be measured. In this research a numerical wave overtopping model in OpenFOAM model is used to perform a sensitivity analysis of the predicted wave overtopping turbulence. By changing the input volume and bottom roughness of the dike, the behaviour and magnitude of the depth-averaged turbulence can be analysed. When the sensitivity of the modelled turbulence is known, the sensitivity of the turbulence intensity parameter can be analysed, to obtain more insights on the range of the turbulence intensity. By gaining more insights on the topic of wave overtopping turbulence in terms of sensitivity, the correctness of the turbulence parameter, used in empirical equations and wave overtopping models, can be analysed. These insights can thereafter be used to explore where and when wave overtopping turbulence should be measured

and to (further) develop field measuring techniques in order to measure wave overtopping turbulence. When the involved mechanisms of wave overtopping turbulence and its relation with wave overtopping failure are better understood, dike safety can be improved, as potential damage can be better estimated and prevented (Hoffmans et al., 2018; Van Bergeijk et al., 2019a; Van Bergeijk et al., 2019b).

1.2. Research objective

The overall objective of this research is to gain more insights in wave overtopping turbulence. This objective is achieved using a numerical wave overtopping model in OpenFOAM to analyse the magnitude, sensitivity and behaviour of wave overtopping turbulence along the dike profile. This can be used to analyse where turbulence can best be monitored during wave overtopping experiments on a simple dike profile. In addition, two empirical calculation methods for the relative turbulence intensity parameter, used directly in the critical flow velocity equation and indirectly in the cumulative overload method (COM), are compared, to obtain insights in the possible range, magnitude, similarities and sensitivity of each calculation method.

The gained insights on the modelled and computed turbulence intensities are used to provide new insights on the correctness of the current approach of wave overtopping turbulence within the empirical COM equations. The main research question in this study is:

'To what extent does the wave overtopping turbulence predicted with an OpenFOAM model for a simple dike profile, with a single slope angle and cover type, vary with the cover roughness and wave overtopping volume and is this variability represented in the turbulence parameter that is used in the empirical models to predict wave overtopping damage on landward dike slopes?'

1.3. Research questions

To help answering the main research question, three research questions have been composed.

- Q1) Which turbulence models can best be selected for this research to simulate wave overtopping turbulence in the OpenFOAM model and how do the predictions of the OpenFOAM model compare to wave overtopping experiments at the Vecht dike?
- Q2) What variabilities of the wave overtopping turbulence are predicted by the OpenFOAM model for a simple dike profile and how sensitive are these predicted wave overtopping turbulence variabilities towards the modelled wave overtopping volume and bed roughness?
- Q3) To what extent does the turbulence parameter, used in the empirical models to predict wave overtopping damage, represent the changes in the wave overtopping turbulence predicted by the OpenFOAM model for different wave overtopping volumes and bed roughnesses?

1.4. Research method

During this research more insights into the topic of wave overtopping turbulence on the landward slope of the dike will be gained by using a numerical wave overtopping model in OpenFOAM. This wave overtopping model can predict turbulence variations along a dike with a simple profile for a single overtopping wave. To construct the numerical mesh and validate this model, field measurements of wave overtopping experiments performed on the Vecht dike have been used. From the different field experiments, one test section was selected. After the selection, the wave overtopping model was set-up to replicate this selected test section. For this model set-up, the most appropriate turbulence model

was selected and implemented into the model. The turbulence model was selected based on (1) the availability of the turbulence model in OpenFOAM, (2) the required computational time of the turbulence model, (3) the required turbulence scale/output accuracy needed for this research and (4) the complexity of the model implementation. After the selected turbulence model was implemented, the numerical mesh was generated and other model settings, such as the boundary conditions, were addressed. The model was validated by comparing the OpenFOAM velocity predictions with wave overtopping velocity data obtained during field measurements at the selected test section. During the validation process, the data sampling and processing methods, used for this study, were set-up.

After the validation, the wave overtopping model was used to analyse the variabilities and sensitivity of wave overtopping turbulence along the dike profile towards changes in wave overtopping volume and bed roughness. In the OpenFOAM model, the wave overtopping volume was changed by implementing different boundary conditions for the wave overtopping velocity (u) and water layer thickness (h) at the inlet. The bed roughness was changed by implementing different roughness heights (k_s). After the sensitivity analysis in OpenFOAM, the relative turbulence intensity, which is used in empirical equations to estimate wave overtopping damage on the landward side of dikes, was computed using two different calculation methods and compared to observe whether the calculated turbulence intensities present similar trends and ranges to one another. Lastly, the obtained trends of the modelled wave overtopping turbulence will be compared to the obtained trends of the computed relative turbulence intensities. Figure 4 presents a flow chart of the overall research process.

This study applies the front velocity data of wave overtopping experiments on the Vecht dike in the Netherlands obtained by Infram Hydren, a numerical 2DV (two-dimensional vertical) OpenFOAM model developed by Van Bergeijk et al. (2020) and the empirical equations of the cumulative overload method (COM) developed by Van der Meer et al. (2010).

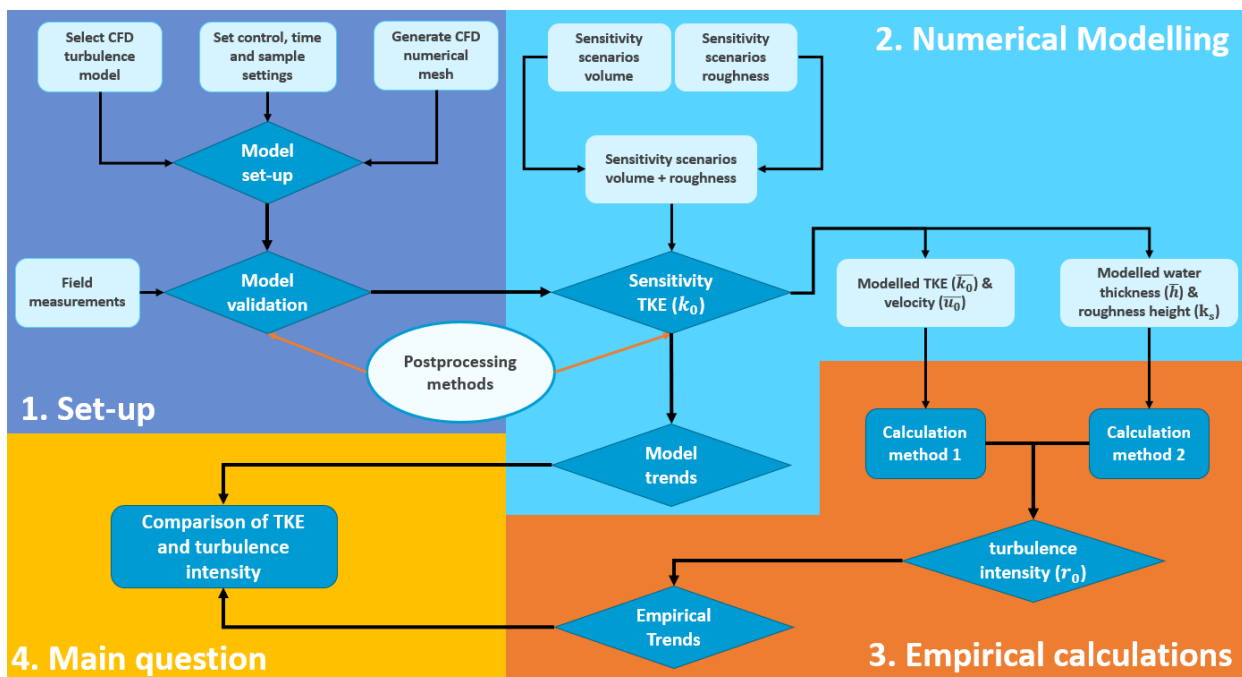


Figure 4 - Flow chart of the research processes showing the research components needed to answer the main research question of this research. The arrows indicate the order in which the research components are obtained.

1.5. Research scope

This study only covers the impact of wave overtopping turbulence on the landward side of a simple dike profile. Herein a simple dike profile refers to a dike with a single slope angle and a single cover type. This means that dike profiles with obstacles, such as trees and streetlights, or cover and/or slope angle transitions, such as roads or berms, are outside of the scope of this research.

To analyse the wave impact of a single overtopping wave, the numerical OpenFOAM wave overtopping model is used. This model will solely be used to analyse the behaviour, intensity and sensitivity of the turbulence maxima during a wave overtopping event. The resulting wave overtopping damage cannot be analysed with the OpenFOAM model and is not calculated afterwards using the COM method.

1.6. Report outline

The outline of this report is as follows. First, a description of the current knowledge on wave overtopping turbulence, the empirical models and the OpenFOAM model is given in chapter 2. Afterwards the study area is introduced in chapter 3, wherein the dike characteristics and field measurement methods are described. Chapter 4 presents a description of the model set-up and the used settings in the OpenFOAM model. In addition, the model calibration, model validation and the wave overtopping volume and roughness scenarios are described. In chapter 5 the sampling and postprocessing methods for the modelled parameters and the computation methods for the turbulence intensities are described. Chapter 6 presents the validation of the OpenFOAM model. The results of the sensitivity analysis of the modelled turbulence are presented in chapter 7 and the comparison between the two different empirical turbulence intensity calculations is presented in chapter 8. In chapter 9 a discussion is presented, wherein the relevance, applicability and limitations of this study are described. The conclusions of this study are presented in chapter 10 and the further recommendations are presented in chapter 11.

| Current knowledge

2.1. Turbulence

Turbulence is often characterised by disorder, chaotic fluid motions in both time and space, the presence of vorticity and the entrainment of air. These vortices, also known as coherent structures, swirl around one another and take on a variety of shapes. In turbulent flows, these vortices, swirls and eddies are continuously and irregularly produced in all three dimensions (Stewart, 1969; Kantha & Clayson, 2000; Loper, 2007; De Serio & Mossa, 2019). In general, turbulence is generated when an excessive amount of kinetic energy is present in some of the water flow layers. This excessive energy can overwhelm the damping effect of the fluid viscosity, causing an increase in perturbations and instabilities in the flow. These perturbations and instabilities will thereafter produce even more disturbances and will eventually destroy the orderly behaviour of the fluid, which then results in turbulence (Figure 5) (Kantha & Clayson, 2000; Loper, 2007).

In turbulent flows most of the kinetic energy is contained in the large-scale eddies. These eddies rapidly dissipate when the kinetic energy is converted into heat by the viscous shear stress near the bottom, making the flow laminar again. This energy dissipation is caused by the continuous conversion of these large-scale structures to smaller and smaller scale structures. When these small scale structures become small enough, the remaining energy gets dissipated through viscous dissipation. This process is called the energy cascade and the scale at which viscous dissipation is possible, is called the Kolmogorov length scale (Vassilicos, 2015). Due to these processes a turbulent flow can only be sustained if a persistent source of energy supply is available in the flow.

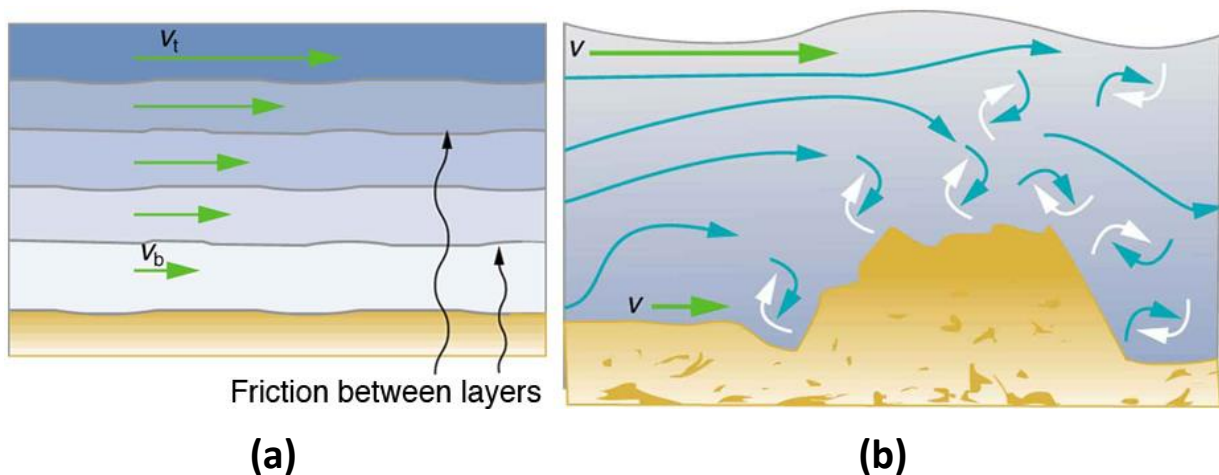


Figure 5 - (a) Laminar flow with flow layers moving at variable velocities. (b) Turbulent flow. The varying flow velocity, bed roughness and viscosity of the water cause drag between each flow layers, while the bed causes friction. This friction disturbs the flow near the bed, while the drag transfers disturbances to the upper layers. These disturbances obstruct the laminar flow structure and cause turbulence. The turbulent flow causes the fluid to mix, which increases the shear, heat and drag within the fluid. Note: reprinted from Urone et al. (2020).

2.2. Turbulent boundary layer

When a fluid flows over a surface, the flow velocity profile near the wall will show a distinctive structure, called the boundary layer. In the boundary layer, the flow velocity of the free stream reduces towards the surface until the velocity is reduced to zero at the surface, which is called the ‘no-slip’ condition. This reduction of the flow velocity and the ‘no-slip’ condition are caused by the increased influence of the viscous forces towards the wall, causing the fluid to ‘stick’ to the boundary (Robert, 2003; Bomers et al., 2018; Horstman et al., 2018; Nikolaidou, 2019). If a flow transitions from laminar to turbulent, the laminar boundary layer will become a turbulent boundary layer. In the turbulent boundary layer, eddies are generated by irregularities of the bed and develop in various sizes over time (Figure 6.a) (Bomers et al., 2018).

The structure of a turbulent boundary layer on an unvegetated surface consists of four flow regions (Figure 6.a) (Robert, 2003). The flow region closest to the bed is the **viscous sub-layer**. In the viscous sub-layer, the flow is laminar, as the velocity reduces to zero due to the dominant viscous forces. Therefore, turbulent shear stresses can be neglected within this sub-layer. In addition, eddies that were generated in the freestream, can rapidly dissipate due to the viscous stresses in this sub-layer. Above the viscous sub-layer, the **transition/buffer layer** is located. Within the transition layer, the viscous shear stresses and the turbulent shear stresses are equally important, which causes energetic small-scale turbulence to be generated by the flow instabilities in this sub-layer. Furthermore, a sharp peak in turbulent kinetic energy (TKE) and turbulent dissipation occurs, as the mean-flow kinetic energy gets converted into TKE. Therefore, the transition layer is often called the turbulence-generation layer. Within **logarithmic layer**, located above the transition layer, the viscous shear stresses become negligible and the turbulent shear stresses become equal to the bottom shear stresses. The **turbulent outer layer** is often the largest flow regime and reaches up to the water surface. In the turbulent outer layer, the velocity is relatively constant due to the strong mixing of the flow. Within this layer, turbulence is dominant and transport of momentum normal to the flow direction, is much more efficient than in the transition layer near the surface (Nikolaidou, 2019).

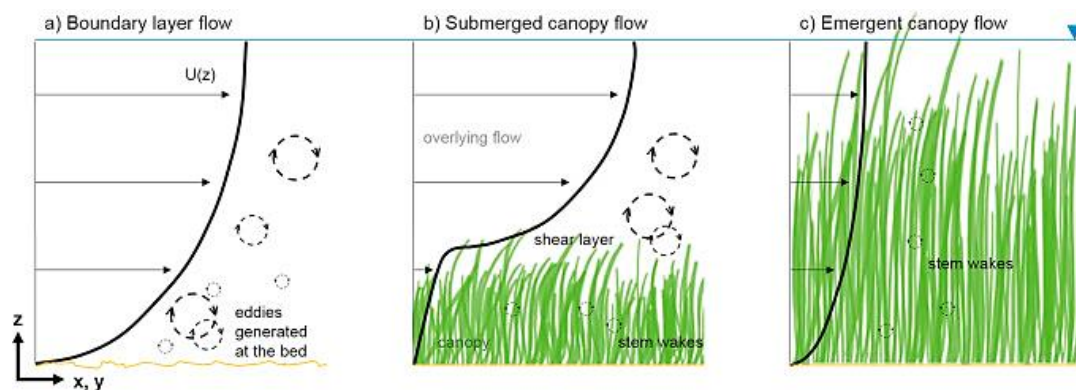


Figure 6 - Three flow regimes wherein the bed, vegetation top and stems are the dominant source of turbulence. Note: reprinted from Beudin et al. (2017)

For flow over a vegetated surface, a turbulent boundary layer is formed due to the difference in velocity between the top of the vegetation and the bottom (Figure 6.b). Due to the canopy shear, caused by this difference in velocity, a peak in turbulence can be observed right above the vegetation as large-scale vortices are generated. These peaks in turbulence increase the exchange of suspended matter and water between the water body and canopy (Horstman et al., 2018). The small-scale vortices are mainly produced by the stems. Nonetheless, at a critical vegetation density, the turbulence intensity on the dike will decrease as a critical bed roughness has been reached, resulting in a reduction of the flow velocity (Horstman et al., 2018) (Figure 6.c).

2.2.1. Hydraulically smooth and rough flows

In turbulent flows, the viscous sub-layer thickness, also called the laminar boundary layer thickness (δ_v), can range from fractions of millimetres to many millimetres (Nikolaidou, 2019). Using this sub-layer thickness, two types of turbulent flows can be distinguished. A turbulent flow is considered hydraulically smooth when the roughness elements at the surface are smaller than the laminar boundary layer thickness ($k_s < \delta_v$), as the elements do not disturb the main body (Figure 7). The flow is considered hydraulically rough when the roughness elements are larger than the laminar sub-layer ($k_s > \delta_v$), as the elements penetrate into the main body of flow, or when the width of the open-channel is much larger than the flow depth ($width \gg depth$) (Robert, 2003; Nortier et al., 2014). Therefore, highly turbulent flows with a small water layer thickness, are more likely to be hydraulically rough.

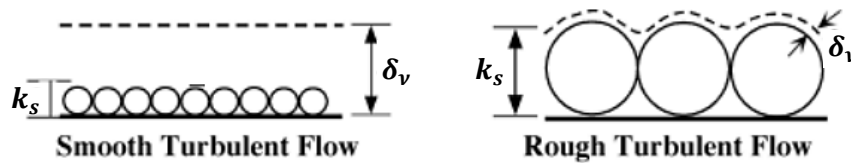


Figure 7 – Left: a hydraulically smooth flow. Right: a hydraulically rough flow. k_s represents the roughness height and δ_v represents the laminar layer thickness. Note: reprinted from MIT (2016)

2.2.2. The effect of acceleration and deceleration

The shape of the boundary layer influence both the amount of pressure drag and skin friction drag in the flow. The pressure drag represents the forces perpendicular to the flow direction (pressure), while the skin friction drag represents the forces tangential to the flow direction (shear stress) (Schiereck, 2001; Robert, 2003; Nikolaidou, 2019). In uniform flows, the boundary layer is often fully developed and reaches up to the water surface, which leads to a logarithmic distribution of the velocity profile (Figure 8.a). However, in reality flows are never uniform and the boundary layer is often not fully developed. Furthermore, acceleration and deceleration of the flow, which have an effect on the boundary layer shape and the amount of turbulence in the flow, are taken into account in non-uniform flows (Schiereck, 2001).

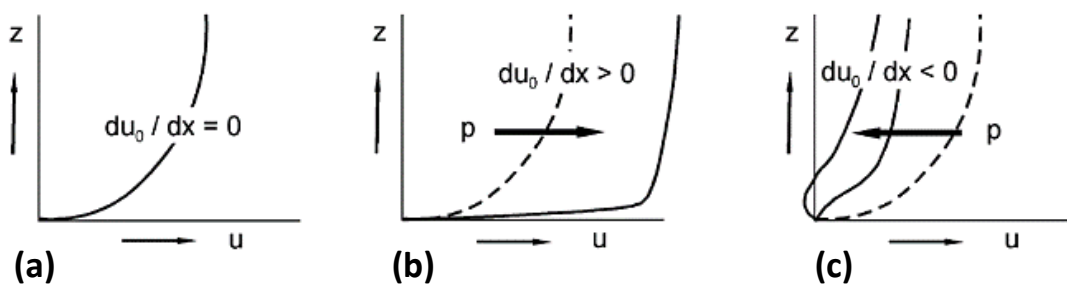


Figure 8 - Influence of pressure gradients on the flow velocity profile. (a) no acceleration or deceleration, (b) boundary layer thickness decreases and the flow starts to accelerate, (c) boundary layer thickness increases and the flow starts to decelerate. Note: reprinted from Schiereck (2001).

Flow acceleration occurs when the pressure gradient in the flow direction increases, which is the case for wave overtopping on the slope as the overtopping waves have a non-uniform distribution (Schiereck, 2001). This means that the mass upstream is smaller than the mass downstream, as the wave front is much larger than the rest of the wave and the flow accelerates due to gravity. When the flow accelerates, the boundary layer thickness will decrease and the velocity gradient between the free stream and the near-wall region will increase (Figure 8.b). This increase in velocity gradient will lead to larger shear stresses, as faster velocities can penetrate closer to the dike surface.

Flow deceleration occurs when the pressure gradient in the opposing direction of the flow increases (Schiereck, 2001). As the pressure gradient increases opposite to the flow direction, the velocity profile

will start to deform, causing the boundary layer thickness to increase and the velocity gradient between the free stream and the near-wall region to become smaller (Figure 8.c). This decrease in velocity gradient, decreases the shear stresses and increases the pressure in the flow. Furthermore, less turbulence will be generated, as the increase in pressure also increases the potential energy of the fluid, which leads to a reduction of the kinetic energy (Ponsioen, 2016). In addition, the risk of flow separation will start to increase when the flow decelerates. Flow separation occurs when the flow near the wall rapidly decelerates compared to the free stream velocity. This will increase the unsteadiness and pressure gradient in the flow, until the boundary layer gets reversed and detaches from the surface (Figure 8.c) (Schiereck, 2001; Robert, 2003; Nikolaidou, 2019). This separation of the flow causes the pressure drag to increase significantly, as a wake of recirculating flow will be created, and will once again increase the amount of turbulence generated (Schiereck, 2001; Robert, 2003; Nikolaidou, 2019). Generally, flow separation occurs when the slope angle changes sharply. Therefore, local peaks in turbulence and flow separation can occur on the dike crest, as the velocity rapidly decelerates due to the horizontal crest until the slope angle changes and the flow can accelerate again. During this slope angle transition, the free stream flow can suddenly accelerate, while the flow near the wall remains much slower as the flow ‘sticks’ to the surface.

2.3. Wave overtopping turbulence

Wave overtopping over a dike generates both momentum and bed shear stress, creating tensile stresses and shear stresses along the entire dike profile. When overtopping waves run down the inner slope due to gravitational acceleration, the overtopping flow will gain energy along the slope. This increase in energy further increases the bed shear stresses on the inner slope of the dike (Van Bergeijk et al., 2019b). The increasing shear stresses between the dike cover and the water body will result high Reynolds numbers and will eventually form a turbulent boundary layer at the bed (Aguilar-López et al., 2018; Bomers et al., 2018). Turbulent overtopping flow has the potential to entrain and stir sediment particles along the inner dike slope and dike crest (Li et al., 2004). This potential entrainment and stirring may result in varying cover erosion across the landward slope.

From experiments it was found, that this erosion is often caused by the front edge of the overtopping wave, as turbulence is strongest in the rising stage of an overtopping wave. The wave overtopping turbulence affects both the location and the amount of erosion, but this turbulence does not solely initiate cover erosion (Bomers et al., 2018). In addition to turbulence, parameters such as pressure, shear stresses and cover strength also play a role in the initiation of cover erosion (Schiereck, 2001; Hoffmans, 2012).

2.4. Wave overtopping erosion

On a simple dike profile with a constant slope and a uniform revetment, the flow velocity is highest towards the toe of the dike due to gravitational acceleration. It was found that, for a simple dike profile, the toe of the landward slope experiences the most erosion (Bijlard, 2015; Bomers et al., 2018; Van Bergeijk et al., 2019b). This vulnerability of the toe compared to other locations on a simple dike is caused by the combination of the gravitational acceleration and the change in slope angle, creating a very turbulent flow near the toe of the dike. During wave overtopping, the soil at the landward side of the dike can be weakened by the wave impact and the saturation of the soil over time. When the cover becomes weak, local scour or erosion holes can be formed by the turbulent flow due to the constant stirring of sediment and pulling of the grass sods. When a scour hole is created, the risk of a breach on the landward side of the dike increases. This is because the scour holes will eventually become bigger, as the soil layers underneath the grass cover are now exposed to the turbulent flow (Figure 9).

The onset of erosion through turbulence is influenced by the bed roughness and geometrical roughness of the dike cover. However, the onset of erosion is significantly more affected by the geometrical roughness (Bomers et al., 2018). The terms bed roughness and geometrical roughness are used to make a separation between two different roughness causes. The bed roughness refers to the roughness caused by the cover material, while the geometrical roughness refers to the roughness caused by irregularities or transitions in the cover (Bomers et al., 2018). These irregularities in the cover, such as animal burrows, bumps or cover transitions, yield an additional increase in the near-bed turbulence.

In general, when the roughness of the bed increases, the velocity will decrease due to drag and friction. Although it could be expected that the onset of erosion is at less risk when the velocity decreases, this is not always the case, as an increase in bed roughness also increases the turbulence production in the flow. This increase in turbulence causes an increasing risk of erosion. Therefore, the rougher the cover type, the more turbulence can be generated throughout the dike profile and the more irregularities in the cover, the more turbulence can be generated locally. Thus, different types of roughness can enhance the onset of turbulence and turbulence intensities, thereby affecting the onset, location, amount and speed of erosion.

Erosion on a dike is more likely to occur at the locations where the cover type changes, for example at the transition of grass to asphalt, as the bed roughness between the different cover materials differ. In these cases, the turbulence increases when the surface changes rapidly from smooth to rough, while the turbulence decreases from rough to smooth (Hoffmans et al., 2018; Van Bergeijk et al., 2019a). In addition, obstacles on the slope, such as trees, also enhance the onset of local erosion. This is because the grass strength is weaker around the obstacle, as the root growth can be hindered by the obstacle, and because local acceleration and deceleration of the flow produces additional turbulence at the front of the obstacle (Bomers et al., 2018; Hoffmans et al., 2018). The amount of erosion around the obstacle depends on the type of cover, as for example grass erodes faster than asphalt, and the location of the obstacle on the slope, as the flow velocity increases towards the toe of the dike.

2.5. The empirical equations

Different empirical equations have been developed over the years to better predict wave overtopping failure on the inner dike slope. These developed empirical equations use known processes that occur during wave overtopping, such as the front velocity and pressure, and can be used to determine the impact of an overtopping wave. These equations often use the discharge distribution data of the wave overtopping experiments and corresponding wave overtopping velocity data to gain a realistic representation of the processes involved with wave overtopping damage (Bijlard et al., 2016).

2.5.1. Cumulative Overload Method

The Cumulative Overload Method (COM) is an empirical relation developed by Van der Meer et al. (2010). The method is used to determine the wave overtopping damage on the landward slope of the

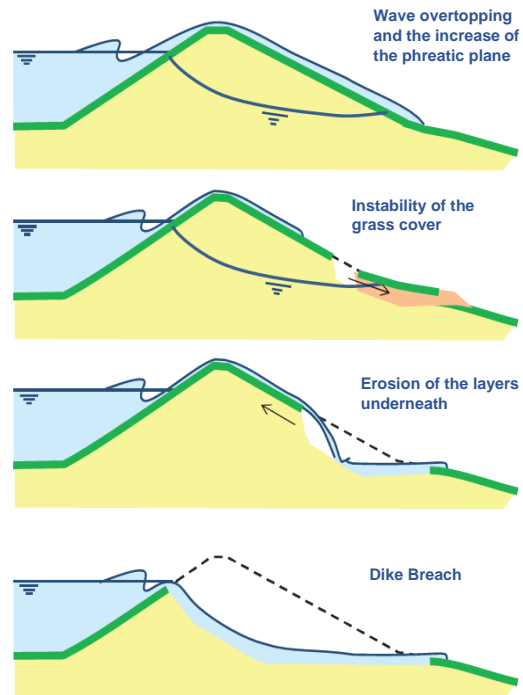


Figure 9 – The process of wave overtopping failure.
Note: reprinted from 't Hart et al. (2016)

dike caused by cumulative wave overtopping. The Cumulative Overload Method can provide a better understanding of the relation between the volume of wave overtopping, the velocity of the overtopping waves and the strength of the grass (Bijlard, 2015). This method predicts the moment when a damage criterion on the landward slope is reached, but can only be used if the wave load as function of time and the grass strength are provided beforehand (Van der Meer, 2011; Hoffmans et al., 2018). The damage that can be predicted after a certain number of overtopping waves are; no damage, start of damage, damage on various locations or failure. The original empirical model developed by Hoffmans is written as follows:

$$\sum_{i=1}^N (U_i^2 - U_c^2) = D \quad \text{for } U_i^2 > U_c^2 \quad [1]$$

In equation [1] D is the damage number [m^2/s^2], which gives an indication of the amount of damage, N is the number of overtopping waves that exceed U_c [-], U_i is the front velocity of the i^{th} overtopping wave at the crest [m/s] and U_c is the critical flow velocity of the cover [m/s]. Herein, the U_c is a strength parameter and the U_i is a load parameter. If U_i is larger than U_c , the overtopping wave volume contributes to the damage number. Through different experiments it was found that the erosion at dikes with geometrical transitions, revetment transitions and/or obstacles differs from erosion at simple dike profiles (dikes consisting of one slope and one cover type). This difference can be explained by the fact that the load increases at these transitions and obstacles, while the grass strength is reduced (Hoffmans et al., 2014). To take the effects of transitions, objects, flow acceleration and the grass strength into account, factors can be added to equation [1]:

$$\sum_{i=1}^N (\alpha_m (\alpha_a U_i)^2 - \alpha_s U_c^2) = D \quad \text{for } \alpha_m (\alpha_a U_i)^2 > \alpha_s U_c^2 \quad [2]$$

In equation [2] the factor α_a represents the gravitational acceleration of the front velocity, which increases the flow velocity along the landward slope of the dike. The factor α_m represents the contribution of geometrical and revetment transitions and obstacles on the dike cover. This factor takes the type of transition and the shape of the obstacle into account. If no transition or object is present, this factor is set to 1.0 and is increased when angle changes, transitions and/or obstacles are present ($\alpha_m > 1.0$). The factor α_s represents the strength of the grass at special locations on the inner dike slope, such as at transitions and obstacles. This factor takes the interruption of grass growth at these locations into account, as the roots cannot grow towards the object or transition. For this reason the grass strength at these locations is smaller ($\alpha_s < 1.0$) than elsewhere on the grass cover ($\alpha_s = 1.0$) (Bijlard, 2015; Hoffmans et al., 2018). Thus, the factors α_a and α_m are load factors, while α_s is a strength factor. In Figure 10, examples of a revetment transition, geometrical transition and obstacle are presented. For the load factor α_m , multiple equations can be used to calculate the contribution of transitions and obstacles depending on the type of transition and/or obstacle on the dike. For the other two factors, only one equation is available. For a simple dike profile with a constant slope and a uniform revetment, this results in the following factor equations (Chen, 2019):

$$\alpha_s = \frac{1.5 F_{m,B} - 0.5 F_{m,A}}{2 F_{m,B} - F_{m,A}} \quad [3] \quad \alpha_a = \frac{U_{i,slope}}{U_{i,crest}} \quad [4]$$

$$\alpha_{m,CS} = 1 - \sin\left(\frac{1}{2}\theta_0\right) \quad [5] \quad \alpha_{m,ST} = 1 + \sin\left(\frac{1}{2}\theta_0\right) \quad [6]$$

Equation [3] is based on experiments with the tensile force test. Within this equation, $F_{m,A}$ describes the maximum tensile force for condition A, when no additional strength is used from the sides, while $F_{m,B}$ describes the maximum tensile force for condition B, when additional strength is used on two

sides. In equation [4], $U_{i,slope}$ represents the overtopping velocity on the slope and $U_{i,crest}$ represents the overtopping velocity at the transition between the crest and slope. Equations [5] and [6] both calculate the load factor α_m and use the steepness of the inner slope (θ_0). Although multiple equations can be used to calculate α_m for different transitions and obstacles, only the geometrical transitions between the crest and slope (calculated with equation [5]) and the slope and toe (calculated with equation [6]) need to be taken into account for a simple dike profile. In general, the average range for α_s between 0.82 and 0.97 and for α_a between 1.2 and 1.5 close to the toe (Chen, 2019).

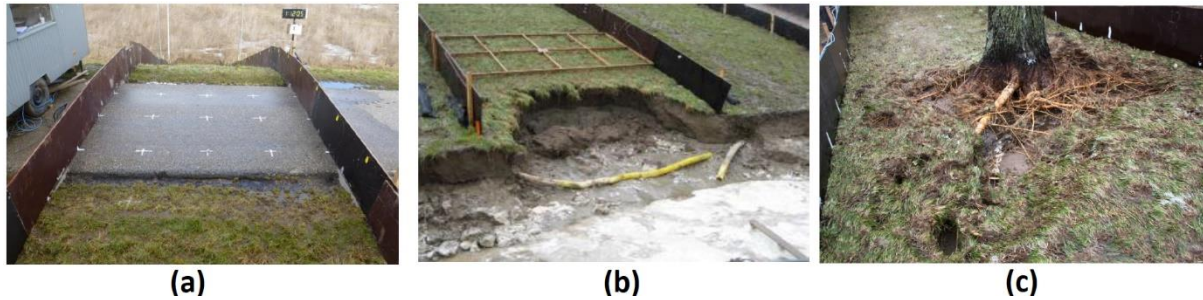


Figure 10 – (a) Transition between a grass and asphalt cover (revetment transition), (b) transition in the slope angle of the dike (geometrical transition), (c) tree on the dike slope blocking the flow (obstacle). Note: reprinted from Hoffmans et al. (2014).

By using equation [2] a damage number can be calculated for each wave overtopping that exceeds the critical velocity. Depending on the damage number, the Cumulative Overload Method indicates whether no damage, start of damage, damage on various locations or failure of the dike occurs (Van der Meer, 2011; Bijlard, 2015). When a scour hole deeper than 20 cm is formed by wave overtopping, the grass cover is considered to have failed. The damage number values at which damage will occur on the dike depend on the calculated critical velocity and alpha factors. The value of the critical velocity and factors need to be calculated for each dike section separately and are used in the equation as constant parameters. When the values of these constants are calculated, the wave overtopping data can be used in equation [2] to calculate the damage numbers. Using the field observations of wave overtopping damage on the selected dike, the damage number can be calibrated. For example, if early damage is observed after the 10th wave and the damage number calculated by equation [2] is 1000 m²/s² at the 10th wave, it is stated that the start of damage occurs when the damage number reaches 1000 m²/s² for all overtopping situations on this particular dike. This means that it is assumed, that damage will occur after the same calculated damage number, but for different wave overtopping volumes. Doing this for all possible COM results, could for example give the following calibrated damage factors:

- | | |
|-------------------------------|---|
| - No damage | $\sum(U_i^2 - U_c^2) < 1000 \text{ m}^2/\text{s}^2$ |
| - Start of damage | $\sum(U_i^2 - U_c^2) = 1000 \text{ m}^2/\text{s}^2$ |
| - Damage on various locations | $\sum(U_i^2 - U_c^2) = 4000 \text{ m}^2/\text{s}^2$ |
| - Failure of the dike | $\sum(U_i^2 - U_c^2) = 7000 \text{ m}^2/\text{s}^2$ |

2.5.2. Critical flow velocity

The critical flow velocity is an input parameter of the Cumulative Overload Method. This critical flow velocity, functions as a threshold parameter that represents the strength of the grass cover during wave overtopping. When the velocity of the overtopping wave exceeds the critical velocity, damage can start to occur as can be seen in equation [2] of the COM (Bijlard, 2015). The critical flow velocity (U_c) can be computed by using either field data of wave overtopping erosion or one of the developed empirical equations.

One of the first empirical equations for U_c was developed by Van der Meer in 2010, which has since then been further researched and improved in different studies (Valk, 2009; Bijlard, 2015; Horstman et al., 2018). One of the more recent approaches to calculate the critical flow velocity is based on the Turf Element Model. The Turf Element Model makes an attempt to link the loads on the grass sod with the strength of the grass sod (Hoffmans, 2012). The load forces are mainly caused by pressure fluctuations that occur perpendicular to the grass cover. These upward pressures are generated by wave overtopping turbulence at the bed, as this creates under pressure. Because an increase in turbulence will cause an increase in pressure fluctuations, it can be stated that turbulence is directly related to the amount of erosion. On the other hand, the downward forces on the soil are characterised by shear forces and the root strength force (Le & Verhagen, 2014). The critical flow velocity using this theory is computed using equation [7].

$$U_c = \alpha_{grass,U} r_0^{-1} \sqrt{\frac{\psi_c(\sigma_{grass,c}(0) - \rho w)}{\rho}} \quad \text{with } \alpha_{grass,U} = 2.0 \quad [7]$$

In this equation, r_0 represents the relative (depth-averaged) turbulence intensity [-], ρ represents the water density [kg/m^3], ρw is the pore water pressure [N/m^2], ψ_c is the critical shields parameter [-], $\alpha_{grass,U}$ is a constant [-] and $\sigma_{grass,c}(0)$ is the critical mean grass normal stress at the ground level [N/m^2] (for example perpendicular to the ground surface). Mainly one constant U_c is used to describe the critical flow velocity for all overtopping waves, but the critical flow velocity can also be computed for each individual wave overtopping event. Using the COM (equation [2]), the critical flow velocities can be used to compute the damage of successive wave overtopping events. The critical flow velocity depends on the type of dike cover and the overall quality of the cover, as these will influence the critical shields parameter and the critical mean normal stresses. Because the critical velocity is often low, erosion can easily take place if no action is taken (Van Bergeijk et al., 2019b).

Generally, one constant value is used to describe the critical flow velocity along the entire dike profile, which would only be a correct assumption if the flow is uniform (Hoffmans et al., 2018). Therefore, to better estimate wave overtopping damage, the critical velocity should also be variable along the dike profile. This is not only because the strength of the cover varies along the dike profile, but also because the turbulence intensity varies along the dike profile, which causes large differences in the local onset of erosion. Hoffmans et al. (2016) stated that when U_c varies, the maximum critical velocity can be found about halfway on the landward slope of the dike.

In addition, when successive waves overtop the dike, the soil will get saturated over time. When the top layer of the grass becomes fully saturated, the suction pressure of the grass will eventually reduce to zero. This saturation of the ground results in liquefaction of the soil, causing the critical flow velocity to become lower and erosion to occur faster. This liquefaction of the soil over time is taken into account in equation [7] through the pore water pressure parameter (ρw) (Bijlard, 2015). Without the pore water pressure parameter, the equation would assume a fully saturated state of the grass sods. As wave overtopping does not always cause full saturation of the soil, the suction pressures must be included in the equation. When the soil becomes fully saturated, ρw becomes equal to zero. In most cases, storms can speed up this saturation process as wave overtopping is often combined with heavy rain during storms (Bijlard, 2015). In Table 1 an overview of the parameters that influence the critical flow velocity is presented.

Table 1 - Overview of the parameters that can increase or decrease the grass strength threshold (U_c).

U_c Increases (Threshold \uparrow)		U_c Decreases (Threshold \downarrow)	
Less turbulence	$rD \downarrow$	More turbulence	$rD \uparrow$
Ground is unsaturated (dry)	$\rho w \uparrow$	Ground is saturated (wet)	$\rho w \downarrow$
Mean grass normal strength is high	$\sigma_{\text{grass},c}(0) \uparrow$	Lower grass strength (Obj/trans)	$\alpha_s \downarrow$
Shields parameter is high	$\psi_c \uparrow$		

2.5.3. Relative (depth-averaged) turbulence intensity

The relative depth-averaged turbulence intensity is computed through an empirical equation and used as a constant parameter in the critical flow velocity equation (equation [7]). The relative depth-averaged turbulence intensity can be calculated using the following equation and provides a dimensionless value (Bijlard, 2015; Hoffmans et al., 2018):

$$r_0 = \frac{\sqrt{k_0}}{U_0} = \frac{\alpha_0 u_*}{U_0} = \frac{\alpha_0 \sqrt{g}}{C} \quad [8]$$

The above presented equation is a combination of the depth-averaged flow velocity (U_0), which represents the velocity in the longitude direction (equation [9]), the depth-averaged turbulent kinetic energy (k_0), which represents TKE in all directions (equation [10]), the bed shear velocity (u_*) (equation [11]) and the Chézy coefficient (C) (equation [12]).

$$U_0 = C \sqrt{R_h S_b} \quad [9] \quad \sqrt{k_0} = \alpha_0 u_* \quad [10] \quad u_* = \sqrt{g R_h S_b} \quad [11] \quad C = 18 \log_{10} \frac{12 R_h}{2d} \quad [12]$$

In the equations above R_h represents the hydraulic radius [m], which is equal to the flow depth, S_b represents the dike slope [-], g represents the gravitational acceleration [m/s^2], α_0 is a constant of 1.21 [-] and d is the particle diameter [m] (Bijlard, 2015; Hoffmans et al., 2018). Bijlard (2015) found that the relative turbulence intensity is mostly between the 0.1 and 0.3 for wave overtopping on a slope, wherein a relative turbulence intensity around 0.1 is often used when most of the damage occurs at the lower half of the slope. If damage occurs near the upper half of the slope, a relative turbulence intensity around 0.2 is used. This is because the turbulence intensity will decrease, while the velocity will increase down the slope due to gravitational acceleration (Bijlard et al., 2016).

The relative turbulence intensity has an important relation with the critical velocity, as this factor can cause major differences in the resulting critical flow velocity computed with equation [7]. This sensitivity is caused by the fact that the critical flow velocity will increase when the turbulence intensity decreases and vice versa, as can be noted from equation [7]. This relation is caused by the fact that turbulence can increase the onset of erosion. Therefore, when less turbulence is present, the risk of the onset of erosion also decreases and thus, the threshold at which grass will erode also increases. This shows that the critical velocity reacts proportional to the turbulence intensity, as can also be noted from equation [7] (Bijlard et al., 2016). Although the turbulence intensity is a small factor, it still has a large impact on the resulting damage estimate. Bijlard (2015) found that when the turbulence parameter is adjusted by 1%, the critical flow velocity, indicating the grass erosion threshold, will change with approximately 8%. Furthermore, the critical flow velocity and turbulence intensity, both depend on factors such as the cover type (roughness) and the overall cover quality (irregularities).

In reality turbulence is a non-constant load factor, however, currently the turbulence parameter is used as a constant and implemented in the critical flow velocity equation, which is a strength factor within the COM. Due to this Bijlard et al. (2016) points out that the current use of the relative turbulence intensity is not fully correct and should be further investigated in future research.

2.6. The numerical wave overtopping model

Numerical models can be used to better understand processes and to analyse hypotheses. These models can calculate hydraulic variables with the use of boundary conditions, initial values and known relations. Within these models different equations can be ‘plugged in’ through the use of solvers or sub-models to simulate different situations and resolve specific parameters. In numerical models, different equations are solved for each cell in the grid. This means that more information can be obtained if a mesh with smaller grid cells is used. Computational Fluid Dynamics (CFD) modelling is one of the more specific types of numerical modelling. One of the more used CFD model software is OpenFOAM. OpenFOAM stands for ‘Open source Field Operation And Manipulation’ and is a free to use open-source CFD toolbox (OpenCFD, 2016; Liu, 2017). OpenFOAM essentially uses a collection of C++ code text files and allows users to run many different tasks on an unlimited amount of processors. Many researchers prefer using OpenFOAM to investigate wave overtopping as it is capable of accurately modelling overtopping processes. As the data is of open-source nature, libraries and toolboxes that prove to be useful are freely shared among users and constantly extended and improved for various purposes (Chen, 2019).

Van Bergeijk et al. (2020) constructed a 2DV numerical model in OpenFOAM in order to simulate individual wave overtopping flows on the crest and landward slope of a grass-covered dike. The developed numerical model provides insights into which hydrodynamic forces are dominant at the dike surface, how these hydrodynamic forces vary along the dike profile and where the highest hydraulic loads occur. The hydraulic loads can be computed at every location of the crest and landward slope of the dike, but also at cover material transitions and geometrical transitions (berms). The model calculates the flow velocity, the near bed velocity, the pressure, the shear stress and the normal stress on the cover along the dike profile per overtopping wave. However, this model does not calculate or estimate wave overtopping erosion. Nonetheless, the output can be used to calculate failure mechanisms, such as wave overtopping failure, giving this wave overtopping model a major advantage compared to other models.

In the next subsections (2.6.1. and 2.6.2.), the model, as developed by Van Bergeijk et al. (2020), will be present. This model will be referred to as the original model within this research. To obtain a better model validation some changes were implemented, which are mentioned in section 4.5. This adjusted model will be referred to as the new model within this research.

2.6.1. Model Input

To use the OpenFOAM model, certain model input, such as initial values, is required. The model input is used to numerically simulate the overtopping wave and solve the loads exerted by the wave impact. In addition to the information, such as simulation time, sample frequency and transport properties, the model also needs restrictions in the form of boundary conditions. Furthermore, sub-models are needed to solve fluid processes, such as the turbulence. To gain a better understanding of the model, these boundary conditions and used sub-models are shortly introduced. The boundary conditions and sub-models mentioned, are used in the original model version developed by Van Bergeijk et al. (2020).

2.6.1.1. The original boundary conditions

In the OpenFOAM numerical model, the overtopping waves at the crest are characterised by the flow velocity in the upper layer (u) in meters per second and the layer thickness of the flow (h) in meters. These two parameters vary along the inner dike profile and depend on the overtopping volume (V) [m^3/m]. In the model, the flow velocity and layer thickness at the crest as a function of time (t) are used as inlet boundary conditions. The maximum flow velocity U_{max} (equation [13]) and maximum layer thickness h_{max} (equation [14]) at the crest can be determined through the empirical formulas

developed by van der Meer (Van Bergeijk et al., 2020). In the original wave overtopping model, equation [14] is used to calculate the maximum layer thickness h_{max} . However, in this study the maximum layer thickness is calculated using equation [22], presented in subsection 4.5.3., instead.

$$U_{max} = 5.00 V^{0.34} \quad [13] \qquad h_{max} = 0.133 V^{0.5} \quad [14]$$

The variation in the maximum flow velocity along the inner dike profile determines the location where erosion is most likely to occur (Van Bergeijk et al., 2020). Previous experiments have pointed out that the flow velocity and layer thickness increase quickly to the maximum value, whereafter a slower decrease to zero occurs as the wavefront passes. The time difference between the arrival of the wavefront and the decrease to zero of the flow velocity and layer thickness, is called the overtopping period (T_0). The overtopping period T_0 is expressed in seconds and also depends on the volume of the overtopping waves. T_0 can be calculated by the following empirical equation, which was also developed by Van der Meer in 2010:

$$T_0 = 4.4 V^{0.3} \quad [15]$$

The overtopping period, the maximum flow velocity and the maximum layer thickness can be used to describe the layer thickness and flow velocity as a function of time (t). This can be done using the following equations (Hughes et al., 2012):

$$h(x, t) = h_{max}(x) \left[1 - \frac{t}{T_0}\right]^a \qquad \text{for } 0 \leq t \leq T_0 \quad [16]$$

$$u(x, t) = U_{max}(x) \left[1 - \frac{t}{T_0}\right]^b \qquad \text{for } 0 \leq t \leq T_0 \quad [17]$$

From the equations can be noted that the maximum layer thickness (h_{max}) and the maximum flow velocity (U_{max}), which occur at the wavefront, both depend on the cross-dike coordinate x (Van Bergeijk et al., 2020). However, because these equations are only used at the dike crest, no cross-dike coordinate (x) is needed to determine the boundary conditions. The factor a in equation [16] and the factor b in equation [17], both describe the shape of the decreasing flow velocity and layer thickness over time. As the shape of the flow velocity and layer thickness is assumed to be triangular, the shape factors a and b both become equal to one ($a = b = 1$). Because the three empirical formulas of Van der Meer et al. (2010) (eq. [13], eq. [14] and eq. [15]) were based on overtopping volume measurements in the range of 0.2–5.5 m³/m, the OpenFOAM model also uses this wave range.

2.6.1.2. The original turbulence model

The developed numerical model also takes turbulence into account through the use of a turbulence model. The implemented turbulence model solves a two-phase Reynolds-averaged Navier–Stokes (RANS) equation using the finite volume method (Van Bergeijk et al., 2020). The term ‘two-phase’ refers to the fact that the overtopping flow consists of both gas and liquid. The (highly) turbulent wave overtopping entrains air, creating a two-phased flow. In equation [18], the Reynolds-averaged Navier–Stokes equation is presented, wherein ρ is the density and μ is viscosity.

$$\rho \bar{u}_j \frac{\partial \bar{u}_i}{\partial x_j} = \rho \bar{f}_i + \frac{\partial}{\partial x_j} \left[-\bar{p} \delta_{ij} + \mu \left(\frac{\partial \bar{u}_i}{\partial x_j} + \frac{\partial \bar{u}_j}{\partial x_i} \right) - \overline{\rho u'_i u'_j} \right] \quad [18]$$

In equation [18] can be noted that the u -terms (velocity), δ -term (Kronecker delta) and f -term (external forces), in both the i -direction and j -direction, are denoted in Reynolds-averaged terms ($u(x, t) = \bar{u}(x) + u'(x, t)$). The Reynolds decomposition divides the flow variables into a mean time-averaged component ($\bar{u}(x)$) and a component which fluctuates in time and space ($u'(x, t)$). This fluctuating

component in equation [18], represents the turbulence in the flow and is denoted at the right-hand side of the equation ($\rho \overline{u'_i u'_j}$). The OpenFOAM model uses the averaged values to calculate the fluctuation in time and space by solving the rearranged RANS equation:

$$\frac{\partial \rho \overline{u'_i u'_j}}{\partial x_j} = -\rho \bar{u}_j \frac{\partial \bar{u}_i}{\partial x_j} + \rho \bar{f}_i + \frac{\partial}{\partial x_j} \left[-\bar{p} \delta_{ij} + \mu \left(\frac{\partial \bar{u}_i}{\partial x_j} + \frac{\partial \bar{u}_j}{\partial x_i} \right) \right] \quad [19]$$

Along the slope, the simulated hydraulic load is determined by the turbulence and velocity of the overtopping wave close to the bed. To account for the effect of turbulence on the hydraulic forces, the RANS-based $k - \omega$ SST (Shear Stress Transport) turbulence model was incorporated into the OpenFOAM model. In appendix A, a detailed description is given of the RANS-based turbulence models and in section 1.1. of appendix A the $k - \omega$ SST turbulence model is described.

2.6.1.3. The original cover roughness

In the model, the roughness of the dike surface is implemented through the use of a dimensionless roughness constant (C_s) and the Nikuradse roughness height (k_s) in meters. The roughness constant (C_s) describes the shape and spacing of the roughness elements and can range from 1.0 to 0.5, wherein 1.0 indicates a strong non-uniform shape and spacing, and 0.5 represents an uniform shape and spacing. Because the roughness constant (C_s) can only describe both, the shape and spacing at the same time, the exact definition of each C_s value cannot always be tracked down. Therefore, multiple combinations in shape and spacing can be represented by the same roughness constant.

The Nikuradse roughness height (k_s) describes the height of these roughness elements, but can also be used to partly describe the shape of the roughness elements by using the average height of different roughness elements for k_s . During the calibration of the OpenFOAM model, the roughness constant (C_s) was set to 0.5, as is done in most CFD studies, while the Nikuradse roughness height (k_s) was set to 0.8 cm (Van Bergeijk et al., 2020). The roughness constant (C_s) and the Nikuradse roughness height (k_s) are adjusted within the turbulent eddy viscosity boundary condition, as explained in subsection 4.1.4., and can only capture the small irregularities on the grass cover. For larger irregularities on the grass cover, such as scour holes and bumps, the roughness needs to be resolved in the mesh. This means that roughness elements much larger than the grid size cannot be modelled with use of the roughness height (k_s), and therefore need to be resolved in the mesh itself. In this research these larger roughness elements will not be applied.

2.6.2. Model Output

The OpenFOAM model developed by Van Bergeijk et al. (2020) can numerically calculate high hydraulic loads along the dike profile, for loads that are caused by (1) high flow velocities at the front of the wave, (2) wave impact at slope angle or cover type transitions and (3) turbulence, which leads to high stresses. The OpenFOAM model is used to calculate the near bed velocity (u_*), pressure (p), shear stress (τ) and normal stress (σ) on the crest and landward slope of the dike.

The flow velocity and water fraction (α) are also calculated by the OpenFOAM model for every cell at every time step. Using the model output of the water fraction (α), the layer thickness is determined. The layer thickness is represented by the highest grid cell with a water fraction larger than 0.6. This means that when a grid cell is filled for more than 60% with water, it is assumed that the cell is completely filled with water. At the same time, it is assumed that grid cells with less than 60% water are empty, and thus holding no water at all.

3

| Study area

In this research, a numerical wave overtopping model has been used. In order to validate the performance of this numerical model, the simulated model output needs to be compared to field measurements, such as the flow velocity, water layer thickness and/or pressure. In addition, a measured dike profile is required to generate a more realistic numerical mesh.

From December 2020 to March 2021 destructive wave overtopping tests were performed in the Netherlands on grass covered slopes at sand dikes along the river Vecht. In these tests, the resistance of a grass cover against wave overtopping was analysed. The results of these tests are used to determine the critical flow velocity (U_c), which can be used in erosion models for grass covers on sand dikes. This is necessary, as the current empirical equations used to calculate the critical flow velocity are based on grass covers on clay dikes. However, these equations are not suitable for sand dikes, as grass covers on clay dikes are stronger.

At three test locations along the Vecht dike, wave overtopping tests were performed with different simulators. The performed research was part of the Hoogwaterbeschermingsprogramma (HWBP)¹.

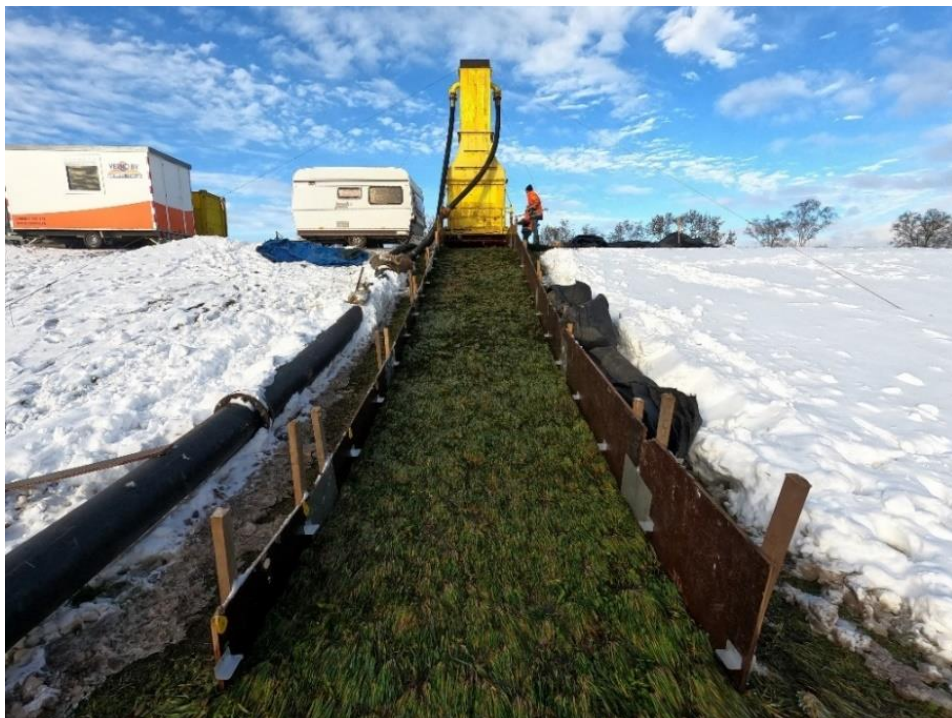


Figure 11 – The wave run-up simulator set-up for test section 2 at test location one at the Vecht dike. The wave run-up simulator was developed by Van der Meer Consulting B.V. and Infram. Note: reprinted from Mom et al. (2021)

¹ a flood protection program in the Netherlands

3.1. Performed wave overtopping tests

For this study the front velocities measured at test location 3 at the Vecht dike are used (Mom et al., 2021). This location was chosen, as the dike consists of a single cover type and slope angle. At this location three different test sections were used to perform the wave overtopping tests with the wave run-up simulator (Figure 11). The wave run-up simulator is used to mimic wave overtopping discharges in the field. This is done by filling the simulator reservoir and opening the butterfly valve, which is located at the bottom of the reservoir, to release the target fill height/volume. The fill height is defined beforehand and is used to operate the simulator, as this fill height corresponds to the target wave overtopping volume.

3.1.1. Simulated wave overtopping volumes

The wave overtopping tests were performed by applying an increasing wave overtopping discharge (Van der Meer, 2011). The stopping criterion of the experiments is reached when the top layer of the cover, which can have a thickness of 20 cm, fails.

The first wave overtopping discharges used are 1, 10, 30 and/or 60 l/s per meter. Only when the grass cover did not fail after a discharge of 60 l/s per meter, the discharges of 50, 100 and/or 190 l/s per meter were simulated. The volume and amount of simulated waves depend on the wave conditions, slope angle of the outer slope and the simulated storm duration. The following conditions were used:

Table 2 – The simulator conditions used to simulate wave overtopping (Mom et al., 2021)

	Discharges of 1-60 l/s per m	Discharges of 50-190 l/s per m
Significant wave height (H_s)	0.5 m	1.0 m
Peak period (T_p)	2.53 s	3.58 s
Wave slope (S_{0p})	0.05	0.05
Outer slope angle ($\cot \alpha$)	3.0	3.0
Storm duration	5 h	5 h

3.1.2. Front velocity field measurements

The front velocity of an overtopping wave is known to produce the fastest velocities, and therefore has the most impact on wave overtopping damage (Van der Meer et al., 2011; Bomers et al., 2018). In order to determine the front velocity, the overtopping wave was filmed from above to determine the position of the wave front along the dike profile using distance markers. These markers were located at every meter, along the sides of the test section, relative to the simulator outlet. After the experiments, the film was analysed frame-by-frame. The number of frames between the wave front moving from one to the next distance marker were counted and translated into a front velocity using the known capture frequency of the camera (60 Hz). The margin of error of this measuring method is approximately 0.5 m/s.

The original wave overtopping model developed by Van Bergeijk et al. (2020), was calibrated and validated using velocity (and pressure) measurements as a function of time. These velocity measurements were obtained using a paddle wheel that measures the flow velocity continuously, providing a depth-averaged velocity. The measurement method using the paddle wheel was replaced by the measurement method using the video camera, which is used to capture the front velocity. This was done, as the use of the camera is less disruptive and more user-friendly. This is because the paddle wheel needs to be buried, in order to measure the velocity at the dike surface, which could slightly alter the test results. Therefore, these measurements require the need of an additional test section. In addition, these paddle wheels can only be used at a few locations along the dike profile, resulting in

local velocity profiles, while the method using the camera can be used to capture the front velocity along the whole dike profile. Earlier research pointed out that both measurement methods provide the same range and behaviour of the front velocity (Van der Meer, 2021). Therefore, the less disruptive and more user-friendly, camera measurement method is more preferred and better suitable.

Note: Mom et al. (2021) points out that the simulated wave front does not represent a realistic wave front for the first 3 to 4 meters relative to the position of the simulator. This means that the front velocity for this part is not correctly simulated. It is unknown whether the front velocity in the first 3 to 4 meters is under- or overestimated.

3.2. The selected test section

For this research, test section 3-2 was selected out of the three sections at test location 3 (Mom et al., 2021). This test section was chosen due to the fact that all wave overtopping volumes (200 to 2500 l/m) have been measured without interruption, as the stopping criterion was not reached. Therefore, this test section provides a large range of measured front velocities, which can be used for the validation of the model.

In Figure 12, the measured dike profile (test section 3-2) has been visualised, which is used to generate the numerical mesh in the OpenFOAM model (section 4.2.). The dike profile has a height difference between the crest and toe of circa 3 meter. The length, measured per meter along the slope, is about 16 meters from the simulator outlet to the toe.

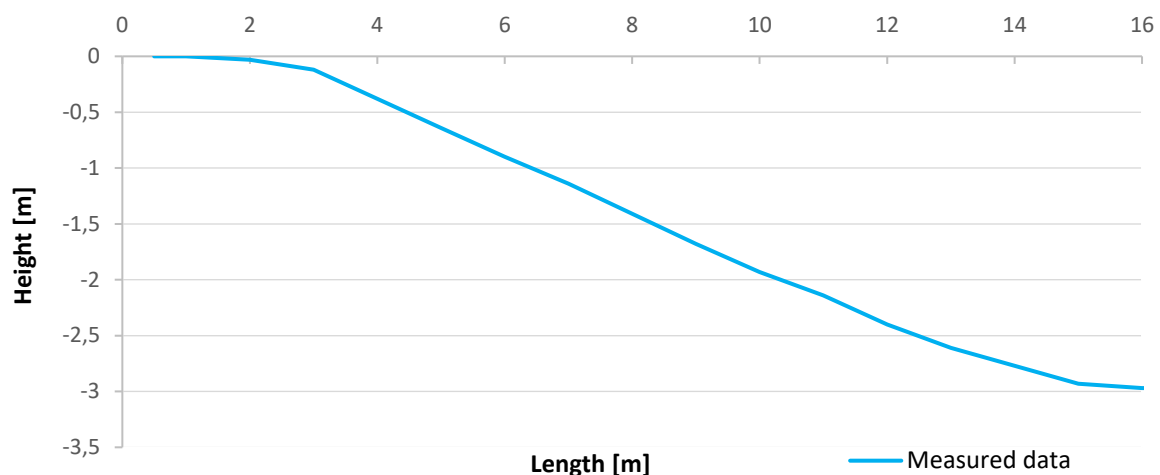


Figure 12 - The measured dike profile used in the OpenFOAM wave overtopping model. The inner crest is located from 0.5 to 2 meter and the toe is located from 15 to 16.5 meter. The dike has a height difference of circa 3 meters and length of 16 meters.

3.2.1. Experiment results

For the validation of the model, three of the seven simulated wave overtopping volumes have been modelled. During the validation, only the mean flow velocity, calculated using velocity measurements obtained during two separate experiments, was compared to the modelled velocity. Figure 13 presents the measured front velocities along the dike profile of the three selected wave overtopping volumes (500 l/m, 1500 l/m and 2500 l/m). The front velocity of each wave overtopping volume is measured at least twice during every wave overtopping test (GO190_1.0-A and GO190_1.0-B). Only for a wave overtopping volume of 500 l/m, four measurements were used, as this volume was simulated for both, the overtopping discharges of 50 and 190 l/s per meter (GO50_1.0 and G0190_1.0) (Mom et al., 2021). For the validation, the mean front velocity of the different test results are used., Figure 13 presents

the front velocities at every 0.5 meter relative to the crest, because the video camera measurement method represents the front velocity between two distance markers.

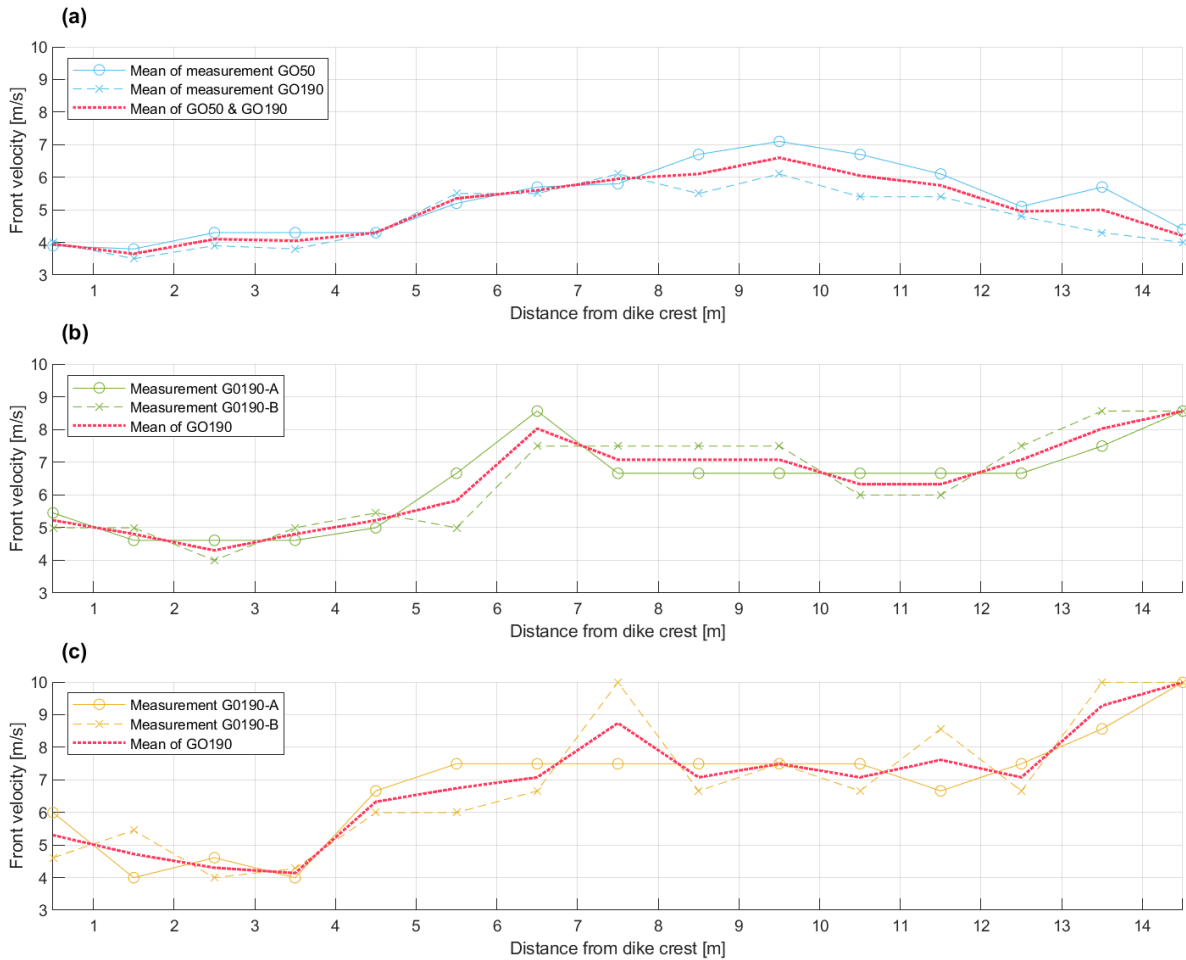


Figure 13 - Velocity measurements with the corresponding mean velocity along the dike profile for a volume of: (a) 500 l/m, (b) 1500 l/m and (c) 2500 l/m. GO50 and GO190(-X) refer to the simulated overtopping discharges of 50 and 190 l/s per m. For the volume of 500 l/m, the mean velocity consists of two mean velocities of other field measurements (GO50 and GO190). The crest starts at 0.5 m, the slope at 2 m and the toe at 15 m.

4

| CFD model set-up in OpenFOAM

The OpenFOAM model is capable of numerically calculating the wave impact of a single overtopping wave. However, in order to do this accurately, the model needs to be set-up correctly. In this chapter, first, the available turbulence models are analysed and re-evaluated to find the most suited turbulence model in OpenFOAM for this study. Afterwards, the model set-up, used in this research, is described.

4.1. Turbulence model

To study turbulence using a CFD model, it is important to select an appropriate turbulence model that can accurately simulate the turbulence in wave overtopping. The chosen turbulence model can greatly affect the quality of the results. Nowadays the most popular turbulence models used, are based on the Reynolds-Averaged Navier-Stokes (RANS), Large Eddy Simulation (LES), Direct Eddy Simulation (DES) or Direct Numerical Simulation (DNS) (OpenCFD, 2016; Nikolaidou, 2019). These models have different limitations and can solve turbulence in the overtopping flow using different input parameters and calculation processes. In appendix A, a detailed description is given on what RANS-based, LES-based, DES-based and DNS-based turbulence models are.

The most appropriate turbulence model can be selected by weighting the pros and cons up against one another and by comparing the accuracy of the model output with the accuracy needed for the specific research. In OpenFOAM, only RANS-based, LES-based and DES-based models are available (OpenCFD, 2016). It is possible to adjust the available turbulence models or develop a 'new' turbulence model. However, changing or creating turbulence models takes up much time in terms of developing and testing. Therefore, only the available turbulence models are evaluated during the selection. In appendix B, an overview of the limitations for each turbulence model type is given.

4.1.1. The selected turbulence model

The current wave overtopping problem can best be analysed using a RANS-based turbulence model. The RANS-based model is the most suitable turbulence model for this case due to the accuracy of the output, the small calibration and computational time needed and the low complexity of the model set-up. Although the RANS-based model can only present time averaged turbulence quantities, a more accurate estimation of small scale turbulent processes in the boundary layer is less useful for this study. This is because verification of the more detailed turbulence processes is currently not possible, as no turbulence data is available to verify specific processes near the bed. In addition, the relative turbulence intensity (r_0) describes the wave overtopping turbulence over the full water depth (subsection 2.5.3.). Therefore, an averaged turbulence output would be sufficient for this study.

For this research, the least suitable turbulence model from the three possible models would be the LES-based, as this model type would need the most computational time and requires a lot of computer capacity to overcome its limitations, which makes the implementation still very challenging. More accurate turbulence models can be implemented to capture small length scale vortices (eddy scale) in the overtopping flow without time-averaging when the processes of wave overtopping turbulence are better understood, (more) turbulence measurement data is available or when near-bed turbulence processes are of interest. Figure 14 presents the difference between a RANS-based and LES-based turbulence model simulation. From the figure can be noted how the turbulence predictions are time-averaged for the RANS-based model, while the LES-based model estimates each eddy in the system throughout time.

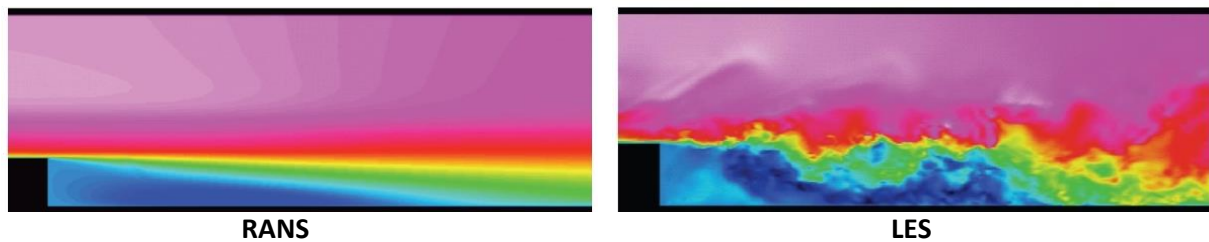


Figure 14 - Comparison between a RANS-based and LES-based turbulence model simulation. Note: reprinted from Estrado (2019)

From the different RANS-based turbulence models, the $k - \omega$ shear stress transport ($k - \omega$ SST) turbulence model is the most suitable for wave overtopping modelling. The $k - \omega$ SST is the most suitable model, because it can accurately resolve the turbulence in both the near-wall region and the freestream (Liu, 2017; Nikolaidou, 2019). This means that the same turbulence model, as incorporated in OpenFOAM by Van Bergeijk et al. (2020), can be used for this research. The $k - \omega$ SST turbulence model switches between the $k - \epsilon$ ($k - \epsilon$) turbulence model, which is more suitable to study turbulence in the free-stream region, and the $k - \omega$ turbulence model near the wall, which is more accurate near boundary layers. The model makes use of the turbulent kinetic energy (k), the turbulent dissipation rate (ϵ) and the specific turbulent dissipation rate (ω) to predict the effects of turbulence. In section 1.1. of appendix A, a more detailed description, with the corresponding equations, of the $k - \omega$ SST turbulence model is presented.

4.1.2. The turbulent kinetic energy

The symbol k represents the turbulence kinetic energy or TKE in m^2/s^2 and is used in both the $k - \epsilon$ and $k - \omega$ equations. This parameter represents the amount of turbulence in the flow, as it represents the available energy in the largest eddies, which carry the most energy. In the OpenFOAM model, the TKE is used as a wall function along the dike profile, which is used to provide a zero-gradient condition for the volume field flow. Without the implementation of this 'boundary condition', the volume field would likely have a gradient. In OpenFOAM the turbulent kinetic energy is implemented through the use of the $kqRWallFunction$ (OpenCFD, 2016; Liu, 2017). In addition, this wall function has an initial intensity value of $0.05 \text{ m}^2/\text{s}^2$ at the inlet of the domain (subsection 4.5.1.).

4.1.3. The specific turbulent dissipation

The symbol ω represents the specific turbulent dissipation in s^{-1} . This parameter is used in the $k - \omega$ equations and can also be used to calculate the turbulent dissipation rate (ϵ). This parameter describes the amount of TKE that dissipates and switches between two equations to solve omega depending on the cell distance from the wall. In OpenFOAM, the omega is also implemented as a type of boundary condition to provide a wall constraint through the use of the $\omega WallFunction$. This wall function is needed in RANS-based models to solve the dissipation rates in the near-wall region using the log-law theory (OpenCFD, 2016; Liu, 2017).

4.1.4. The kinematic turbulent viscosity

The term 'Nut' is used to express the kinematic turbulent viscosity (ν_t) in m^2/s . The kinematic turbulent viscosity is a very important parameter within the turbulence model, as it influences the onset of turbulence within the flow. In the OpenFOAM model, the turbulent eddy viscosity is also used as a type of boundary condition along the dike profile and used to constrain the turbulence at the wall. Due to the way the turbulent eddy viscosity is incorporated, the parameter functions as a type of wall function in the turbulence model. This wall function will give more realistic estimates of the near wall processes, as it will switch between different equations depending on the cell distance from the wall. In OpenFOAM, the turbulent eddy viscosity is implemented through the use of the *nutRoughWallFunction* (OpenCFD, 2016; Liu, 2017). This wall function uses a roughness height (k_s) and roughness constant (C_s), which are used to define the roughness of the surface of the dike profile (subsubsection 2.6.1.3.) to solve the viscosity near the wall.

4.2. Numerical mesh

The domain that is generated contains the surface of the dike crest, slope and toe and a part of the atmosphere above the dike. Apart from the bed surface, the ground underneath the dike was not simulated, as this was not needed to simulate the wave impact. To realise the detailed mesh, first, a simplified mesh was generated. This simplified mesh had a cell length (x-direction) of 2 centimetres, a height (y-direction) of 1.5 centimetres and a width (z-direction) of 20 centimetres. The simplified mesh had a height of 2.50 meters and a length of 16 meters, creating a total of 82500 cells in the domain.

After generating the simplified mesh, the *SnappyHexMesh*-tool was used to accurately 'cut-out' the measured dike profile from the simplified mesh, giving the mesh the same dimensions as the dike profile presented in section 3.2.. To create a smooth dike surface, the number of cells in the domain and the angle of some cells have been adjusted. In addition, the cells in the near-wall region are split in layers to increase the accuracy of the near-bed turbulence solutions. The resulting mesh has six layers near the wall, giving a near-wall thickness of 0.0054 meter with an overall cell thickness in the boundary layer of 0.032 meter. In the mesh, the cells at the bed are the smallest and increase in size further from the bed. Figure 15 presents the generated numerical mesh of the measured dike profile.

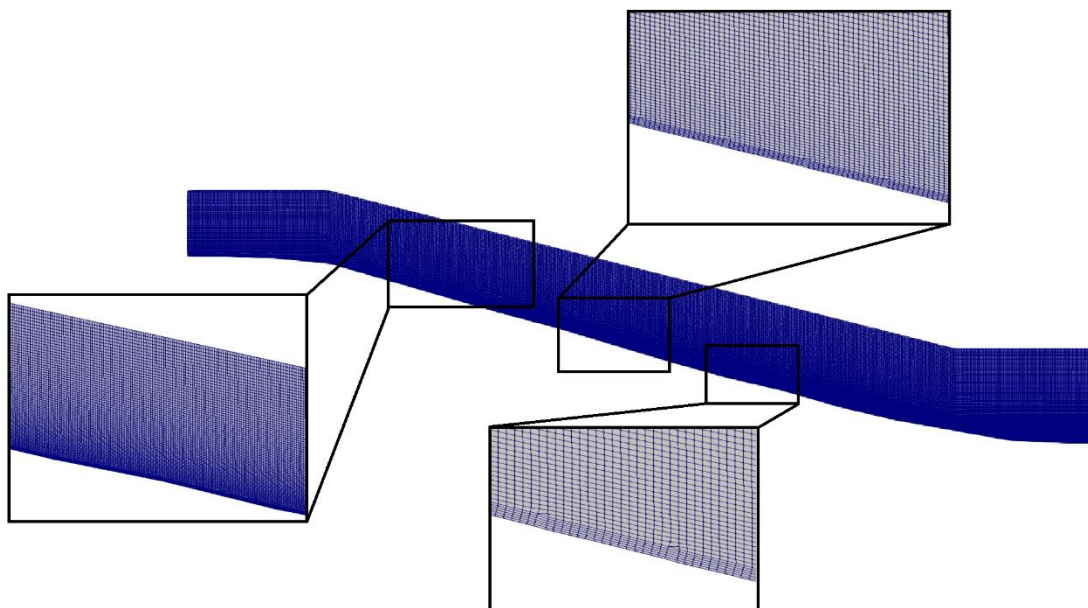


Figure 15 - The numerical mesh of the Vecht dike generated in OpenFOAM. The grid uses the measured dike profile with a grid size in the cross-dike direction (Δx) of 2 cm and in the vertical direction (Δz) of 0.54 cm for the bottom layer and 1.5 cm for the top layer.

4.3. Time settings

In the OpenFOAM model, time settings need to be assigned to specify the model scenario. These time settings can provide different output sizes and may influence the data quality. In the model, it is possible to use a different time step for the calculations and to sample the model output. This is because the accuracy necessary to solve the flow equations is not always needed for the output data. By appointing different the time steps for solving and sampling, the total run time can be reduced.

During this research, the start time in the model was always set to 0 seconds and the end time to 30 seconds, as this is the duration that captures the complete wave overtopping process for all wave overtopping volumes. To accurately solve the high velocity fluctuations and turbulence in the flow, the numerical time step used to solve the flow was set to 0.001 seconds. In the model, an option was enabled that allows the model to slightly adjust this numerical time step of 0.001 seconds in order to coincide with the write interval for the data sampling mentioned in section 5.1.

4.4. Constants

To accurately solve the two phased flow, some constants are needed. In the OpenFOAM model, these constants describe the transport properties of the water and air in the system and are used as input values within the different solvers. In Table 3, an overview of these constants is given. In addition, the gravitational acceleration is set to 9.81 m/s^2 in OpenFOAM. The presented constants are used in every OpenFOAM run and are not changed throughout this study.

Table 3 - An overview of the transport properties within the OpenFOAM model.

Parameter	Density (ρ) [kg/m^3]	Viscosity (ν) [m^2/s]	Friction coefficient (σ) [kg/s^2]
Water	1000	1.00E-06	0.07
Air	1.00	1.48E-05	

4.5. Initial and boundary conditions

Numerical models need initial and boundary conditions to solve simulated problems. These initial conditions are used as start values, while the boundary conditions are used as limitations. The model uses both conditions to solve the unknown parameters. In the wave overtopping model the initial and boundary conditions are used to describe the flow processes at the inlet and are mainly related to the velocity and the water layer thickness. When the model over- or underestimates the front velocities along the dike profile, the velocity simulated by the model can be improved by adjusting the boundary conditions. In the subsections below, the used initial and boundary conditions are presented.

4.5.1. Initial turbulence

Within the selected turbulence model, an initial condition for the TKE (k) is needed (subsection 4.1.2). In the original model an initial intensity value of $0.05 \text{ m}^2/\text{s}^2$ at the inlet of the domain is applied (Van Bergeijk et al., 2020). This value is left unchanged in this study. However, the sensitivity of the modelled wave overtopping turbulence towards this initial intensity has not been not analysed.

4.5.2. Velocity

In OpenFOAM, the symbol U is used to represent the velocity in m/s . The velocity is calculated along the dike profile throughout time and is used to solve other parameters, such as the TKE and pressure. In the wave overtopping model, the maximum flow velocity (U_{max}) determines the velocity at the entrance of the simulation and is calculated using an empirical equation, and thereby functioning as a type of boundary condition for the velocity. The highest velocities are simulated at the beginning of

the overtopping wave and the lowest velocities are simulated at the end of the overtopping period, as the velocity will decrease over time. Table 4 presents the maximum velocities calculated with equation [13] and the front velocities, measured at the crest of the selected test section, for all simulated wave overtopping volumes during the field experiments (section 3.2.). The wave overtopping volumes of 500, 1500 and 2500 l/m are highlighted in green, as these volumes were used for the validation of the model in chapter 6.

Table 4 - Overview of the calculated velocity using equation [13] and the front velocity measured at the crest of test section 3-2 for each performed wave overtopping volume (selected test section). The volumes 2.5, 1.5 and 0.5 m³/m have been highlighted in green, because these volumes are simulated. In the last column, the difference between the velocities is presented by subtracting the calculated from the measured velocity (measured-calculated).

Volume [l/m]	Calculated velocity [m/s]	Measured velocity [m/s]	Difference [m/s]	Difference [%]
200	2.78	3.90	1.12	33.5
400	3.42	5.20	1.78	41.3
500	3.66	3.95	0.29	7.6
1000	4.50	4.55	0.05	1.1
1500	5.08	5.20	0.12	2.3
2000	5.54	5.50	-0.04	0.7
2250	5.74	5.50	-0.24	4.3
2500	5.92	5.30	-0.62	11.1

From the table above, can be noted that the calculated velocities underestimate the flow velocity at lower volumes (< ± 1500 l/m) and overestimate the flow velocity at higher volumes (± 1500 l/m >). Furthermore, these calculated velocities present a more linear trend, while the measured flow velocities is more scattered. The reason for these scattered measured flow velocities could be caused by the incorrect simulation of the wave front for the first 3 to 4 meters, which could result in over- or underestimation of the front velocities (subsection 3.1.2.).

In this research, the boundary condition for the velocity is implemented using the same equation for the maximum flow velocity (U_{max}), as was used in the original model (equation [13]). The calculated velocities are used, instead of the measured front velocities, due to the larger range of applicable wave overtopping volumes. This is done, as the model would not limited to the wave overtopping volumes performed during the field experiments. In addition, the calculated velocities present a clear linear trend, which may give a better representation of the modelled wave overtopping volumes.

4.5.3. Water layer thickness

In OpenFOAM, alpha water [-] is used to calculate the water layer thickness (h) [m] and uses the symbol α . Alpha water describes the amount of water present in each cell in the domain throughout time. During the simulation, the amount of water in each cell is solved by the model. The amount of cells filled with water in the y-direction will eventually be used to determine the water layer thickness. As wave overtopping flow is highly turbulent, a lot of air can be entrained by the flow. To simulate this entrainment, while limiting the run-up time needed for the model to simulate this water-air mixing, an inlet condition is given to the alpha water parameter. This inlet condition will change the water and air ratio of the inflowing water from a 100% water to a ratio of 80% water and 20% air, as was introduced by Van Bergeijk et al. (2022) as an improvement of the original model. In addition to the water-air ratio, the model also uses a boundary condition to limit alpha water at the inlet. This boundary condition describes the maximum water layer thickness at the start of the domain to limit the layer thickness of the incoming wave. The assigned water layer thickness [m] is converted to an alpha water

[-] per cell within the model. This maximum layer thickness will decrease over time, as can be noted from equation [16] in subsection 2.6.1.1., just as the boundary condition for the velocity.

In the original model, the maximum water layer thickness (h_{max}) is calculated using equation [14]. However, when this equation is used, the wave overtopping volume of the boundary conditions ($\sum_0^{T_0} h(T_0) \cdot u(T_0)$) do not correspond to the target volumes for the simulation. To correct the simulated volume at the inlet, the maximum water layer thickness (h_{max}) is adjusted by replacing equation [14] with an equation that incorporates more parameters than the wave overtopping volume alone. It is not possible to use field measurements to adjust the maximum water layer thickness, as the water layer thickness was not measured during the field experiments (subsection 3.1.2.). The new equation for the h_{max} can be obtained by combining equation [20], used to calculate the overtopping volume in m^3/m , and equation [21], used to calculate the overtopping discharge in m^3/s (Hughes et al., 2012).

$$V = \int_0^{T_0} q(t) dt \quad [20] \quad q(t) = h_{max} U_{max} \left[1 - \frac{t}{T_0} \right]^m \quad [21] \quad h_{max} = \frac{V(m+1)}{U_{max} T_0} \quad [22]$$

In equation [22], the maximum layer thickness is calculated with help of the maximum flow velocity (U_{max}), the wave overtopping volume (V) and the overtopping period (T_0), which can be obtained with equation [15]. The constant m [-] in equation [22] can be calculated by summing up the constants a and b ($a + b$), as stated in subsection 2.6.1.1. Since $a = b = 1$, the constant m has a value of 2. In Table 5, the outcome and difference between the original and adjusted h_{max} can be observed for the volumes 500, 1500 and 2500 l/m, as these volumes have been compared in the validation phase.

Table 5 – The maximum water layer thickness calculated with the original and adjusted equation for the volumes 2.5, 1.5 and 0.5 m^3/m . In the last column, the difference between the maximum water layer thickness is presented by subtracting the original outcome from the adjusted outcome (adjusted-original).

Volume [l/m]	Original h_{max} [m]	Adjusted h_{max} [m]	Difference [m]	Difference [%]
500	0.094	0.145	0.051	42.7
1500	0.163	0.189	0.026	14.8
2500	0.210	0.213	0.003	1.4

Table 5 shows that the adjusted equation provides higher results for the maximum layer thickness than the original equation. The original equation seems to underestimate the h_{max} more for the lower wave overtopping volumes than for the larger volumes. This decreasing difference for an increasing volume could indicate that the original equation could start overestimating the h_{max} at volumes larger than 2500 l/m. This is, however, not analysed in this research.

In this research, the boundary condition for the water layer thickness is implemented using the adjusted equation for the maximum water layer thickness (h_{max}) (equation [22]). The adjusted equation for h_{max} is used, instead of the original equation, as this results in wave overtopping volumes equal to the target volumes. In addition, it was observed that this adjusted equation can correct the volume balance for any combination of U_{max} , V and T_0 , as the equation is interconnected with these parameters.

4.6. Model calibration and validation

During the development of the OpenFOAM model by Van Bergeijk et al. (2020), the model was calibrated by adjusting the roughness height (k_s). In later studies performed by Van Bergeijk et al. (2021), the model proved to be applicable for other wave overtopping scenarios and dike profiles than

the ones used during the development of the model. Therefore, Van Bergeijk et al. (2021) stated that the wave overtopping model does not need to be re-calibrated when a new dike profile is used to simulate. However, the model still needs to be validated to ensure that the model correctly mimics the wave overtopping discharge and velocities. For this reason, the model is not re-calibrated and the original value of 0.008 meters will be used for the roughness height (k_s) in the volume scenarios that are mentioned in subsection 4.7.1..

To obtain a better validation of the wave overtopping model, an adjustment was made to the boundary condition of the original model. The adjusted boundary condition of the water layer thickness, implemented for this research, is presented in subsection 4.5.3.. It is assumed that the vertical flow structure is solved correctly by the current OpenFOAM model, as the performance of the boundary layer was validated for the original model set-up, and as this was also not re-validated in later studies performed with this numerical model (Van Bergeijk et al., 2020, 2021, 2022). The velocity predictions of the validated model are presented in chapter 6.

4.7. Scenarios for the sensitivity analysis

After the model validation, the wave overtopping volume and bed roughness scenarios can be simulated in OpenFOAM. These scenarios were used to analyse the sensitivity of wave overtopping turbulence towards the wave overtopping volume and bed roughness and are used to explore how these characteristics influence the location where turbulence is produced during wave overtopping. This will provide more insights on the processes involved in wave overtopping turbulence and can provide a better understanding of the locations where turbulence can best be measured during field experiments. In section 5.3. is described which turbulence parameters will be sampled and how these turbulence parameters will be compared. In chapter 7, the results of the mentioned sensitivity scenarios are presented.

4.7.1. Volume scenarios

Seven scenarios for the wave overtopping volume were simulated to analyse the sensitivity of wave overtopping turbulence towards volume (V) changes. All other conditions remained unchanged in these scenarios. For each wave overtopping volume, a different set of boundary conditions was generated, using equation [22] for the maximum water layer thickness (h_{max}), equation [13] for the maximum flow velocity (U_{max}) and equation [15] for the wave overtopping period (T_0). The variation in maximum water layer thickness and flow velocity during this overtopping period can be calculated using equation [16] and equation [17]. Table 6 presents the seven volume scenarios with the corresponding boundary conditions.

Table 6 – Overview of the wave overtopping volumes used for the sensitivity analysis of wave overtopping turbulence. In the last column, the maximum layer thickness (h_{max}), maximum velocity (U_{max}) and overtopping period (T_0) corresponding to each volumes are given. The green rows represent the volumes that have been used for the validation.

Volume [l/m]	Roughness constant (C_s) [-]	Roughness height (k_s) [cm]	h_{max} [m]	U_{max} [m/s]	T_0 [s]
500	0.5	0.8	0.145	3.66	2.84
1000	0.5	0.8	0.171	4.50	3.90
1500	0.5	0.8	0.188	5.08	4.70
2500	0.5	0.8	0.213	5.92	5.94
3000	0.5	0.8	0.223	6.26	6.46
3500	0.5	0.8	0.231	6.55	6.94
5000	0.5	0.8	0.252	7.29	8.18

The volumes that are simulated for these scenarios were selected to observe the sensitivity for overtopping volumes that are more likely to occur at sand dikes. In the Netherlands, sand dikes have only been constructed along rivers with relatively small wave overtopping probabilities, such as the Vecht river. For this reason, wave overtopping volumes larger than 3500 l/m have a very small probability of occurrence and are, therefore of less interest for this study. However, to observe whether trends and behaviour in turbulence changes for higher volumes, a volume of 5000 l/m was also analysed. The lowest volume that was simulated is a volume of 500 l/m. In most cases volumes lower than 500 l/m do not cause wave overtopping damage, as the maximum velocity and layer thickness significantly decrease for these volumes. Therefore, lower volumes are not of interest in this research.

4.7.2. Roughness scenarios

The sensitivity of wave overtopping turbulence towards the bed roughness was analysed by comparing four different roughness scenarios for a wave overtopping volume of 1000 l/m. All other conditions remained unchanged. The wave overtopping volume of 1000 l/m was simulated for these scenarios, as this is a high, but realistic, wave overtopping volume for the Vecht dike and is the mean simulated volume simulated during the field experiments.

In the model, the bed roughness is implemented through the use of a roughness constant (C_s), which represents the shape and spacing of the roughness elements, and the Nikuradse roughness height (k_s), which represents the height of these roughness elements. The Nikuradse roughness height (k_s) can also be used to partly describe the shape of the roughness elements by using the average height of the different roughness elements for k_s . Due to the definition of these two roughness parameters, the roughness constant (C_s) is set to 0.5, representing an uniform shape and spacing of the grass cover, as is done in most CFD studies, while the roughness height (k_s) is changed to represent different heights of the grass cover. This roughness height is noted in meters within the model. In subsection 2.6.1.3. more details on the implementation of these two roughness parameters is given.

Table 7 presents the four different roughness scenarios with the corresponding boundary conditions, noted in the last three columns. During the selection of the roughness heights for these roughness scenarios, it was assumed that the reference roughness height (0.8 cm) represents a rough dike cover. For this reason, the other roughness heights were selected in order to represent a nearly smooth (0.008 cm), a mildly rough (0.08 cm) and a very rough (4 cm) dike cover.

Table 7 - Overview of the roughness settings that were applied in the OpenFOAM model, to analyse the sensitivity of wave overtopping turbulence. In the last column, the maximum layer thickness (h_{max}), maximum velocity (U_{max}) and overtopping period (T_0) are given. The green row represents the roughness settings that have been used for the volume scenarios.

Volume [l/m]	Roughness constant (C_s) [-]	Roughness height (k_s) [cm]	h_{max} [m]	U_{max} [m/s]	T_0 [s]
1000	0.5	4.0	0.171	4.50	3.90
	0.5	0.8			
	0.5	0.08			
	0.5	0.008			

Before the roughness height of 4.0 cm was selected, the model predictions were analysed for three different roughness heights (4.0, 8.0 and 10.0 cm). This was done, to check whether the roughness height is not oversized compared to the cell sizes near the wall, as oversizing will cause the model to incorrectly schematise the roughness. It was found that the model predictions for the roughness heights of 8.0 cm and 10 cm present questionably high turbulence results, especially at the crest of the dike. However, the overall results seemed more reliable when the results for a roughness height of 4.0

cm are compared with the results for a roughness height of 0.8 cm. Only the magnitude of the turbulence results are (significantly) increased, while the overall behaviour along the dike profile remained relatively equal and only presented slightly more and much higher peaks. Therefore, the roughness height of 4.0 cm was selected to represent a very rough dike cover.

Using equation [23], each roughness height is translated into a Manning coefficient. The resulting n -values range from 0.0121 to 0.023 [-], which are in range of the Manning coefficient for grass covers (Arcement & Schneider, 1989).

$$n = 0.04k_s^{1/6} \quad [23]$$

Nevertheless, the use of a roughness height of 4.0 cm is still questioned during this research, as this roughness height is likely to be a misrepresentation of natural grass covers, as the grass cover will eventually be pressed onto the surface by the pressure of the overtopping wave. Therefore, the actual grass length and roughness height will be decreased. In addition, there is still a chance that the model incorrectly schematises this roughness height.

4.7.3. Combination scenarios

To analyse whether the observed trends in wave overtopping turbulence towards the previously mentioned scenarios (Table 6 and Table 7) also apply to other scenarios, the combination of both scenarios is analysed. For this combination scenario, the same four roughness heights (k_s) are applied as used for the roughness scenarios. Each roughness height will be applied to four different wave overtopping volumes, resulting in a total of sixteen scenarios. Table 8 presents the sixteen different scenarios with the corresponding boundary conditions, noted in the last three columns.

Table 8 - Overview of the volume and roughness settings used to analyse the sensitivity of wave overtopping turbulence. In the last column, the maximum layer thickness (h_{max}), maximum velocity (U_{max}) and overtopping period (T_0) are given. The green rows represent the volume and roughness settings were also used for the volume scenarios and roughness scenarios.

Volume [l/m]	Roughness constant (C_s) [-]	Roughness height (k_s) [cm]	h_{max} [m]	U_{max} [m/s]	T_0 [s]
500	0.5	4.0	0.145	3.66	2.84
	0.5	0.8			
	0.5	0.08			
	0.5	0.008			
1000	0.5	4.0	0.171	4.50	3.90
	0.5	0.8			
	0.5	0.08			
	0.5	0.008			
2500	0.5	4.0	0.213	5.92	5.94
	0.5	0.8			
	0.5	0.08			
	0.5	0.008			
3000	0.5	4.0	0.223	6.26	6.46
	0.5	0.8			
	0.5	0.08			
	0.5	0.008			

5

| Data processing

When a model simulation has been performed, the model output needs to be post processed to obtain a compact and ready-to-use version of the relevant data. Part of the post processing is already executed within the OpenFOAM model, however, post processing is finalised using a MATLAB script, specially created by Van Bergeijk et al. (2020), to post process the data output of this wave overtopping model. In this chapter, the sampling and processing of the relevant model output is explained.

5.1. Data sampling

In this research, the velocity (u), the water fraction (α) and the turbulent kinetic energy (k) from the model simulations were sampled. The sample time (Δt) for all these parameters was set to 0.1 seconds. This time step is more appropriate than the numerical time step of 0.001 seconds, because the data will eventually be averaged in time during the postprocessing. The sample distance (Δx) was set to 0.05 meter in order to closely observe the changes along the dike profile. Due to the large fluctuations that the turbulent flow can present, the sample time and sample distance were set to a relative small values. These sampling settings will provide enough data to observe the front velocity and can present the sensitivity of turbulence more accurately along the dike and over time.

5.2. Overtopping front velocity and maximum velocity

During this research, the front velocity was obtained in order to validate the model. The front velocity is the term used to describe the velocities present in the front of the overtopping wave. These front velocities are assumed to have a large contribution to wave overtopping damage, due to the highest overtopping velocities being produced by the wave front, resulting in more wave overtopping turbulence (Van der Meer et al., 2011; Bomers et al., 2018). From the model output, the surface velocity of the wave front is used instead of the depth-averaged velocity. This is because the method used for the field measurements also only takes the top layer of the wave front into account (subsection 3.1.2.). By obtaining the front velocity in a similar way, the velocities are more likely to match during the validation. The front velocity for each location was collected by selecting the first velocity that occurs in time at any point along the dike slope. This method assumes that the measured front velocity corresponds with the first computed velocity at each location. This means that, the velocity that occurs when the wave front enters each sample distance ($\Delta x = 0.05$ m) is used as the front velocity. This sample method is used to obtain a single velocity for each location. The water surface velocity throughout time was not used, because the velocity as function of time (u_t) was not measured during the field experiments at the Vecht dike (subsection 3.1.2).

In theory the highest velocities are produced at the front of the wave. However, this does not directly imply that the highest velocity occurs at the first moment in time that water enters a location. In the model, it is possible that the maximum velocity, caused by the wave front, occurs at a later time step for some locations along the dike. This means that the highest velocity, which is associated with the front velocity, could occur milliseconds after the wave front passes in the model. By analysing both the

front velocity and the maximum velocity, more certainty on the model performance can be obtained. Although no measurements have been performed to obtain the actual maximum velocity, it is assumable that these maximum velocities should be either in the same range or larger than the front velocities. For this reason, the maximum velocity is also used to validate the model, as it is much harder to validate the model solely using this sampling method. The maximum velocity is collected by selecting the highest velocity over time for each location. If the front velocity is underestimated, this could imply that either the sample method for the front velocity is inappropriate or that the model predicts a different velocity profile than in reality occurs. If both, the front velocities and maximum velocities, are underestimated, the model will also underestimate the output. However, it is still likely that the model presents correct turbulence predictions.

5.3. Modelled wave overtopping turbulence

During this research, the turbulent kinetic energy or TKE (k) output is used to quantify the variability of turbulence. The TKE is used, because this parameter is a measure of the turbulence intensity in all dimensions and determines the dissipation rates, pressure fluctuations and shear stresses in the flow (Stull, 1988). When, for example, less kinetic energy is present, the largest eddies will become smaller and, thus decreasing the amount of energy that can dissipate. This results in a lower amount of vortices being dissipated into smaller vortices, causing less shear stresses and pressure fluctuations to occur. This means that other important wave overtopping (load) parameters are largely related to the amount of available TKE. Furthermore, additional turbulence can be generated when these load parameters increase. Therefore, the TKE gives a good impression of how much turbulence is present in the flow.

To analyse the turbulence intensities within wave overtopping, the modelled TKE at any cell in the mesh (k) was used to calculate a depth-averaged TKE (k_0) for each position on the profile (every 0.05 m). The depth-averaged TKE was calculated with equation [24] in m^2/s^2 , wherein the symbol $k_{x,z}$ represents the TKE at a cell in the mesh, $h_{x,z}$ represents the cell height of this cell and h_x represents the total water layer thickness. Using this equation the depth-averaged TKE for each location and time step can be obtained.

$$k_0(x) = \frac{\sum_{z=0}^h k_{x,z} h_{x,z}}{h_x} \quad [24]$$

In this research, the turbulence maxima were analysed in order to explore the magnitude of the TKE peak values and the locations at which these peaks occur. During this research, the following depth-averaged TKE maxima were used to analyse wave overtopping turbulence for each scenario.

- 1) The maximum TKE
 - Represents the maximum value and location of the highest depth-averaged TKE.
- 2) The maximum significant TKE
 - Represents the maximum value and location of the averaged 33% highest depth-averaged TKE.
- 3) The maximum mean TKE
 - Represents the maximum value and location of the mean depth-averaged TKE.

The significant depth-averaged TKE represents the mean of the highest 33% of the TKE per position along the dike profile. The significant TKE is used in addition to the maximum TKE, due to the fact that the maximum TKE could be a short and incidental peak in turbulence. These short and incidental peaks are generally less likely to cause wave overtopping damage than when the TKE reaches this significant value for a longer period of time. However, as the maximum TKE can still give much insights on the range of turbulence and the behaviour of these large and spontaneous peaks, both values will be observed.

5.4. Empirical relative turbulence intensity

After the sensitivity of the wave overtopping turbulence has been analysed with the OpenFOAM model, the sensitivity of the relative depth-averaged turbulence intensity (r_0) is analysed. This is done by calculating r_0 , using the modelled depth-averaged TKE (k_0) and other modelled parameters for two different approaches presented in equation [8] and by comparing the resulting trends of these relative turbulence intensity calculations. For these r_0 calculations, the data, obtained during the sensitivity analysis for the combination scenarios, is used (subsection 4.7.3.).

Both the turbulence parameter (r_0) and the modelled TKE (k_0) represent the depth-averaged turbulent (intensity) in all dimensions (u', v', w') of the flow (Hoffmans, 1993; Schiereck, 2001; Hoffmans, 2012). Therefore, the modelled depth-averaged TKE can be used to directly calculate the relative turbulence, by using the first notation in equation [8] (subsection 2.5.3.). In the first notation, the depth-averaged flow velocity (U_0) and the depth-averaged turbulent kinetic energy (k_0) are used. In this equation, the mean depth-averaged TKE ($\overline{k_0}$) is applied for k_0 and the mean depth-averaged velocity in the longitude direction (\overline{u}) along the profile is applied for U_0 . The depth-averaged flow velocity (U_0) is calculated using equation [25], wherein $u_{x,z}$ represents the velocity at a cell in the mesh, $h_{x,z}$ represents the cell height and h_x represents the total water layer thickness. The relative depth-averaged turbulence (r_0) is first calculated for each position along the profile and then averaged to obtain a single r_0 value for each wave overtopping scenario.

$$U_0(x) = \frac{\sum_{z=0}^h u_{x,z} h_{x,z}}{h_x} \quad [25]$$

The other approach, presented in the last notation of equation [8] (subsection 2.5.3.), is a less time excessive method, used to calculate the relative depth-averaged turbulence intensity. This is because, the input does not necessarily require complex modelling or field measurements. In the last notation, the Chézy coefficient (C) of each wave overtopping scenario is calculated using equation [12] (subsection 2.5.3). In this equation, the hydraulic radius (R_h) can be replaced with the water layer thickness (h) and the particle diameter ($2d$) can be replaced by the roughness height (k_s). These adjustments results in equation [26], which is also called the White-Colebrook relationship for hydraulic rough walls.

$$C = 18 \log_{10} \left(\frac{12h}{k_s} \right) \quad [26]$$

To use equation [26], the dike surface needs to be hydraulically rough (2.2.1.). Generally, wave overtopping arrives highly turbulent at the dike crest, and covers a relatively larger width of the dike section during an overtopping events. Therefore, it is assumed that both conditions ($k_s > \delta_v$ and $width \gg depth$) mentioned in section 2.2.1. apply for the performed sensitivity scenarios. In equation [26], the average water layer thickness (\overline{h}) of each sensitivity scenario is used, as the water layer thickness (h) was not measured during the field experiments.

6

| Model validation

To validate the OpenFOAM model, the simulated velocities are compared to the front velocities measured during the field experiments. The model is valid when the front velocities and the maximum velocities of the model are in range and/or show trends similar to the field measurements. In the new model set-up, the maximum water layer thickness (h_{max}) is adjusted, as stated in subsection 4.5.3.. Figure 16 presents the simulated front and maximum velocities of the new model for a volume of 500, 1500 and 2500 l/m. Figure 16 shows that the modelled velocities do not fully mimic the measured velocities in terms of magnitude, especially at the lower volumes. On the other hand, the trend along the dike profile is rather similar. Because the field measurements have an error margin of ± 0.5 m/s and the wave run-up simulator cannot represent a realistic wave front in the first 3 to 4 meters relative to the crest (section 3.1.2.), the measured velocities could be much higher near the crest and lower near the toe. Furthermore, Van Bergeijk et al. (2020) points out that the model performance decreases at lower volumes. Therefore, the new model set-up provides a good enough fit for this study. The validation steps and the simulated velocities of the original model are presented in Appendix C. The new set-up provides higher velocity maxima and more similar front velocities along the dike profile.

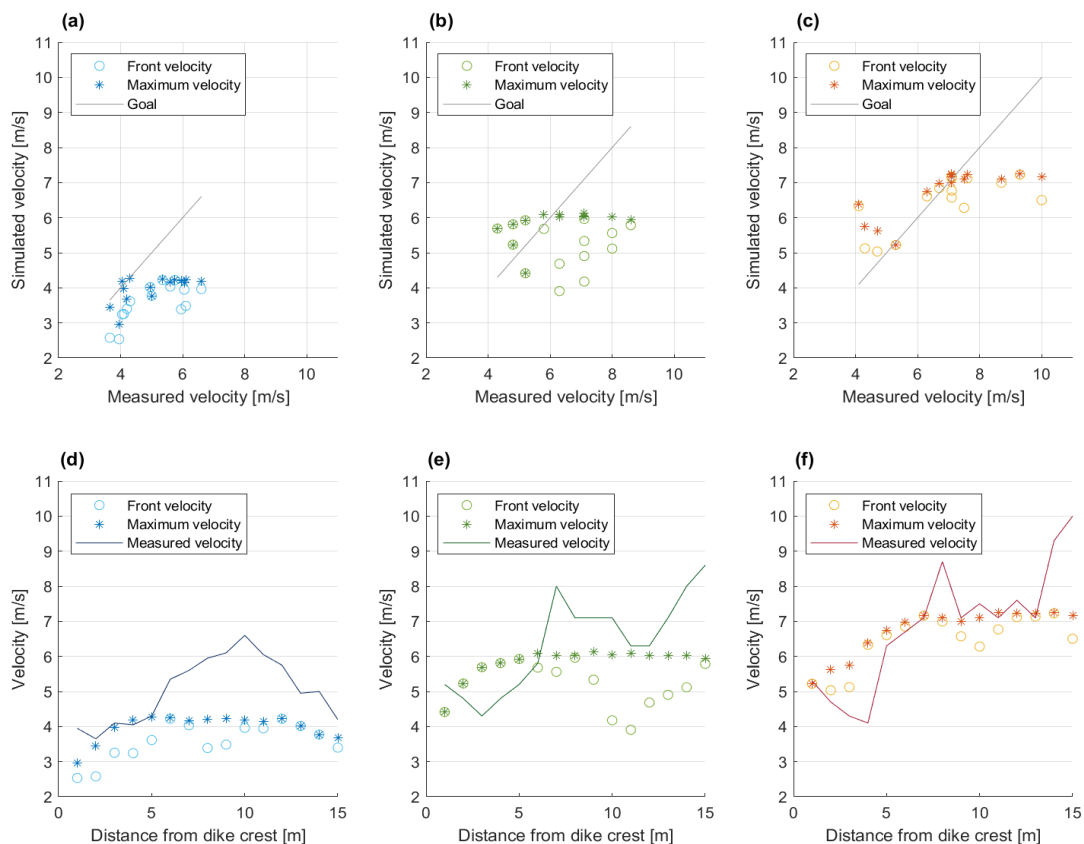


Figure 16 - The value and location of the front and maximum velocity for the wave overtopping volumes of: (a, d) 500 l/m (blue), (b, e) 1500 l/m (green) and (c, f) 2500 l/m (orange). The goal-line represents the target range for the velocities. The measured velocity represents the target trend along the profile with the crest at 0.5 m and the toe at 15 m.

Wave overtopping turbulence

After the validation of the OpenFOAM model, the sensitivity of wave overtopping turbulence was analysed. For the sensitivity analysis, only the volume (V) and the roughness height (k_s) are adjusted, as explained in section 4.7.. In this chapter, the sensitivity of turbulence towards the wave overtopping volume, the roughness height and a combination of both are presented. In Appendix D, larger versions of the plotted results can be found.

7.1. The sensitivity towards the volume

The sensitivity of wave overtopping turbulence towards the wave overtopping volume (V) is analysed by comparing the wave overtopping volumes of 500, 1000, 1500, 2500, 3000, 3500 and 5000 l/m. Figure 17 presents the highest TKE maxima and Figure 18 presents the TKE along the dike profile.

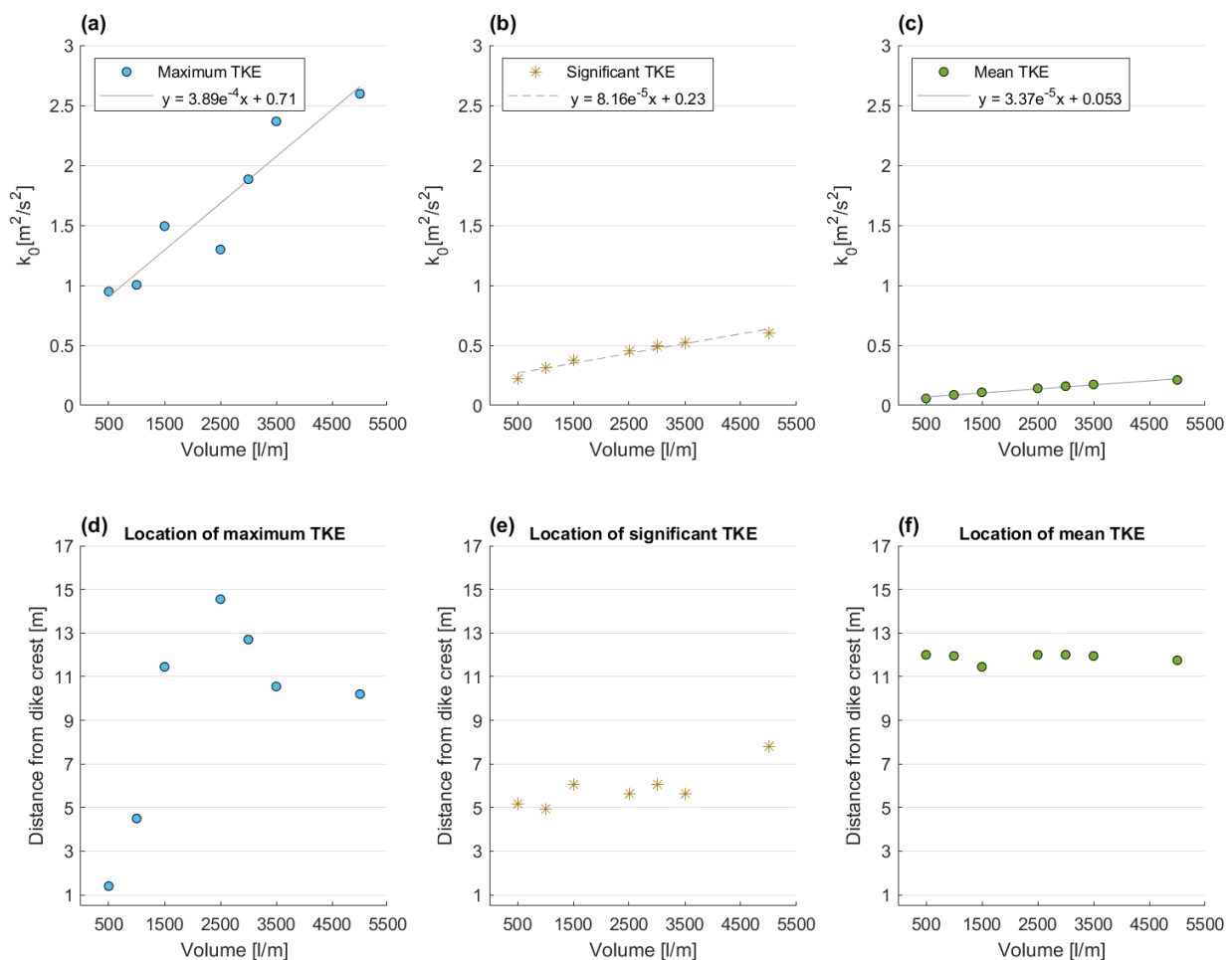


Figure 17 – Values and locations of the turbulence maxima of: the maximum TKE (a, d), the maximum significant TKE (b, e) and the maximum mean TKE (c, f). The crest starts at 0.5 m, the slope at 2 m and the toe at 15 m.

From the three upper subplots in Figure 17, the linearity of the trend lines stands out. The trend shows that the maximum, significant and mean TKE increase quite linearly for an increasing wave overtopping volumes. Furthermore, it can be noted from the trends that the maximum TKE presents a greater increase, for an increasing wave overtopping volume, than the significant and mean TKE. This shows that the peak in wave overtopping turbulence (maximum TKE) increases significantly more than the significant and mean wave overtopping turbulence for increasing wave overtopping volumes. The reason that the TKE increases for increasing wave overtopping volumes is, because larger volumes contain larger velocities and water layer thicknesses. These larger velocities cause the boundary layer thickness to decrease and more bubbles to be induced into the flow. This will result in more tensile and shear stresses along the dike profile, increasing the kinetic energy generated along the profile (subsection 2.2.2.). On the other hand, the increase in water layer thickness enables the increase in maximum eddy size, which carries the most energy according to the Kolmogorov theory (Wolanski & McLusky, 2011; Ting & Reimnitz, 2015; Vassilicos, 2015; Bomers et al., 2018). Therefore, flow acceleration in the model may mainly affect the magnitude of the turbulence parameters and only slightly affects the course along the dike profile. Therefore, the amount of turbulence is dependent on the flow velocity.

In the lower three subplots of Figure 17, the location at which each turbulence maximum occurs is presented. From these subplots it can be noted that, the mean TKE occurs around the same location for each wave overtopping volume (12 m). This is also true for the significant TKE, which occurs higher up the profile, at 5.5 m below the crest for all wave overtopping volumes. However, when Figure 17.e is closely observed, it stands out that the significant TKE presents a slight shift towards the toe of the dike profile for an increasing wave overtopping volume. On the other hand, the location at which the maximum TKE occurs is more scattered along the dike profile. This could indicate that the maximum TKE has random occurring peaks, without a notable trend.

When the maximum TKE is observed along the dike profile in Figure 18.c, it stands out that the maximum TKE presents more and larger fluctuations for higher wave overtopping volumes. The largest volume (5000 l/m), for example, shows more and higher peaks along the dike profile than the smallest volume (500 l/m), which shows a relatively steady course along the slope with one large peak occurring at the crest. This further proves that the turbulence fluctuations (maximum TKE) increases exponentially, compared to the significant and mean TKE for increasing wave overtopping volumes. Furthermore, the trends along the profile show that the TKE maxima presents a similar pattern along the profile for each wave overtopping volume and a linear magnitude increase. Meaning that the magnitude of the turbulence maxima increase, but that the course of the TKE along the profile remains equal for increasing wave overtopping volumes.

In addition, it can be noted from Figure 18.c that all wave overtopping volumes present large peaks at the crest. These large peaks in TKE at the crest are caused by the highly turbulent entrance of the flow at the crest, which is implemented in the model using an initial turbulence condition (subsection 4.5.1.), and by the rapid deceleration of the large flow velocities due to the horizontal angle of the crest. This deceleration of the highly turbulent and fast moving flow will increase the boundary layer thickness at the crest, which initially reduces the amount of turbulence. However, when the boundary layer thickness becomes too large, flow separation will occur, which will cause a significant increase in pressure drag and local turbulence peaks (section 2.2.2.). In addition, a (larger) water jet is more likely to occur as the flow separated on the crest can jump directly onto the slope, leading to possible scour holes near the crest (Valk, 2009; Ponsioen, 2016; Nikolaidou, 2019).

Lastly, it can be noted from Figure 18.a and Figure 18.b, that the mean and significant TKE decreases at the toe of the dike. This is likely caused by the large dissipation of TKE before the toe, as a result of the transition in slope angle, which decelerates the flow. However, it is likely that the flow does not decelerate enough to cause flow separation.

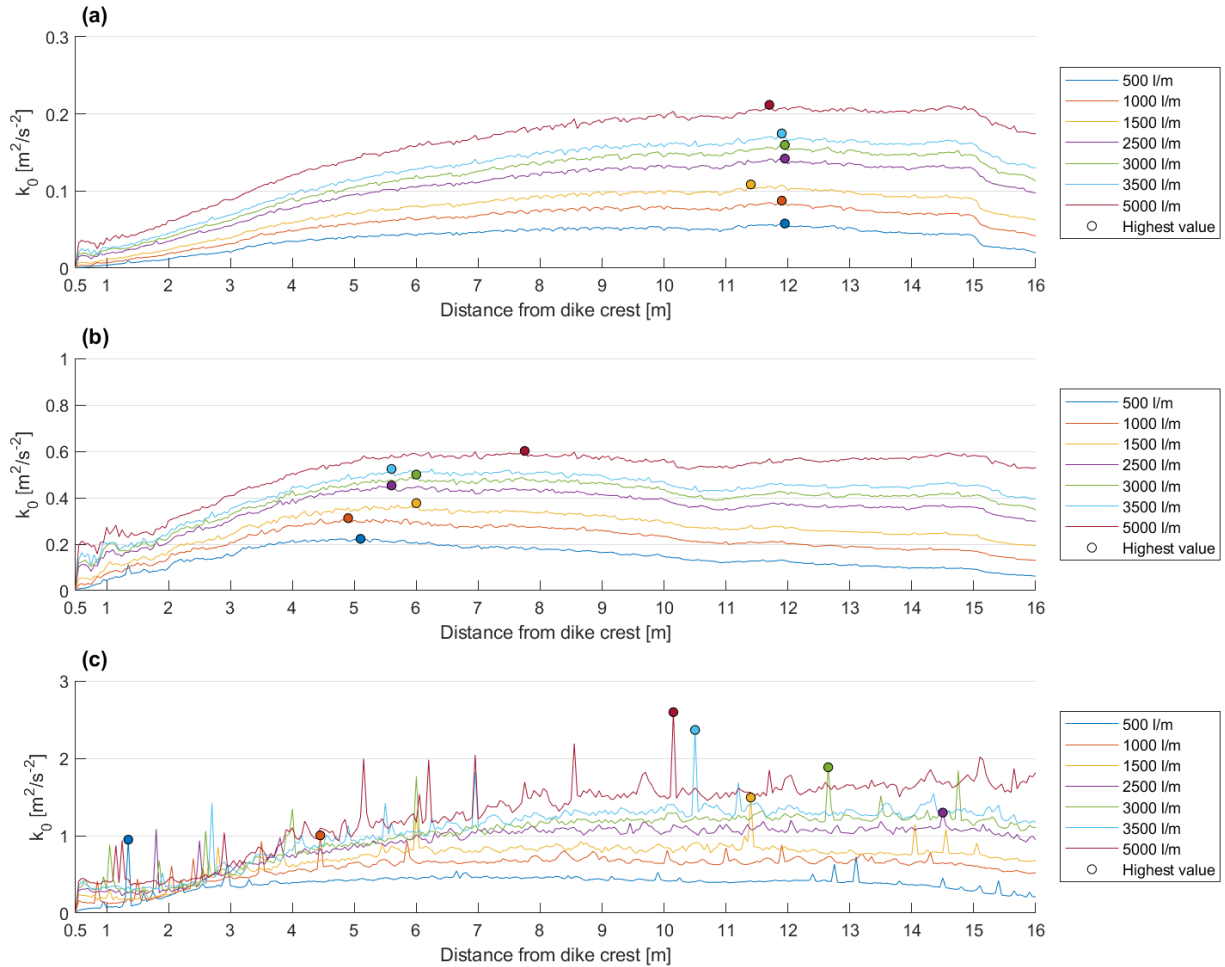


Figure 18 – The depth-averaged turbulence maxima plotted over the dike profile. (a) The maximum mean depth-averaged TKE, (b) the maximum mean significant depth-averaged TKE and (c) the maximum depth-averaged TKE have been plotted. The crest starts at 0.5 m, the slope at 2 m and the toe at 15 m. Note: The y-axis uses different scales.

7.2. The sensitivity towards the roughness height

The sensitivity of wave overtopping turbulence towards the roughness height (k_s) is analysed, by comparing four different roughness heights for a wave overtopping volume of 1000 l/m, as described in subsection 4.7.2.. Figure 19 presents the highest turbulence maxima and Figure 20 presents the TKE along the dike profile.

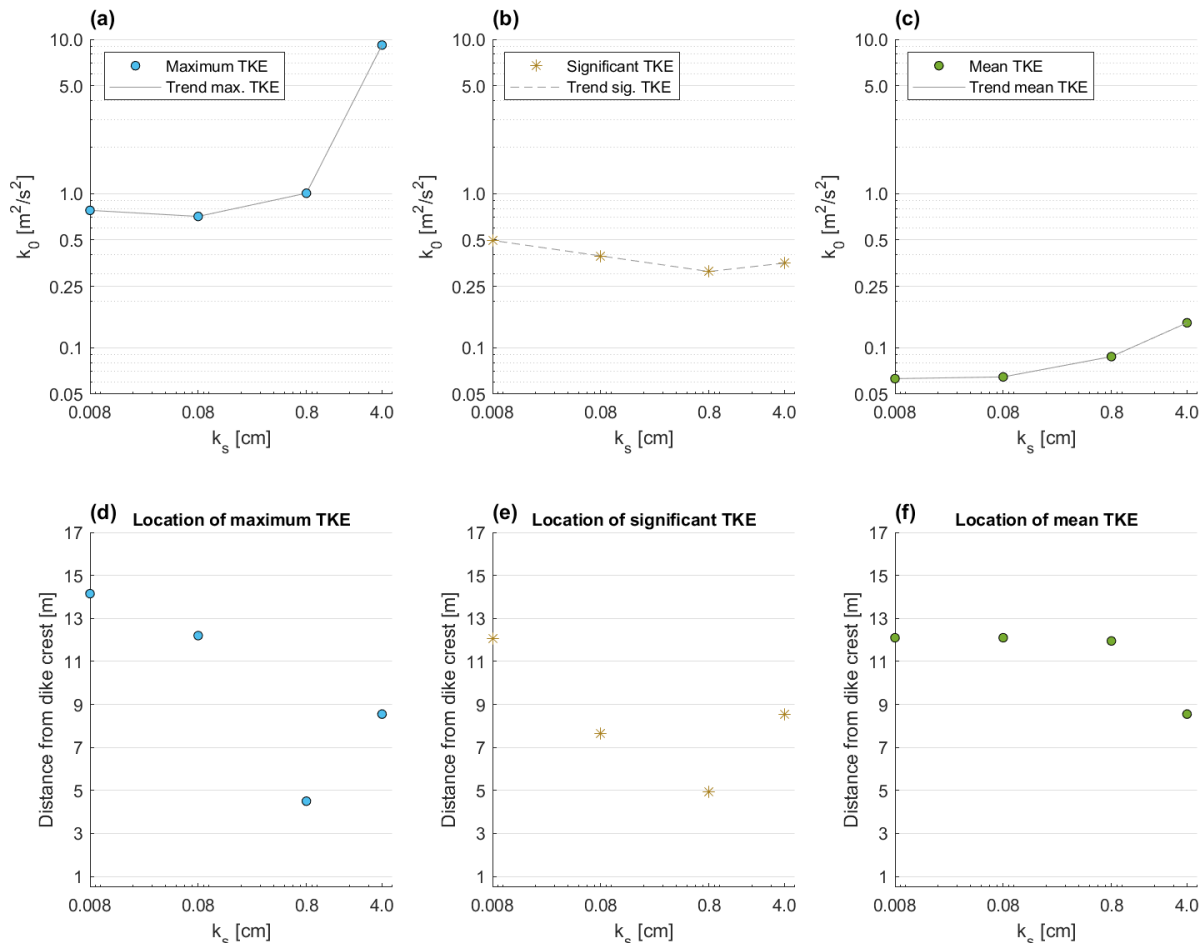


Figure 19 - Values and locations of the turbulence maxima of: the maximum TKE (a, d), the maximum significant TKE (b, e) and the maximum mean TKE (c, f). The crest starts at 0.5 m, the slope at 2 m and the toe at 15 m. Note: The y-axis in sub-plots (a, b, c) use a logarithmic-scale.

From the three upper subplots in Figure 19, it can be noted that the maximum, significant and mean TKE present different trends. The mean TKE, presented in Figure 19.c, shows a clear and steady increase for an increasing roughness height. On the other hand, the maximum significant TKE decreases for an increasing roughness height (Figure 19.b). Only for a roughness heights of 4.0 cm the significant TKE increases again. Lastly, the maximum TKE, presented in Figure 19.a, also shows an increase for an increasing roughness height. However, between the roughness heights of 0.008 and 0.08 cm, the maximum TKE shows a slight decrease. This slight decrease in peak turbulence could be caused by a slight increase in flow velocity, as the flow could become hydraulically smooth for a roughness height of 0.008 cm (subsection 2.2.1.). This slight increase in velocity will generate additional energy along the slope, thereby slightly increasing the range of the peaks compared to a slightly rougher surface (0.08 cm). However, because this decrease in maximum TKE is so small, this opposing trend can be neglected. Since, the maximum and mean TKE both clearly increase for an increasing roughness height, it can still be concluded that the overall amount of turbulence increases

for increasing roughness heights. If the mean TKE did not present a clear increase for increasing roughness heights, it would not be possible to conclude that the overall turbulence increases. This is because the mean TKE represents the increase in TKE for the whole overtopping period, as both, the higher and lower turbulence fluctuations at a location are taken into account. Therefore, representing the highest total wave overtopping turbulence. This increase in TKE for an increasing roughness is not linear, but shows a rather exponential trend.

In the lower three subplots of Figure 19, the location at which each turbulence maximum occurs is presented. It stands out that the maximum and significant TKE present an overall shift towards the dike crest for an increasing roughness height. The mean TKE, on the other hand, remains at the same location (12 m) for increasing roughness heights. Only between the roughness heights of 0.8 and 4.0 cm, the location of the maximum, significant and mean TKE shows a different trend, as the location shifts to the same position for all TKE maxima. The reason that the roughness height of 4.0 cm shows such deviations from the trends of the turbulence maxima, in both magnitude and positioning, is that the maximum TKE (fluctuations) significantly increases. In Figure 19.a, it stands out that the trend of the maximum TKE becomes significantly steeper between the roughness heights of 0.8 cm and 4 cm. In addition, when subplots (d, e, f) of Figure 19 are compared, it stands out that for a roughness height of 4.0 cm, the maximum, significant and mean TKE occur at exactly the same location (8.5 m). These observations indicate that the maximum turbulence peak, generated for a roughness height of 4.0 cm, significantly impacts the magnitude of the significant and mean TKE, compared to lower roughness heights. This means that one location will experience significantly large turbulence fluctuations, when a large roughness height is applied (4.0 cm). However, this roughness height also generates high turbulence peaks at other locations along the profile, as can be noted from Figure 20. This large increase of the maximum TKE at multiple locations along the dike profile could be caused by the size of the roughness height, which becomes significantly larger than the viscous sub-layer. This could cause the roughness height to perturb the flow excessively, resulting in additional turbulence being generated in the turbulent boundary layer (subsection 2.2.1.). However, this large increase of the turbulence maxima for a roughness height of 4.0 cm, could also be the result of an incorrect schematisation of the roughness for these larger roughness heights. The range of the turbulence peaks becomes significantly larger along the entire dike profile, and the peaks seem to occur rather systematic (\pm every 0.5 m), compared to the other maximum TKE results.

When the subplots of Figure 20 are compared, it can be observed that the locations of the turbulence maxima overlap. In the figure can be noted that the location of the significant and mean TKE are equal for a roughness height of 0.008 cm, the maximum and mean TKE are equal for a roughness height of 0.08 cm and the maximum and significant TKE are equal for a roughness height of 0.8 cm. This overlap is mainly caused by a large peak in maximum turbulence (0.08, 0.8 and 4.0 cm) and/or the increase in turbulent peaks (0.008 and 0.08 cm). These observations of the turbulence maxima together, indicate that the increase in roughness height increases the overall wave overtopping turbulence, but decreases the overall intensity of the peaks. However, when larger roughness heights (4.0 cm) are applied, the peak in wave overtopping turbulence (maximum TKE) will influence the significant and mean turbulence and cause the intensity of the peaks to increase again.

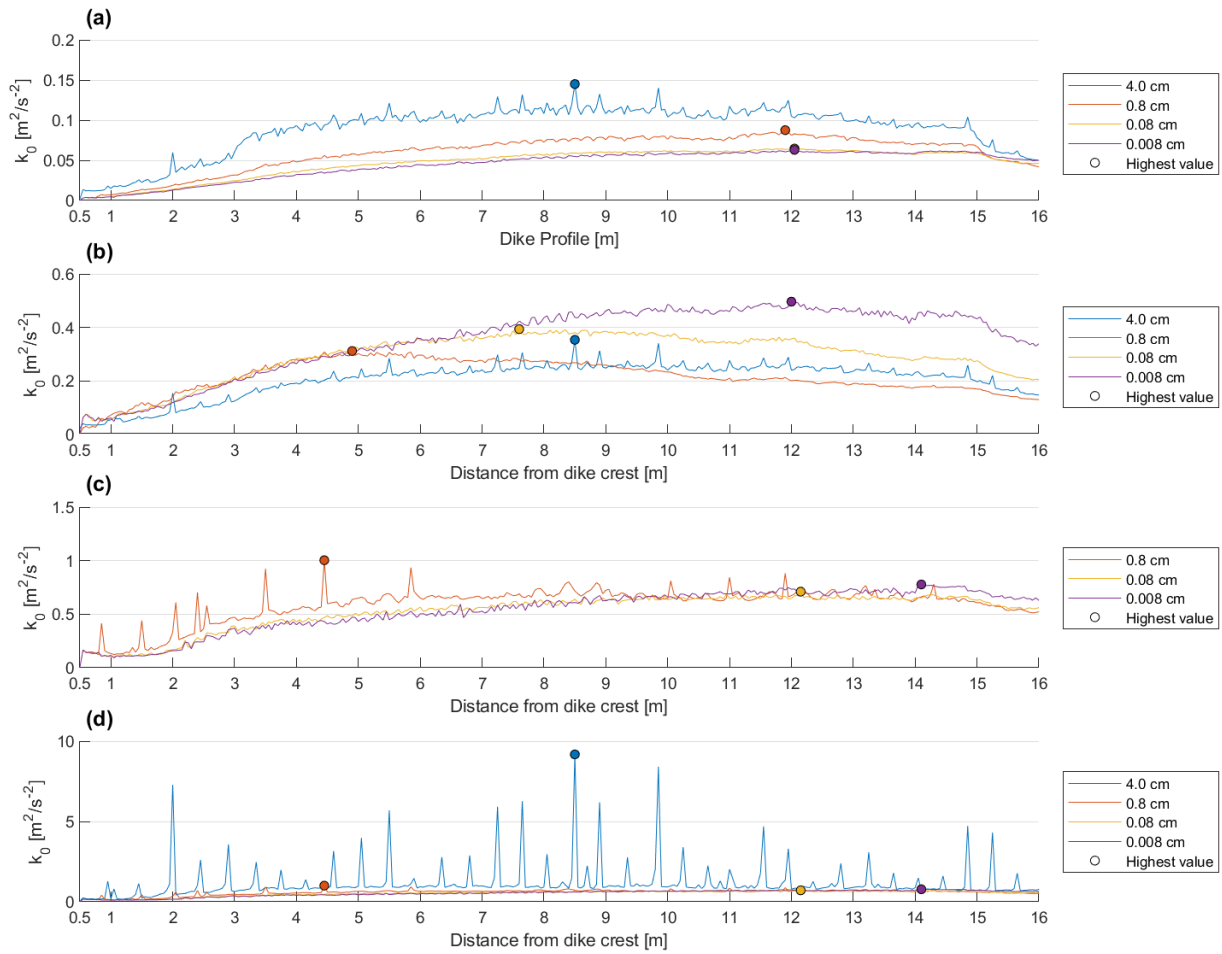


Figure 20 – The depth-averaged turbulence maxima plotted over the dike profile. (a) The maximum mean depth-averaged TKE, (b) the maximum mean significant depth-averaged TKE and (c, d) the maximum depth-averaged TKE have been plotted. The crest starts at 0.5 m, the slope at 2 m and the toe at 15 m. Note: The y-axis uses different scales.

7.3. The sensitivity towards the volume and roughness height

The sensitivity of wave overtopping turbulence towards the wave overtopping volume (V) and roughness height (k_s) are analysed by comparing four different wave overtopping volumes for four different roughness scenarios. The resulting sixteen scenarios are described in subsection 4.7.3. in more detail. Figure 21 presents the magnitude and location of each turbulence maxima for the wave overtopping volumes of 500 l/m, 1000 l/m, 2500 l/m and 3000 l/m.

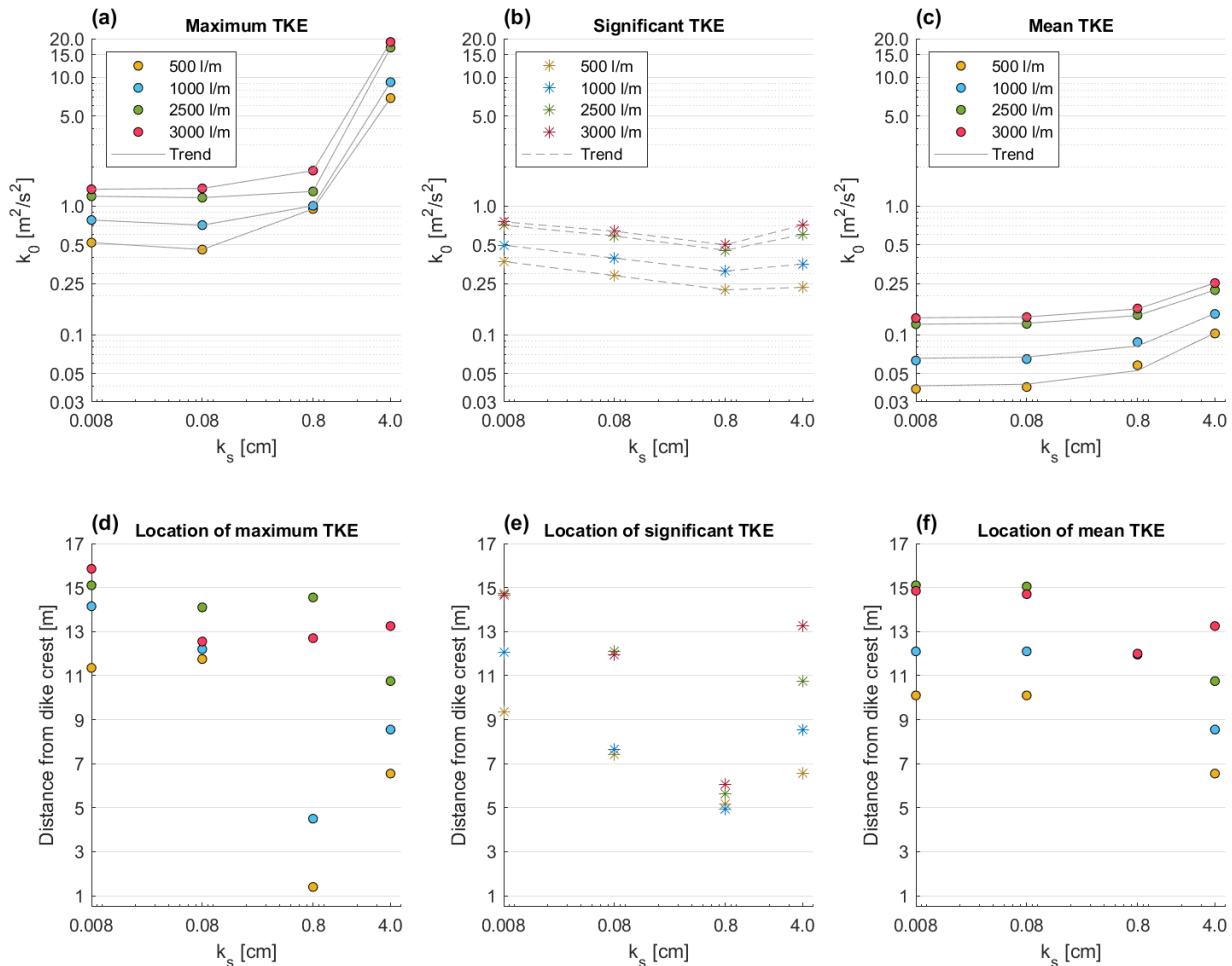


Figure 21 – Values and locations of the turbulence maxima for the wave overtopping volumes of 500 l/m (yellow), 1000 l/m (blue), 2500 l/m (green) and 3000 l/m (red): (a, d) The maximum depth-averaged TKE, (b, f) the maximum mean significant depth-averaged TKE and (c, e) the maximum mean depth-averaged TKE have been plotted. The crest starts at 0.5 m, the slope at 2 m and the toe at 15 m. Note: The y-axis in sub-plots (a, b, c) use a logarithmic-scale.

From the three upper subplots in Figure 21, it directly stands out that all turbulence maxima increase for increasing wave overtopping volumes. This shows that, in case of a fixed roughness height, the wave overtopping turbulence increases for increasing wave overtopping volumes, regardless of the applied bed roughness. What stands out as well, is that the mean TKE has a much smaller range than the maximum and significant TKE. Furthermore, it can be noted that the maximum and significant TKE have similar ranges for roughness heights between 0.008 and 0.8 cm, but show significantly higher values for a roughness height of 4.0 cm.

When only Figure 21.a is observed, it stands out that the maximum TKE still shows a decreasing trend between the lowest two roughness heights (0.008 and 0.08 cm). However, this decreasing trend becomes smaller for increasing wave overtopping volumes and even becomes positive for a wave overtopping volume of 3000 l/m. Furthermore, it can be noted from Figure 21.b, that the previously

observed decrease and increase in trend of the maximum significant TKE (subsection 7.2.) also occurs for wave overtopping volumes other than 1000 l/m. Because this decreasing trend in significant TKE occurs for all wave overtopping volumes, this could indicate that a threshold roughness height exists at which the lowest possible maximum mean significant TKE is obtained.

When the locations of the turbulence maxima are observed in subplots (d, e, f) of Figure 21, it stands out that the location of all turbulence maxima present an overall shift towards the toe of the dike for increasing wave overtopping volumes, regardless of the applied roughness height. The distance of this shift towards the toe of the dike, for increasing wave overtopping volumes, does depend on the applied roughness height. When the location of the mean TKE is observed in Figure 21.f, it stands out that the mean TKE, for a roughness height of 0.008, occurs at the exact same location as the mean TKE for a roughness height of 0.08 cm, regardless of the applied wave overtopping volume. This indicates that when the roughness height changes from smooth (0.08 cm) to smoother (0.008 cm), only the magnitude and intensity of the turbulence peaks are affected, while the mean TKE will remain equal in both positioning and magnitude. Only the location of the mean TKE for a roughness heights of 0.8 cm does not shift for an increasing wave overtopping volume, but remains at one location (12 m). Furthermore, it can be noted that the previously observed overlap in the locations of the turbulence maxima for a roughness height of 4.0 cm (subsection 7.2.), also occurs for wave overtopping volumes other than 1000 l/m.

Comparison of the turbulence intensity calculations

The sensitivity of the relative turbulence intensity is analysed by comparing the results of r_0 for two different calculation methods. In this chapter, the trends and magnitudes of the turbulence intensities are compared for different combinations of wave overtopping volumes and roughness heights. In addition, the differences between both r_0 approaches will be analysed and the found trends of the relative turbulence intensity will be compared to the found trends of the modelled TKE.

8.1. Comparison per wave overtopping volumes

For this analysis, the relative turbulence intensity was computed at each location along the dike profile and afterwards averaged to obtain one turbulence intensity, as described in subsection 5.4.. Figure 22 presents the sensitivity of the turbulence intensity (r_0) for changes in wave overtopping volume. Figure 22.a presents the relative turbulence intensity, calculated using the modelled mean depth-averaged TKE ($\overline{k_0}$) and mean velocities (\overline{u}) directly. For this approach the first notation of equation [8] is used. Figure 22.b presents the relative turbulence intensity, calculated using the modelled mean water layer thicknesses (\overline{h}) and the implemented roughness heights (k_s) to calculate the Chézy coefficient using equation [26]. For this calculation, the last notation of equation [8] is used. This means that for both approaches the OpenFOAM model output is used as input for the calculation.

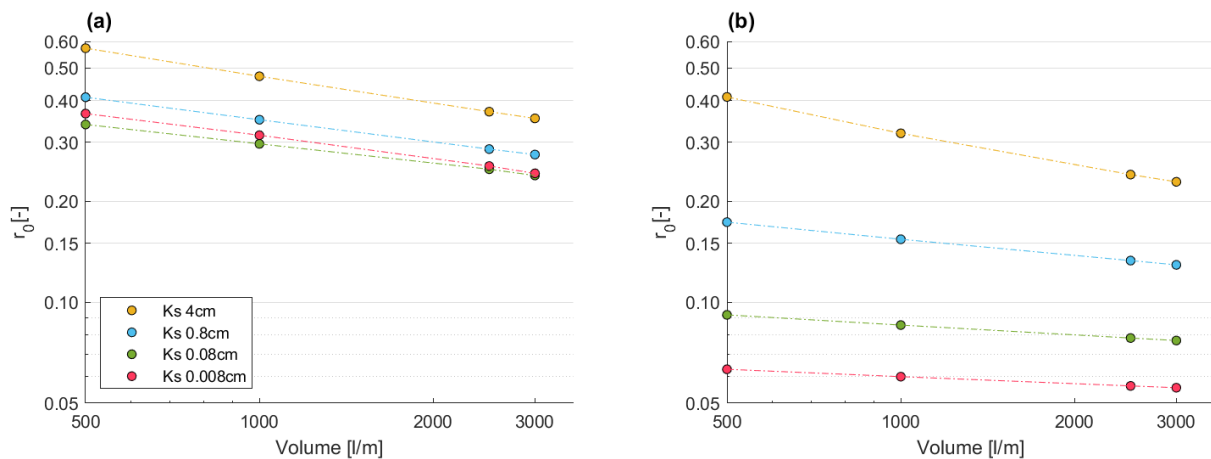


Figure 22 - The relative depth-averaged turbulence intensity for the roughness heights of 4.0 cm (yellow), 0.8 cm (blue), 0.08 cm (green) and 0.008 cm (red). (a) r_0 calculated using the modelled TKE (k_0) directly, (b) r_0 calculated using the White-Colebrook Chézy equation with the modelled water layer thickness (h). Note: For the y-axis a logarithmic-scale is used.

In Figure 22, it stands out that both calculations of the relative turbulence intensity present a decreasing trend for an increasing wave overtopping volume. These decreasing trends are relatively linear in both calculation methods. The reason why the turbulence intensity (r_0) decreases for an

increasing wave overtopping volume can be found in both notations of equation [8]. In the first notation of the equation, the turbulence intensity (r_0) decreases when the depth-average velocity (U_0) increases. The turbulence intensity (r_0) also decreases when the Chézy coefficient (C) increases (equation [8]), which happens when the roughness of the cover reduces or when the water layer thickness (h) becomes thicker (equation [26]). As both, the flow velocity and water layer thickness, increase when the wave overtopping volume increases, it is expected that this decreasing trend would occur. However, when purely the empirical equations for the critical flow velocity (U_c) are analysed, the relation between the relative turbulence intensity and the wave overtopping volume would mean that the risk of erosion would be higher at the crest than at the toe of a simple dike profile. This is indirectly caused by the flow acceleration towards the toe of the dike, due to gravitational acceleration. If r_0 is calculated for multiple locations along the dike profile, the turbulence intensities would be higher near the crest than near the toe, since, the only variables in the equations that change significantly, would be the depth-average velocity (U_0) and the water layer thickness (h). Herein, assuming that the TKE (k_0) remains equal or increases proportional to the flow velocity and layer thickness. When the turbulence intensity becomes larger, the critical flow velocity (U_c) will decrease, resulting in a lower risk of erosion, as U_c represents the grass strength threshold. In addition, the empirical equations indicate that the risk of erosion is higher for lower wave overtopping volumes. This is because the critical flow velocity will increase for an increasing wave overtopping volume, as both, the flow velocity and water layer thickness increase. However, the grass strength threshold (U_c) and the load on the dike (U_i) will both increase in the COM method for an increasing wave overtopping volume. Meaning, that the current approach of the relative turbulence intensity within the critical flow velocity equation could still provide appropriate damage predictions for the COM, as the parameters balance one another out.

It can also be noted from Figure 22, that when the relative turbulence intensity is calculated using the modelled TKE directly, the decreasing trends are slightly steeper for the lower roughness heights, than when the Chézy coefficient is used. In addition, the difference in magnitude also stands out. In Figure 22.a, the turbulence intensities are much larger than the turbulence intensities in Figure 22.b for all combinations of wave overtopping volume and roughness height. Therefore, the first notation of equation [8] seems to overestimate the turbulence intensities compared to the last notation. This overestimation is especially large when lower roughness heights are applied.

8.2. Comparison per roughness height

For this analysis, the relative turbulence intensity was computed in the same way as mentioned in the section 8.1.. In Figure 23, the sensitivity of the turbulence intensity (r_0) for changes in roughness height is presented. Figure 23.a presents the relative turbulence intensity calculated using the modelled mean depth-averaged TKE ($\overline{k_0}$) and mean velocities (\bar{u}) directly, while Figure 22.b presents the relative turbulence intensity calculated using the Chézy coefficient. Therefore, both approaches use the OpenFOAM model output as input for the calculation.

In Figure 23 it stands out that both calculations of the relative turbulence intensity present an increasing non-linear trend for an increasing roughness height. In the figure, it also directly stands out that the overall results of the two calculation methods show a different behaviour. When the relative turbulence intensity is calculated using the modelled TKE directly, it can be noted that the range and increase between the different scenarios is larger than when the Chézy coefficient is used. In addition it can be noted from Figure 23.b, that the deviation between the wave overtopping volumes increase when the roughness height is increased, while the deviation between the wave overtopping volumes remain rather equal for an increasing roughness height in Figure 23.a. This means that the relative

turbulence intensity increases exponentially for the calculation using the Chézy coefficient (Figure 23.b).

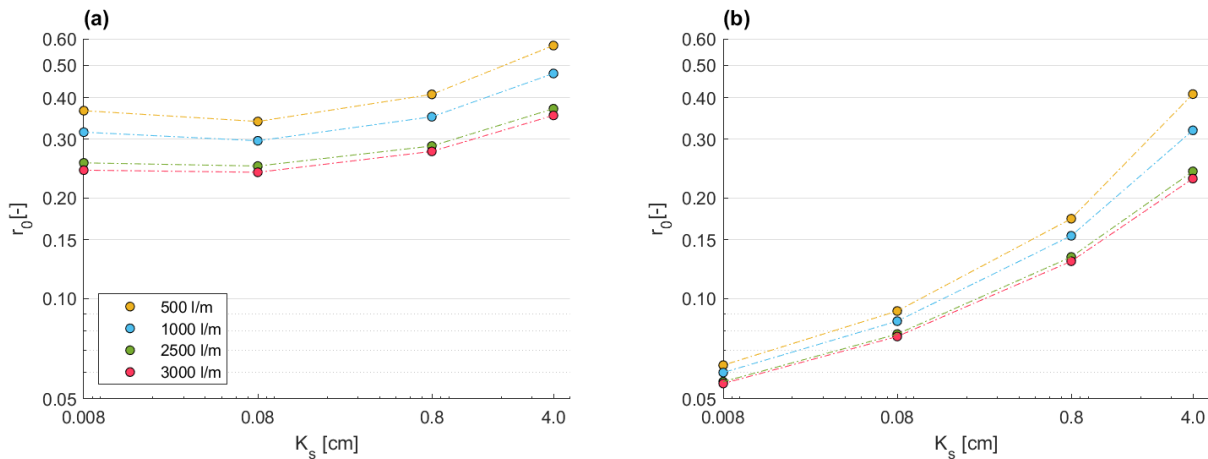


Figure 23 –The relative depth-averaged turbulence intensity for the wave overtopping volumes of 500 l/m (yellow), 1000 l/m (blue), 2500 l/m (green) and 3000 l/m (red). (a) r_0 calculated using the modelled TKE (k_0) directly, (b) r_0 calculated using the White-Colebrook Chézy equation with the modelled water layer thickness (h). Note: For the y-axis a logarithmic-scale is used.

When Figure 23.a is observed it can be noted that for all wave overtopping volumes, the smoother surface (0.008 cm) shows larger turbulence intensities than a less smooth surface (0.08 cm). This decreasing trend between the lowest two roughness heights is caused by the increase in turbulence peaks for a roughness height of 0.008 cm, as explained in the chapter 7. This increase in turbulence peaks will increase the mean depth-averaged TKE ($\overline{k_0}$), but will not significantly increase mean velocities (\overline{u}). In addition, it can be noted that the deviation between these roughness heights, decreases when the wave overtopping volume increases. When looking at the turbulent intensity, computed with Chézy (Figure 22.b), it can be noted that this trend does not occur, as a steady increase in turbulence intensity is presented. Another notable difference is that the calculation, using Chézy, presents a slightly larger deviation between the turbulence intensities when the roughness height increases for a wave overtopping volume of 500 l/m, than for a wave overtopping volume of 3000 l/m. This is also notable by comparing the steepness of the trend in Figure 22.b and the range of turbulence intensities in Figure 23.b for the largest (4.0 cm) and smallest roughness heights (0.008 cm).

When r_0 is calculated with the modelled depth-averaged TKE and depth-averaged velocity directly, the resulting turbulence intensities present a high range of intensities ($r_0 = 0.25 - 0.6$). However, the resulting turbulence intensities present a lower range ($r_0 = 0.055 - 0.4$) when r_0 is calculated with the Chézy coefficient (equation [26]). As the magnitude differs, this could indicate that one of the equations is over- or underestimating the turbulence intensities for lower roughness heights. The larger roughness heights present a more equal range.

8.3. Differences between modelled and empirical predictions

In this section a comparison is made between the found trends for the modelled TKE and the calculated turbulence intensities. Although both turbulence predictions represent turbulence differently, it is still important to understand how and why these turbulence parameters differ. Since, turbulent kinetic energy (k) is generally treated as a measure of (total) turbulence intensity and both of these parameters are depth-averaged for this research, it would be expected that the overall trends would be comparable (Robert, 2003). Therefore, this comparison might give a greater understanding, of whether the relative turbulence intensity is appropriate. In Table 9 an overview of the found trends for both turbulence predictions (r_0 and k_0) are presented.

Table 9 - Overview of the found trends of the modelled depth-averaged turbulent kinetic energy (k_0) and the calculated depth-averaged relative turbulence intensity (r_0) for an increasing wave overtopping volume and roughness height.

	TKE (k_0)	Relative turbulence intensity (r_0)
Wave overtopping volume V ↑	Increases ↑	Decreases ↓
Roughness height k_s ↑	Increases ↑	Increases ↑

In Table 9 stands out that the TKE and the turbulence intensity both increase for an increasing roughness height, but present opposing trends for an increasing wave overtopping volume, as the TKE increases, while the turbulence intensity decreases. These opposing trends are, however, still linearly related to the change in wave overtopping volume and are most likely caused by the fact that both turbulence parameters (r_0 and k_0) represent turbulence in a different manner. The relative depth-averaged turbulent intensity (r_0) represents the turbulence fluctuations in all dimensions (u' , v' , w') relative to the velocity in the longitude direction (u') of the flow, while the modelled depth-averaged TKE (k_0) represents the absolute turbulence fluctuations in all dimensions (u' , v' , w') (Hoffmans, 1993; Schiereck, 2001; Hoffmans, 2012).

From the first notation in equation [8] can be noted, that the contribution of the TKE (k_0) is smaller than the contribution of the velocity (U_0), due to the square-root. This means that r_0 also decreases when the TKE and velocity increase with approximately the same magnitude along the dike profile. However, if the TKE becomes large enough to overcome the influence of the square-root in the first notation of equation [8], the relative turbulence intensity will increase. During this comparison it was observed, that the magnitude of the computed depth-averaged velocity (U_0) and depth-averaged TKE (k_0) both increase linearly along the dike profile for an increasing wave overtopping volume. This could indicate that, if there is indeed a linear relation between the velocity and the TKE, an increasing wave overtopping volume will almost always decrease the r_0 . As the ratio between the TKE and the velocity is not large enough to overcome the influence of the square-root, r_0 becomes smaller. However, this does not necessarily mean that there is less turbulence, as there is still a higher amount of TKE in the system.

On the other hand, it was observed that the TKE and the fluctuations in TKE along the dike profile increase for an increasing roughness height, while the velocity and fluctuations in velocity decrease for an increasing roughness height. This means that a larger roughness will slightly decrease the magnitude and fluctuations in velocity, but will present a very similar behaviour of the velocity along the profile. However, the magnitude and amount of fluctuations in TKE does increase, which means that the ratio between the TKE and velocity increases. Thus, the TKE becomes large enough to overcome the influence of the square-root.

The same applies for the last notation in equation [8], which uses the Chézy coefficient. In this notation, an increasing wave overtopping volume results in a negative trend, as the Chézy coefficient increases for an increasing water layer thickness (equation [26]). As larger volumes over the same dike slope will have a larger water depth, the increase in Chézy will decrease the relative turbulence intensity. On the other hand, the Chézy coefficient will decrease for the same wave overtopping volume when the roughness height increases. Therefore, the last notation also results in a positive trend for an increasing roughness height and a negative trend for an increasing wave overtopping volume.

9

| Discussion

This research presents new insights in terms of magnitude, range and sensitivity of wave overtopping turbulence maxima along a simple dike profile, a dike with a single cover type and slope angle. These findings provide a step towards a better understanding of turbulent processes within wave overtopping. In this chapter the results of this study are compared to findings of other studies, the applicability of the findings are stated and the limitations and/or improvements of this study are discussed.

9.1. Relevance of this research

In this section each discussion subject is introduced with a title and structured per paragraph as follows: first the findings are stated, whereafter the findings will be discussed and lastly, the relevance of the findings is stated.

Possible threshold roughness height to obtain the lowest significant TKE

In this research it was found that an increase in roughness height (k_s) will increase the overall wave overtopping turbulence (mean TKE), but decreases the number of peaks (significant TKE) (Figure 19). This shows that, in case of a fixed wave overtopping volume, the overall wave overtopping turbulence increases for an increasing roughness (Figure 21).

Although, a linear decreasing trend is visible for the significant TKE between the roughness height of 0.008 cm and 0.8 cm (Figure 19.b), the significant TKE increases again when the roughness height is increased to 4.0 cm. The amount of increase between 0.8 and 4.0 cm depends on the applied wave overtopping volume, wherein larger volumes present a larger increase in significant TKE. This increase occurs due to an increasing number of peaks (significant TKE).

This linear decreasing trend of the significant TKE might indicate that a threshold roughness height exists at which the lowest maximum mean significant TKE is obtained, as this decreasing trend occurs for all wave overtopping volumes. This means that the maximum significant TKE will not decrease further when lower or higher roughness heights are applied than this threshold roughness. This threshold would most likely be situated around a roughness height of 0.8 cm.

Contradictions in positioning of the modelled TKE and the wave overtopping theory

In the overall trend for the positioning along the profile, it was found that the turbulence maxima shifts towards the toe of the dike for an increasing wave overtopping volume (Figure 17 (d, e, f); Figure 18). The distance of this shift depends on the applied roughness height (Figure 21 (d, e, f)). For an increasing roughness height an opposite trend was visible, wherein the turbulence maxima shifts towards the crest of the dike (Figure 19 (d, e, f); Figure 20).

The model shows that most of the turbulence maxima occur on the lower half of the slope and shift even further downwards when the wave overtopping volume increases. Generally, wave overtopping damage occurs for larger wave overtopping volumes. Furthermore, in previous studies it is found that

wave overtopping damage often occurs near the toe of a simple dike profile (Bijlard, 2015; Bomers et al., 2018; Van Bergeijk et al., 2019b). Therefore, these trends in positioning of the turbulence maxima, are physically expected for an increasing wave overtopping volume. However, according to the wave overtopping theory, which is based on the turbulence intensity, less turbulence should occur lower on the dike slope due to the increase in velocity caused by gravitational acceleration (Bijlard, 2015; Bomers et al., 2018; Hoffmans et al., 2018; Van Bergeijk et al., 2019a). Although it was stated in previous studies that the damage near the toe of a simple dike profile is most likely caused by the deceleration of the flow due to the change in slope angle, this decrease in velocity is only observed in a few wave overtopping volume measurements at the Vecht dike. In addition, the model does not present a decrease in velocity near the dike toe at all, for most simulated wave overtopping volumes. This means that both, the measurements and the simulated velocities are higher at the toe than at the crest of the dike (Figure 13).

As the model shows that the turbulence maxima occur more often on the lower half of the slope and shift towards the toe for an increasing wave overtopping turbulence, we might be tempted to conclude that the turbulence maxima cause these damages near the toe of a simple dike profile. However, this cannot be stated based on the results of this study alone. Therefore, more research is necessary to validate whether the predicted positioning of the turbulence maxima correlates with the observed positioning of wave overtopping damage in the field.

Reverse engineering may cause underestimation of the relative turbulence intensity

In this research it was found that the relative turbulence intensity decreases linearly for an increasing wave overtopping volume, but increases non-linearly for an increasing roughness height (Figure 22; Figure 23).

When the observed range and magnitude of the relative turbulence intensities for both calculation methods are compared with the turbulence intensities calculated or calibrated in previous studies, we might be tempted to conclude that both calculation methods overestimate the relative turbulence intensity. This is because, in most studies, a range from 0.1 to 0.35 is obtained for r_0 (Hoffmans, 2012; Bijlard et al., 2016; Ponsioen, 2016). However, other studies, which use different erosion prediction models, such as the study of Warmink et al. (2020), state that the turbulence intensity varies between 0.25 for mild slopes and 0.45 for relatively steep slopes. This indicates that there are still large uncertainties concerning the range for the relative turbulence intensity in general. However, the indicative turbulence intensity ranges presented by Hoffmans (2012), do correspond to the range of the calculated r_0 in this study; the modelled TKE approach ($r_0 = 0.25 - 0.6$) and the Chézy approach ($r_0 = 0.055 - 0.4$). Herein, the range for r_0 using the modelled depth-averaged TKE corresponds to the description of an extreme high turbulent uniform flow over a very steep channel slope with limited flow depth ($r_0 = 0.3 - 0.6$). This description of the flow is a better representation of wave overtopping flow than the descriptions that correspond to the range for r_0 using the Chézy equation, which describes channel/river flow.

Originally, the approach for the relative depth-averaged turbulent intensity (r_0) was developed for hydraulically smooth uniform open-channel flows, for which a r_0 with the range of 0.1 to 0.2 can be considered as highly turbulent (Hoffmans, 1993; Schiereck, 2001; Hoffmans, 2012). This is, however, an incorrect assumption for wave overtopping flows, as these flows are highly non-uniform and often very hydraulically rough due to the thin water layer (subsection 2.2.1.). In addition, for non-uniform flows, the mean velocity can either accelerate or decelerate, resulting in higher relative turbulence intensities than for uniform flows (subsection 2.2.2.). Therefore, much higher ranges would be expected for wave overtopping flows. In addition, most studies use reverse engineering to obtain the

critical flow velocity (U_c) after the overtopping experiments, by calibrating U_c with the known wave overtopping damage and front velocity (U_i). Herein, r_0 is either not used or found by reverse engineering. Since, the found ranges of r_0 , obtained using the empirical approach, are much higher than the ranges averagely obtained using reverse engineering, this could indicate that reverse engineering causes the actual turbulence intensity to be underestimated. Especially, since the ranges obtained using an empirical approach could be a better representation of wave overtopping flow, as stated above. If the turbulence intensity is indeed underestimated, this may be caused by an incorrect use of the turbulence parameter within the critical flow velocity equation.

The relative turbulence intensity might misrepresent wave overtopping turbulence

From the found trends in this research, it can be noted that the relative depth-averaged turbulent intensity (r_0), independent of the used calculation method, presents linear opposing trends when compared to the turbulence predictions of the numerical wave overtopping model for an increasing wave overtopping volume (Figure 17 vs Figure 22). On the other hand, both, the calculated and the modelled, turbulence parameters predict a positive trend for an increasing roughness height (Figure 19 vs Figure 23).

According to the wave overtopping theory, which focuses on the relative turbulence intensity, the amount of turbulence should decrease when the velocity increases (Hoffmans, 2012; Van Bergeijk et al., 2019b). This means that when the wave overtopping volume increases, the turbulence (intensity) decreases as larger velocities are generated. This decrease in turbulence for an increasing wave overtopping volume is also estimated by Hoffmans (2012), presenting larger best guess values for lower wave volumes. As the relative depth-averaged turbulence intensity (r_0) represents the wave overtopping turbulence relative to the flow velocity, the wave overtopping turbulence will decrease when the mean velocity and fluctuations increase proportional to one another, which is the case for an increasing wave overtopping volume (subsection 8.3.). However, the absolute turbulence (k) in the flow increases for an increasing wave overtopping volume, as the TKE increases with an increasing velocity. Taking into account that wave overtopping damage mainly occurs near the toe of a simple dike profile, we might be tempted to conclude that the turbulence intensity (r_0) may not be the correct parameter to represent wave overtopping turbulence. Herein, assuming that the grass strength is uniform along the entire cover and that flow velocities are higher near the toe than near the crest of a simple dike profile. Thus, the relative turbulence intensity may be a good parameter to compare the turbulence at different locations, but may not be the correct parameter to describe wave overtopping turbulence related failure.

Based on the performed research it is not possible to conclude whether the turbulence intensity (r_0) is an incorrect representation of the wave overtopping turbulence. Based on the performed research it can only be concluded that the currently used turbulence intensity (r_0) is a good first approximation of wave overtopping turbulence, but presents physically unexpected trends for an increasing wave overtopping volume when compared to the trends of the TKE and observed wave overtopping damages. Therefore, further research is necessary to validate whether the predicted turbulence maxima (TKE) could be a better representation of wave overtopping turbulence or whether a different turbulence intensity parameter, such as the turbulence intensity (I), could provide a better representation wave overtopping turbulence forces.

9.2. Applicability of this research

In this section each discussion subject is introduced with a title and structured per paragraph as follows: first the findings are stated, secondly the findings will be discussed and lastly, the applicability of the findings are stated.

Contribution of the turbulence maxima to wave overtopping failure

In this research it was found that the location of the turbulence maxima along the profile shift towards the toe of the dike for an increasing wave overtopping volume and shift towards the crest of the dike for an increasing roughness height. The distance of this shift depends on the applied roughness height. Furthermore, it was also found that for an increasing wave overtopping volume, the peak in wave overtopping turbulence (maximum TKE) increases exponentially compared to the increase in significant and mean TKE.

Wave overtopping turbulence is closely related to the pressure gradients, tensile stresses and shear stresses. Previous studies established that the maximum turbulence levels occur at the position of the maximum shear stress (MIT, 2016). It is expected that peaks in wave overtopping turbulence, which increase significantly for an increasing wave overtopping volume, cause high variations in turbulence intensities and lead to extreme shear stresses along the profile (Ponsioen, 2016). Although, it is important to understand which of the predicted turbulence maxima contribute (more) to wave overtopping damage, it is not possible to conclude, based on the performed research, which turbulence maxima has the largest contribution to wave overtopping damage.

Currently, turbulence cannot be directly measured yet during wave overtopping experiments in the field. Therefore, the positioning of the turbulence maxima, predicted in OpenFOAM, can be used as a guideline to find where turbulence maxima are likely to occur during different wave overtopping scenarios on a simple dike profile. The found positioning of the turbulence maxima can then function as a starting point to monitor wave overtopping turbulence in the field. This can be done by analysing whether the predicted positioning of the turbulence maxima in OpenFOAM correlate with the observed positioning of the wave overtopping damage on a simple dike profile in the field. In addition, the OpenFOAM model can also be used to obtain shear stress maxima along the dike profile. The obtained positioning of the shear stress maxima can then be compared to the positioning of the TKE maxima, to observe whether the maximum turbulence levels indeed correlate with the position of the maximum shear stress. Furthermore, the sensitivity of the shear stress maxima can be analysed and compared to the sensitivity of the TKE maxima. This can provide insights on whether these extreme shear stresses increase proportional to wave overtopping turbulence peaks (maximum TKE). When the positioning of the TKE maxima, the positioning of the shear stress maxima and the sensitivity of both, the TKE and shear stress maxima, are observed and compared, it might be possible to identify which turbulence maxima contribute (the most) to wave overtopping failure.

Developing a 'new' load-term to separate the turbulence parameter from the U_c

In this research two calculation methods for the relative depth-averaged turbulent intensity (r_0) were compared. From the found trends between the relative turbulence intensities, calculated with the two different calculation methods, and the turbulence predictions of the numerical wave overtopping model, it can be concluded that both turbulence parameters present opposing trends for an increasing wave overtopping volume.

The current representation of the wave overtopping turbulence seems contradicting, as MIT (2016) also states that the general rule of thumb is that the turbulence level increases with the free stream velocity. Originally, the approach for the relative depth-averaged turbulent intensity, was developed for uniform, hydraulically smooth open-channel flows (Hoffmans, 1993; Schiereck, 2001; Hoffmans, 2012). However, these assumptions do not fit for wave overtopping as these flows are highly non-uniform and often very hydraulically rough (subsection 2.2.1.). Furthermore, the parametrisation of the relative depth-averaged turbulence intensity (r_0) was derived from the relative turbulence

intensity equations that use the Root-Mean-Square (RMS) of the turbulence fluctuations. The RMS turbulence intensity, represents the relative turbulence intensity in one flow direction (r_u, r_v or r_w), by dividing the mean velocity in one direction (\bar{u}) by the fluctuations in one direction (u') (Hoffmans, 1993; Schiereck, 2001; Hoffmans, 2012). On the other hand, the turbulence intensity (I) also represents the turbulence intensity in one direction, but uses the mean velocity in all directions ($u'v'w'$). The fluctuations in one direction (u') can be calculated using the square-root of 2/3 TKE ($\sqrt{2/3 k}$) (CFD, 2006). However, the relative turbulence intensity, uses the depth-averaged TKE ($\sqrt{k_0}$) in all directions ($u'v'w'$) and the mean depth-averaged velocity in one direction (\bar{u}), which is an opposite approach compared to the other turbulence intensity parameters. These contradicting observations and theories could indicate that the turbulence intensity (r_0) may be an incorrect representation of the wave overtopping turbulence, as pointed out in section 9.1.. However, this cannot be concluded based on this study alone.

A starting point to find whether the turbulence intensity (r_0) is a correct representation of the wave overtopping turbulence would be, to investigate whether the combination of the relative turbulence intensity, calculated with the Root-Mean-Square (RMS) turbulence fluctuations in the longitude (r_u) and transverse (r_w) direction of the flow, could improve the approach of wave overtopping turbulence. This combination of r_u and r_w could provide a more realistic turbulence trend for an increasing wave overtopping volume, as these turbulence intensity parameters provide an opposite reaction to flow acceleration and deceleration (Schiereck, 2001). Another option is to investigate whether another turbulence parameter can be used instead of r_0 . By implementing another turbulence parameter, such as the depth-averaged TKE (k_0) or the turbulence intensity (I), into the critical flow velocity equation, the empirical approach of wave overtopping turbulence would be changed. This is because the turbulence parameter might develop another relation towards U_c and might even need to be re-located. If the 'new' turbulence parameter is implemented, the sensitivity of the turbulence parameter can be re-evaluated by comparing the new trends with the wave overtopping observations and theories, as was done in this research. In addition, the use of the turbulence intensity within the critical flow velocity (U_c) equation should be re-evaluated, as the turbulence parameter is a load-term and not a strength-term (Bijlard, 2015; Bomers et al., 2018). This could provide a more realistic representation of the flow and erosion processes. A good starting point for this would be, to analyse whether a 'new' load-term can be introduced in which the transition and obstacle factor (α_m), the gravitational acceleration factor (α_a) and a turbulence parameter are combined. This 'new' load-term can then be directly used within the COM to increase or decrease the critical flow velocity (U_c), which represents the strength of the grass cover (strength-term), or the front velocity of the overtopping wave (U_i), which represents the load on the grass cover (load-term). Herein, the latter (increase or decrease the U_i) would be more appropriate.

9.3. Research limitations

In this section each discussion subject is introduced with a title and structured per paragraph as follows: first the subject is introduced, than the limitations of this subject will be discussed and lastly, a solution for the discussed limitations will be stated.

Applicability of the performed research for dikes with complex profiles

In this research, wave overtopping turbulence is analysed for a dike with a single slope angle and a single cover type. This means that the turbulence predictions only apply for dikes with a simple profile, especially for dikes with a slope of 1:4, as used in this research.

For this reason, the found trends, conclusions and recommendations are not (always) applicable for complex dike profiles with geometrical transitions (berms), cover material transitions and/or

obstacles. In addition, it is unknown whether the found trends and conclusions are applicable for dike slopes with different angles than the used slope angle of 1:4. Slope angle changes could largely affect the predicted turbulence maxima in OpenFOAM, as the flow acceleration, caused by the gravity, is related to the slope angle. Therefore, a steep slope will cause a greater acceleration of the flow and will cause the flow to gain more (turbulent kinetic) energy along the slope (Warmink et al., 2018).

To gain more insights into wave overtopping turbulence, the sensitivity of wave overtopping turbulence should also be analysed for wave overtopping scenarios at these complex dike profiles separately and combined. In addition, it is suggested to analyse the sensitivity of wave overtopping turbulence towards slope angle changes as well, for both a simple dike profile and complex dike profiles. If the same wave overtopping scenarios are applied (section 4.7.), the differences in sensitivity can be compared to each other, as well as, to the findings of this study for a simple dike profile. For the sensitivity analysis the same numerical wave overtopping model can be used as applied in this research. Only for the analysis of a dike profile with an obstacle, the applied OpenFOAM model cannot (yet) be used. This is because the current wave OpenFOAM model is a 2DV model, while obstacles can only be correctly simulated in a 3D model.

Applicability of the empirical equations for the boundary conditions

During this research, the wave overtopping model was validated using an adjusted equation for the maximum water layer thickness (h_{max}). This adjusted equation was used to increase the front and maximum velocity of the modelled flow. In addition, the adjusted equation corrected the volume balance of the boundary conditions used to simulate the target wave overtopping volume (subsection 4.5.3.).

Currently, the empirical equations for the maximum flow velocity (U_{max}), the overtopping period (T_0) and the original equation of h_{max} , only depend on the wave overtopping volumes. Overall, these empirical equations provide a good approximation of the wave overtopping distribution, but resulted in an underestimation of the target volume in this study.

Because the empirical equations only use the wave overtopping volume as an input variable, it is possible that this causes some errors. To improve the volume balance of these equations, the empirical equations can best be interconnected with each another, as was done with the adjusted equation for h_{max} . This way, the parameters can 'correct' one another. In addition, more measurable dike and wave overtopping characteristics could then be implemented into the empirical equations, instead of the wave overtopping volume alone. This could increase the applicability and accuracy of the empirical equations and can improve the validation process of the numerical model. Examples of measurable characteristics are; the slope angle of the outer slope, the height difference of the dike, the significant wave height and other simulation conditions (Table 2).

Uncertainties of the field measurement method

For the validation of the model, front velocity measurements of wave overtopping experiments at the Vecht dike were used. These wave overtopping tests were performed using the wave run-up simulator, to simulate overtopping waves on the crest and landward side of the dike. During the validation of the model, the modelled velocities and measured velocities presented a rather similar trend along the dike profile. However, the magnitude of the modelled velocities remained lower than the measured velocities (chapter 6).

The reason the measured and modelled front velocity differ in magnitude, could be caused by the used measurement method for the front velocity in the field. It is known that the measurement method, using the video camera, has a certain error. This error margin is now estimated to be approximately

0.5 m/s (subsection 3.1.2.). This measurement error is caused by the limited frequency of the used video camera (60 Hz) and the risk of human-error, as the captured film is manually analysed frame-by-frame. If the measurement error using of the video camera method is much larger than the approximated margin of 0.5 m/s, this could result in a large over- or underestimation of the critical flow velocity (U_c).

Because the impact of a large error margin on the resulting critical flow velocity and damage predictions is not known, it is suggested to analysis the impact of different front velocities (U_i) on the resulting critical flow velocity using the reverse engineering method with and without the use of the empirical equations for the U_c and r_0 . This could provide insights on the sensitivity of the critical flow velocity towards changes in front velocities. Furthermore, the error margin of video camera method could be reduces by using a camera with a higher frequency. To reduce the labour time of processing the frames and decrease the sensitive for human-error, it is possible to develop a postprocessing method. A starting point could be to investigate whether a computer program can be used to automatically calculate the front velocity using the distance markers along the profile to determine the position of the wave front. A way to let the program distinguish the wave front could be to, for example, change the contrast settings of the frames and using bright colours for the distance marker.

Unknown sensitivity of the water-air ratio and the initial TKE condition

In this study, model simulations in OpenFOAM have been performed, wherein a water-air ratio and an initial condition for the turbulent kinetic energy (k) were applied to the inlet of the numerical mesh. The water-air ratio was set to 80%-20% and the initial condition for the TKE was set to $0.05 \text{ m}^2/\text{s}^2$ (subsection 4.5.1. and 4.5.3.).

The use of a water-air ratio of 80/20 instead of 100/0, could also be a reason that the simulated flow is underestimate, as part of the assigned water layer thickness is likely replaced by air, causing the absolute amount of water entering the system to decrease. Another limitation is that the sensitivity of the model towards the initial condition for the turbulent kinetic energy (k) is relatively unknown.

To understand how the OpenFOAM model implements the water-air ratio into the water layer thickness, it is suggested to perform a model sensitivity analysis on the water-air ratio. This can be done by analysing the effects of water-air ratio changes on the modelled predictions, such as the flow velocity, shear stresses, water layer thickness and TKE. The obtained insights on the sensitivity can determine whether the empirical equation of the maximum water layer thickness should be adjusted to compensate for the water that is replaced by air. However, a water-air ratio is mainly needed when the water layer thickness is measured with a measuring method that does not measure the difference between water or air (Van Bergeijk et al., 2021). Because the water layer thickness was not measured at the selected test section at the Vecht dike, the need for a water-air ratio in this study can be questioned. In addition, it is suggested to perform a comparable model sensitivity analysis for the initial condition for the TKE.

Questionable TKE predictions for a roughness height of 4.0 cm

In order to select a roughness height (k_s) higher than the reference roughness height of 0.8 cm, a check was performed with three different roughness heights (4.0, 8.0 and 10.0 cm). This was done, to find whether the roughness height is not oversized compared to the cell sizes near the wall (section 4.7.2.). After the check, the roughness height of 4.0 cm was selected, because this roughness height presented, to some degree, similar turbulence predictions to the results for a roughness height of 0.8 cm. In addition, the Manning coefficient, calculated with a k_s of 4.0 cm (equation [23]), presented a n -value in range with grass covers.

Although, the roughness height of 4.0 cm presented similar turbulence predictions and a n -value in range with grass covers, there is still a chance that the model incorrectly schematises this roughness height. This is because the roughness height of 4.0 cm is rather larger, as it is close to the water layer thickness of the smaller overtopping waves (Table 5). In addition, it is questionable how realistic this roughness height is, as the overtopping wave will put pressure on the grass. This will reduce the grass length, hence decreasing the roughness height. This indicates that the grass has a changing and maximum roughness height. Therefore, it is possible that an 'absolute' grass length, was used, while a 'relative' grass length would be more appropriate.

It is suggested to analyse at which roughness heights the behaviour of the modelled turbulence drastically changes. Thereafter, analysing whether this increase occurs due to an incorrect schematisation of the applied roughness height. A starting point for this would be, to observed turbulence maxima for roughness heights larger than 0.8 cm. In addition, it is suggested to find the maximum 'relative' grass length, as this can provide an indication of the maximum roughness height for grass covers during wave overtopping. This could be done by, for example, measuring the grass length of different grass covers with the grass both, up straight and tilted. Thereafter, the measurements can be analysed to find a range and/or limit for the roughness height. For this tilted measurement it is might be needed to analyse how the grass can be tilted in the most realistic way.

Linking the roughness parameters to grass cover and wave overtopping characteristics

In this research, four roughness heights (0.008, 0.08, 0.8 and 4.0 cm) were selected to be used for the sensitivity analysis of wave overtopping turbulence within the OpenFOAM model.

During the selection of the four roughness heights, it could not easily be confirmed whether the applied roughness heights correspond to grass covers. This is because the roughness height (k_s) is not directly linkable to cover roughnesses or materials in the field. A method to indicate which cover material could apply for a selected roughness height, is to use the roughness height to calculate the Manning coefficient (subsection 4.7.2.). The calculated Manning coefficient can be used to find what type of cover corresponds to the applied roughness height (Arcement & Schneider, 1989). In this study, it was found that the roughness height influences the amount of fluctuations and behaviour along the profile of the turbulence maxima. This could indicate that the roughness height has a large influence than originally expected. Therefore, it would be beneficial if the roughness height can also be linked to cover characteristics, as this would make the roughness heights more applicable within wave overtopping turbulence calculations and modelling.

For this reason, it is suggested to directly link the applied roughness heights to the dike cover characteristics and wave overtopping characteristics. A starting point could be, to develop a parametrisation or chart, that uses, for example, the grass length of the cover, water layer thickness and/or velocity of the flow as an input. Herein, the grass length can determine the maximum roughness height, while the water layer thickness and/or flow velocity determines how much the grass height is reduced by the pressure of the water body of the overtopping wave. In addition, the roughness constant (C_s) can also be linked to the dike cover characteristics, such as the cover density and cover quality, through the use of a parametrisation or chart. This parametrisation or chart can be used to obtain a realistic roughness constant, which can represent the unevenness of the grass and damages on the cover. As the cover density and cover quality are not directly measurable, it is suggested to use/develop a type of quantification. This quantification can then also be used to describe the grass condition during wave overtopping experiments.

10

| Conclusion

The goal of this research is to gain more insights on wave overtopping turbulence, using a numerical wave overtopping model in OpenFOAM, and in the sensitivity of the empirical depth-averaged turbulence predictions. These insights could be used to improve the turbulence intensity parameter, which is used in various empirical equations, such as the critical flow velocity that is used in the COM, and in wave overtopping models. This can be used as a starting point to find at which locations wave overtopping turbulence can best be measured on a simple dike profile. To achieve this goal, three research questions and one main research question were defined. The conclusion of these research questions will be given per research question.

10.1. Validation of the wave overtopping model

The first research question states: *“Which turbulence models can best be selected to simulate wave overtopping turbulence in the OpenFOAM model and how do the predictions of the OpenFOAM model compare to wave overtopping experiments at the Vecht dike?”*

The most suitable turbulence model for the goal of this research, is the RANS $k - \omega$ SST model. The RANS-based turbulence model requires the least computational time and has a less complex model set-up. The time averaged turbulence output of this turbulence model is also more appropriate for this study, as more accurate estimates of small scale turbulent processes cannot be validated and would therefore be less useful for this research. From the available RANS-based turbulence models, the $k - \omega$ SST model was chosen, as this model is the most suitable for wave overtopping modelling. This RANS-based model can accurately resolve the turbulence in both, the near-wall region and the freestream.

The original numerical wave overtopping model developed by Van Bergeijk et al. (2020) provides appropriate wave overtopping front velocity predictions. However, a validation needed to be performed, using different settings, to improve the velocity predictions. In addition, the used empirical equations for the boundary conditions in the original settings, resulted in slightly lower wave overtopping volumes than the target volumes. Therefore, an adjusted equation for the maximum water layer thickness (h_{max}) was used for the boundary condition of the water layer thickness at the inlet. This adjustment improved the predicted wave overtopping front velocities, as the modelled velocities were increased and the boundary conditions resulted in the target volume. Based on the performed validation, it can be concluded that the current empirical equations, used to calculate the maximum flow velocity (U_{max}), the maximum layer thickness (h_{max}) and the overtopping period (T_0), do not present the correct target wave overtopping volume for the selected section of the Vecht dike. However, the target volume of these empirical equations can be improved by incorporating more wave overtopping characteristics than solely the wave overtopping volume, as was done in this study.

10.2. Sensitivity of turbulence towards volume and roughness

The second research question states: *“What variabilities of the wave overtopping turbulence are predicted by the OpenFOAM model for a simple dike profile and how sensitive are these predicted wave overtopping turbulence variabilities towards the modelled wave overtopping volume and bed roughness?”*

Wave overtopping turbulence seems to be sensitive towards changes in wave overtopping volume, roughness height and the combination of both. The change of these parameters provides different trends, depending on the simulated combination. Overall, the wave overtopping volume affects the magnitude of the TKE, while the roughness height affects the number of fluctuations and the behaviour of the TKE along the dike profile. It was found that the wave overtopping turbulence increases linearly when the wave overtopping volume increases, regardless of the applied roughness height. In addition, when the wave overtopping volume increases, the observed maximum turbulence increases exponentially. This means that the maximum turbulence within a wave overtopping becomes significantly larger than the maximum significant and maximum mean TKE for increasing wave overtopping volumes. Furthermore, it was found that the difference between the maximum TKE and the significant and mean TKE is especially large when a roughness height of 4.0 cm is applied. This shows that the turbulence peaks become significantly higher when significantly large roughness heights are used (4.0 cm). There is, however, still a possibility that this roughness height is incorrectly schematised by the model.

In general, wave overtopping turbulence also increases when the roughness height is increased, as the mean TKE increases for an increasing roughness height. On the other hand, it was found that the significant TKE decreases when the roughness height increases, except between the roughness heights of 0.8 and 4.0 cm, where the significant TKE increases. As this decreasing trend occurs for all wave overtopping volumes between the roughness heights of 0.008 and 0.8 cm, this could indicate that a threshold roughness height might exist at which the lowest possible significant TKE can be obtained. Furthermore, it stands out that for an increasing wave overtopping volume at a roughness height of 4.0 cm, the significant turbulence increases exponentially. This exponential growth is caused by the large influence of the peak in turbulence, which increases exponentially for an increasing the wave overtopping volume.

The location along the dike profile where the modelled turbulence maxima occur, during wave overtopping, are also found to be sensitive to the change in wave overtopping volume and roughness height. In general, the position of the turbulence maxima shifts towards the toe of the dike when the wave overtopping volume increases. Whereas, the turbulence maxima shifts towards the crest of the dike for increasing roughness heights. Furthermore, it was found that the distance between the location of the turbulence maxima depends on the applied roughness height. When large enough roughness heights (4.0 cm) are applied, it was found that the maximum, significance and mean TKE occur at the same location. This is because the significant increase of the maximum TKE, for these larger roughness heights, largely influence the significance and mean TKE. If the roughness height of 4.0 cm is correctly schematised by the model, it could be possible that the maximum TKE is responsible for wave overtopping damage at larger roughness heights (4.0 cm), but that all three TKE maxima become important when lower roughness heights are used (<0.8 cm). To conclude, whether one of the turbulence maxima or the combined effort of all three turbulence maxima contribute the most to wave overtopping damage, it is suggested to validate whether the predicted positioning of the turbulence maxima correlates with observed location of damage in the field.

10.3. Similarities and differences in turbulence predictions

The third research question states: *“To what extent does the turbulence parameter, used in the empirical models to predict wave overtopping damage, represent the changes in the predicted wave overtopping turbulence for different wave overtopping volumes and bed roughnesses?”*

The relative depth-averaged turbulence intensity (r_0), used in the empirical relations, can be calculated using different equations. In this research, two approaches for the relative turbulence intensity have been compared to analyse the sensitivity of this turbulence parameter. In equation [27], the modelled mean depth-averaged TKE ($\overline{k_0}$) and the modelled mean depth-averaged velocities (\overline{u}) are used directly. In equation [28], the Chézy coefficient (equation [26]) is calculated using the modelled mean water layer thicknesses (\overline{h}) and the implemented roughness heights (k_s). This means that both approaches use the OpenFOAM model output as input for the calculation.

$$r_0 = \frac{\sqrt{\overline{k_0}}}{U_0} \quad [27] \quad r_0 = \frac{\alpha_0 \sqrt{g}}{C} \quad [28]$$

The results of this sensitivity analysis show that both calculation methods for the relative depth-averaged turbulence intensities (r_0) present a linear decrease for an increasing wave overtopping volume and a non-linear increase for an increasing roughness height. This decreasing trend for an increasing volume, is caused by the fact that both the velocity and water layer thickness increase when the wave overtopping volume increases. It can be noted from equation [27] that the turbulence intensity (r_0) will decrease when the TKE increases proportional to the depth-average velocity (U_0). On the other hand, it can be noted from equation [28] that the turbulence intensity (r_0) will also decrease when the Chézy coefficient (C) increases, which happens when either the roughness height reduces or the water layer thickness (h) becomes thicker (equation [26]). This means that the critical flow velocity (U_c) increases for an increasing flow velocity, resulting in a lower risk of erosion for an increasing wave overtopping volume. Herein, assuming that the grass strength is uniform along the dike profile. If a turbulence intensity would be calculated for multiple locations along the dike profile, this would result in a higher risk of erosion at the dike crest than near the toe for a simple dike, as the flow velocity over a simple dike profile will increase towards the dike toe due to gravitational acceleration. Previous studies, however, established that wave overtopping failure is more likely to occur near the toe of a simple dike profile, which seems contradicting.

In general, when r_0 is calculated with equation [27], the resulting turbulence intensities show high intensity values ($r_0 = 0.25 - 0.6$). On the other hand, the resulting turbulence intensities show lower intensity values for each scenario when r_0 is calculated with equation [28] ($r_0 = 0.055 - 0.4$). Although both calculation methods provide the same trends, it can still be stated that the turbulence intensity varies largely, depending on the approach. This is because the range, magnitude and sensitivity of both turbulence intensity calculations are quite different, which could largely impacts the predicted wave overtopping damage of the COM due to the change in U_c . In addition, it was found that the range of the computed turbulence intensities could be realistic intensities for wave overtopping turbulence, as previous studies mainly used reverse engineering to obtain the turbulence intensity. This reverse engineering approach, could cause the turbulence to be underestimated, as the relative turbulence intensity equations were originally developed for hydraulically smooth uniform open-channel flows.

10.4. Comparison of the modelled and calculated turbulence

The main research question states: *“To what extent does the wave overtopping turbulence predicted with an OpenFOAM model for the slope of a simple dike profile, with a single slope angle and cover type, vary with the cover roughness and wave overtopping volume and is this variability represented in the turbulence parameter that is used in the empirical models to predict wave overtopping damage on the landward dike slopes?”*

According to the findings in this study, the relative depth-averaged turbulent intensity (r_0), independent of the used calculation method, and the turbulence predictions of the numerical wave overtopping model, both present a non-linear increase for an increasing roughness height. However, the relative turbulence intensity (r_0) presents contradicting trends compared to the modelled TKE for an increasing wave overtopping volume. This difference in trend between the turbulence maxima and the relative turbulence intensity is caused by the fact that both turbulence parameters represent different turbulence quantities. However, because both parameters represent the amount of turbulence within a flow, it is important to validate whether the relative turbulence intensity is a correct representation of wave overtopping turbulence. As often reverse engineering is used to obtain the r_0 , it is possible that another turbulence parameter, such as the depth-averaged TKE (k_0) or the root mean square (RMS) turbulent intensity in multiple flow directions (r_u, r_w), would provide a more appropriate representation of wave overtopping turbulence.

Furthermore, the turbulence intensity parameter is currently often used to help calibrate the critical flow velocity in order to fit the field measurements. This is possible as U_c reacts proportional to r_0 . This suggests that the processes of turbulence, are applied to correct the critical flow velocity for each wave overtopping scenario. This could easily lead to misrepresentations of the processes that occur in reality, as wave overtopping turbulence, pressure, tensile stresses and shear stresses are closely related to one another and to the onset of wave overtopping erosion. Therefore, it is pointed out in this research that the relative depth-average turbulence intensity is probably used incorrectly. It would be more appropriate to separate the turbulence intensity from the critical flow velocity (U_c) equation. This separation can be done by introducing a ‘new’ load-term, in which the transition and obstacle factor (α_m), the gravitational acceleration factor (α_a) and a turbulence parameter are combined. This ‘new’ load-term can then be directly used within the COM to increase or decrease the critical flow velocity (U_c), which represents the strength of the grass cover (strength-term), or the front velocity of the overtopping wave (U_i), which represents the load on the grass cover (load-term). Herein, the latter (increase or decrease the U_i) would be more appropriate.

| Further recommendations

In this chapter, some recommendations are presented. These recommendations can be used by Infram Hydren and other researchers as a starting point for further research. In addition, further work, which are subjects for further research that have not been researched in this study, are pointed out.

11.1. Recommendations for the empirical equations in the COM

In this research, two calculation methods for the relative depth-averaged turbulent intensity (r_0) were compared. It was found that both calculation methods for the relative turbulence intensity present the similar trends. However, the magnitude and range of the results and the sensitivity towards changes in wave overtopping volume and roughness height, depend on the used approach. It is recommended to evaluate the sensitivity, magnitude and range of the relative turbulence intensity using different formulations. This can be done by, firstly, empirically computing the r_0 for a certain set of wave overtopping volume and roughness height scenarios using these different formulations. Secondly, r_0 should be computed using the (different) reverse engineering method(s) for the same set of wave overtopping volume and roughness height scenarios and for the same r_0 formulations. After the relative turbulence intensities are obtained, using empirical equations and reverse engineering, it is possible to compare the sensitivity, magnitude and range of r_0 for each r_0 formulation. For this evaluation, it would be best to first, separately analyse the empirically obtained turbulence intensities and the turbulence intensities obtained using reverse engineering. When the behaviour of each relative turbulence intensity formulation is known, it is possible to analyse the differences in sensitivity, magnitude and range between the empirically obtained r_0 and the r_0 obtained using reverse engineering. This can provide more insights on the possible range, appropriateness and accuracy of r_0 for wave overtopping scenarios.

It is also recommended to make the turbulence parameter and critical flow velocity variable towards changes in wave overtopping scenarios, by incorporating more non-constant parameters into the empirical equations. For example, the slope angle, maximum velocity, maximum water layer thickness and overtopping period could be implemented. Hoffmans (2012) does present an empirical equation that incorporates some of these wave overtopping scenario dependent parameters, wherein the turbulence intensity on the slope is estimated using a different equation than the turbulence intensity on the crest (Van Bergeijk et al., 2019a).

Furthermore, it is possible to make the critical flow velocity somewhat variable along the dike profile, by assigning, for example, critical velocities to different sections of the dike profile, such as the crest, upper slope, lower slope and toe.

In addition it is recommended, to analyse the sensitivity of wave overtopping turbulence towards the water layer thickness and wave overtopping velocities separately. This can give insights in how wave overtopping turbulence is related to the wave overtopping volume at a simple dike profile. This can be done by using separate scenarios for the water layer thickness and wave overtopping velocities in

OpenFOAM, to find out which of these parameters has more influence on the predicted TKE. In addition, these volume scenarios can be combined with slope angle scenarios to analyse how an increase in acceleration (due to gravity) and different transitions in slope angles affect the wave overtopping turbulence.

11.2. Recommendations for further model research

During this research, field measurements were used to validate the numerical wave overtopping model. To validate the model, a new postprocessing method was needed to obtain the front velocity in the model, as only the front velocity was measured at test section 3-2 of the Vecht dike. Therefore, specific velocity data needed to be sampled per location in time (section 5.2.). Due to the used sampling method for the model output and the small amount of available field data, increased the uncertainty of the validation. For the development of the original model, more field data as a function of time was available, which increased the certainty of the validation, as the sample time of the model and field measurements could be set to the same interval (subsection 3.1.2.). However, because the measuring method with the video camera is currently the preferred method, it is recommended to test various sampling methods for the front velocity. This will to help obtain better comparable front velocities and increases the certainty of the model validation. The postprocessing method of the front velocity can be investigated and improved by testing different postprocessing methods and by comparing the results of each modelled front velocity with the field data of the front velocity, for different wave overtopping volumes and dike profiles. Furthermore, it is recommended to measure the maximum and/or mean water height for each test section at least once, using, for example, the surfboard method, as the water height is an important input parameter for the empirical equations and wave overtopping models. These measurements can used to validate the (trend of the) h_{max} .

In this study, turbulence quantities have been extracted from a numerical wave overtopping model in order to analyse the sensitivity of turbulence. Herein, the choice was made to only analyse the (depth-averaged) turbulent kinetic energy (k_0). However, in addition to the TKE, the dissipation rate is also known as an important indication of turbulence. The dissipation rate determines the amount of kinetic energy that is converted into heat, due to large velocity gradients in the turbulent flow and the viscous forces near the wall. Therefore, the TKE and dissipation rate are important parameters within the energy cascade of turbulence (section 2.1.). Furthermore, it is possible that both, the TKE and dissipation rate, are responsible for wave overtopping turbulence erosion. For this reason it is highly recommended, that the dissipation rate is also analysed for a simple dike profile using the same wave overtopping volume and roughness height scenarios, as used in this research.

| References

- Hart, R., de Bruijn, H., & de Vries, G. (2016). *Fenomenologische beschrijving faalmechanismen wti*. Retrieved from Deltares:
- Aguilar-López, J., Warmink, J., Bomers, A., Schielen, R., & Hulscher, S. (2018). Failure of grass covered flood defences with roads on top due to wave overtopping: A probabilistic assessment method. *Journal of Marine Science and Engineering*, 6(3). doi:10.3390/jmse6030074
- Arcement, G. J., & Schneider, V. R. (1989). *Guide for selecting manning's roughness coefficients for natural channels and flood plains*.
- Beudin, A., Kalra, T. S., Ganju, N. K., & Warner, J. C. (2017). Development of a coupled wave-flow-vegetation interaction model. *Computers & Geosciences*, 100, 76-86. doi:10.1016/j.cageo.2016.12.010
- Bijlard, R. W. (2015). *Strength of the grass sod on dikes during wave overtopping*. (MSc). TU Delft and Infram,
- Bijlard, R. W., Steendam, G. J., Verhagen, H. J., & Van der Meer, J. (2016). Determining the critical velocity of grass sods for wave overtopping by a grass pulling device.
- Bomers, A., Aguilar Lopez, J. P., Warmink, J. J., & Hulscher, S. J. M. H. (2018). Modelling effects of an asphalt road at a dike crest on dike cover erosion onset during wave overtopping. *Natural Hazards*, 93(1), 1-30. doi:10.1007/s11069-018-3287-y
- CFD, O. (2006, 2021). Turbulence intensity. Retrieved from https://www.cfd-online.com/Wiki/Turbulence_intensity
- Chen, W. (2019). *Study on wave overtopping of flood defenses*. (Literature report). University of Twente,
- De Serio, F., & Mossa, M. (2019). Experimental observations of turbulent events in the surfzone. *Marine Science and Engineering*, 15.
- Estrado, E. (2019). *Optimisation of complex geometry buildings based on wind load analysis*. Fluid Mechanics (Producer). (2019). [cfd] the k - epsilon turbulence model. Retrieved from <https://www.youtube.com/watch?v=fOB91zQ7HJU&list=PLVKU8cvQithfqvjusvDzqmRTCdNdwb4sL&index=2&t=5s>
- Fluid Mechanics (Producer). (2020). [cfd] large eddy simulation (les). Retrieved from https://www.youtube.com/watch?v=r5vP45_6fB4&list=PLVKU8cvQithfqvjusvDzqmRTCdNdwb4sL&index=6&t=29s
- Hoffmans, G., Stuparu, D., Van Hoven, A., & Labrujere, A. (2016). *Effects of transitions and objects on the erodibility of grass revetments on dikes*. Paper presented at the 8th International Conference on Scour and Erosion, Oxford, UK.
- Hoffmans, G., van Hoven, A., Harderman, B., & Verheij, H. (2014). Erosion of grass covers at transitions and objects on dikes. In *Scour and erosion* (pp. 643-649).
- Hoffmans, G., Van Hoven, A., Steendam, G.-J., & Van der Meer, J. (2018). *Summary of research work about erodibility of grass revetments on dikes*. Paper presented at the International Conference on Protection against Overtopping (third), The United Kingdom.
- Hoffmans, G. J. C. M. (1993). *A study concerning the influence of the relative local turbulence on local-scour holes* (W-DWW-93.251). Retrieved from
- Hoffmans, G. J. C. M. (2012). *The influence of turbulence on soil erosion*: Eburon.
- Horstman, E. M., Bryan, K. R., Mullarney, J. C., Pilditch, C. A., & Eager, C. A. (2018). Are flow-vegetation interactions well represented by mimics? A case study of mangrove pneumatophores. *Advances in Water Resources*, 12.

- Hughes, S. A., Thornton, C. I., Van der Meer, J. W., & Scholl, B. N. (2012). Improvements in describing wave overtopping processes. *Coastal Engineering Proceedings*, 1(33). doi:10.9753/icce.v33.waves.35
- Jüpner, R. (2018). Coping with extremes - experiences from event management during the recent elbe flood disaster in 2013. *Journal of Flood Risk Management*, 11(1), 15-21. doi:10.1111/jfr3.12286
- Kantha, L. H., & Clayson, C. A. (2000). *Small scale processes in geophysical fluid flows* (Vol. 67): International Geophysics.
- Kok, J. (2000). Resolving the dependence on freestream values for the k-omega turbulence model. *AIAA journal*, 38. doi:10.2514/3.14547
- Launder, B., & Sharma, B. I. (1974). Application of the energy-dissipation model of flow near a spinning disc. *Lett. Heat Mass Transfer*, 131-138.
- Launder, B., & Spalding, D. B. (1974). The numerical computation of turbulent flows. *Comput. Methods Appl. Mech. Eng.*, 103, 456-460.
- Le, H. T., & Verhagen, H. (2014). Damage to grass covered slopes due to overtopping. *Coastal Engineering Proceedings*, 1, 9. doi:10.9753/icce.v34.structures.9
- Li, T., Troch, P., & De Rouck, J. (2004). Wave overtopping over a sea dike. *Journal of Computational Physics*, 198(2), 686-726. doi:10.1016/j.jcp.2004.01.022
- Liu, F. (2017). *A thorough description of how wall functions are implemented in openfoam*. Retrieved from
- Loper, D. E. (2007). *Turbulence and small-scale dynamics in the core* (Vol. 8): Elsevier.
- Marisa, N. (2014). Application of rans/pdf & les/fdf methods to prediction of premixed turbulent flames. Retrieved from <https://www.slideserve.com/marisa/application-of-rans-pdf-les-fdf-methods-to-prediction-of-premixed-turbulent-flames>
- Menter, F. R. (1992). Influence of freestream values on k-omega turbulence model predictions. *AIAA journal*, 30(6), 1657-1659. doi:10.2514/3.11115
- Menter, F. R. (1994). Two-equation eddy-viscosity turbulence models for engineering applications. *AIAA journal*, 32(8), 1598-1605. doi:10.2514/3.12149
- MIT, M. I. o. T. (2016). Basics of turbulent flow. Retrieved from <http://www.mit.edu/course/1/1.061/www/dream/SEVEN/SEVENTHEORY.PDF>
- Mom, R., Daamen, E., Overduin, M., Wauben, C., & Wegman, R. (2021). *Factual report praktijkproeven gras op zand*. Retrieved from
- Nikolaidou, L. (2019). *Wall-modelled large eddy simulation of fully rough non-uniform flow for the purpose of predicting stone stability*
- (MSc). Delft University of Technology,
- Nortier, I. W., Nortier, J. W., & de Koning, P. (2014). *Toegepaste vloeistofmechanica: Hydraulica voor waterbouwkundigen*: Stam Techniek.
- OpenCFD, L. (2016). Openfoam: User guide v2012 - turbulence. Retrieved from <https://www.openfoam.com/documentation/guides/latest/doc/guide-turbulence.html>
- Ponsioen, L. A. (2016). *Overflow and wave overtopping induced failure processes on the land-side slope of a dike*. (MSc). TU Delft,
- Robert, A. (2003). *River processes: An introduction to fluvial dynamics*: Arnold.
- Schiereck, G. J. (2001). *Introduction to bed, bank and shore protection*: Delft University Press.
- Stewart, R. W. (Writer) & E. D. Center (Director). (1969). Film notes for turbulence. In *National Committee for Fluid Mechanics Films*. The United States of America: Encyclopaedia Britannica Educational Corporation.
- Stull, R. B. (1988). Turbulence kinetic energy, stability and scaling. In R. B. Stull (Ed.), *An introduction to boundary layer meteorology* (pp. 151-195). Dordrecht: Springer Netherlands.
- Ting, F. C. K., & Reimnitz, J. (2015). Volumetric velocity measurements of turbulent coherent structures induced by plunging regular waves. *Coastal Engineering*, 104, 93-112. doi:10.1016/j.coastaleng.2015.07.002

- Urone, P. P., Hinrichs, R., Dirks, K., & Sharma, M. (2020, 2020). Viscosity and laminar flow; poiseuille's law. Retrieved from [https://phys.libretexts.org/Bookshelves/College_Physics/Book%3A_College_Physics_\(OpenStax\)/12%3A_Fluid_Dynamics_and_Its_Biological_and_Medical_Applications/12.04%3A_Viscosity_and_Laminar_Flow_Poiseuilles_Law](https://phys.libretexts.org/Bookshelves/College_Physics/Book%3A_College_Physics_(OpenStax)/12%3A_Fluid_Dynamics_and_Its_Biological_and_Medical_Applications/12.04%3A_Viscosity_and_Laminar_Flow_Poiseuilles_Law)
- Valk, A. (2009). *Wave overtopping - impact of water jets on grassed inner slope transitions*. (MSc). TU Delft,
- Van Bergeijk, V. M., Warmink, J. J., Frankena, M., & Hulscher, S. J. M. H. (2019a). *Modelling dike cover erosion by overtopping waves: The effects of transitions*. Paper presented at the Coastal Structures 2019, The Netherlands.
- Van Bergeijk, V. M., Warmink, J. J., & Hulscher, S. J. M. H. (2020). Modelling the wave overtopping flow over the crest and the landward slope of grass-covered flood defences. *Journal of Marine Science and Engineering*, 8(7). doi:10.3390/jmse8070489
- Van Bergeijk, V. M., Warmink, J. J., & Hulscher, S. J. M. H. (2021). *Experimental set-up and modelling tools for the load by overtopping waves in erosion models*. Retrieved from
- Van Bergeijk, V. M., Warmink, J. J., & Hulscher, S. J. M. H. (2022). The wave overtopping load on landward slopes of grass-covered flood defences: Deriving practical formulations using a numerical model. *Coastal Engineering*, 171, 104047. doi:<https://doi.org/10.1016/j.coastaleng.2021.104047>
- Van Bergeijk, V. M., Warmink, J. J., Van Gent, M. R. A., & Hulscher, S. J. M. H. (2019b). An analytical model of wave overtopping flow velocities on dike crests and landward slopes. *Elsevier*, 11.
- Van der Meer, J. W. (2011). The wave run-up simulator - idea, necessity, theoretical background and design. 75.
- Van der Meer, J. W. (2021). *Hydraulische metingen voor de golfoverslagen golfoploopsimulator*. Retrieved from Van de Meer Consulting B.V.:
- Van der Meer, J. W., Hardeman, B., Steendam, G. J., Schüttrumpf, H., & Verheij, H. (2011). Flow depths and velocities at crest and landward slope of a dike, in theory and with the wave overtopping simulator. *Proceedings of the International Conference on Coastal Engineering; No 32 (2010): Proceedings of 32nd Conference on Coastal Engineering, Shanghai, China, 2010.; structures.10*.
- Van der Meer, J. W., Schrijver, R., Hardeman, B., van Hoven, A., Verheij, H. J., & Steendam, G. J. (2010). *Guidance on erosion resistance of inner slopes of dikes from three years of testing with the wave overtopping simulator*. Paper presented at the 9th International Conference Coasts, marine structures and breakwaters, Edinburgh, UK - London.
- Vassilicos, J. C. (2015). Dissipation in turbulent flows. *Annual Review of Fluid Mechanics*, 47(1), 95-114. doi:10.1146/annurev-fluid-010814-014637
- Wang, G., Yang, F., Wu, K., Ma, Y., Peng, C., Liu, T., & Wang, L.-P. (2021). Estimation of the dissipation rate of turbulent kinetic energy: A review. *Chemical Engineering Science*, 229. doi:10.1016/j.ces.2020.116133
- Warmink, J., van Bergeijk, V., Chen, W., Aguilar Lpez, J. P., Bomers, A., & Hulscher, S. (2018). *Modelling wave overtopping for flood defense reliability*.
- Warmink, J. J., Van Bergeijk, V. M., Frankena, M., Van Steeg, P., & Hulscher, S. J. M. H. (2020). *Quantifying the influence of transitions on grass cover erosion by overtopping waves*. Paper presented at the 37th International Conference on Coastal Engineering, ICCE 2020. <https://doi.org/10.9753/icce.v36v.papers.39>
- Wolanski, E., & McLusky, D. (2011). *Treatise on estuarine and coastal science*: Elsevier.
- Yuan, S., Li, L., Amini, F., & Tang, H. (2014). Turbulence measurement of combined wave and surge overtopping of a full-scale hptrm-strengthened levee. *Journal of Waterway, Port, Coastal and Ocean Engineering*, 14.
- Zhang, H., Nakagawa, H., Kawaike, K., & Baba, Y. (2010). Experiment and simulation of turbulent flow in local scour around a spur dyke. *International Journal of Sediment Research*, 24, 13.

Explanation of the turbulence models

The first turbulence models were based on the mixing length approach. These models used the mixing length (l_m), which describes the size of turbulence eddies in the flow, to calculate the eddy viscosity (μ_t) (Launder & Spalding, 1974). However, because the mixing length is specified algebraically, the mixing length approach (l_m) became less popular when resolving turbulence.. This is because the mixing length, as can be seen in equation 2, only depend on the distance from the wall. This means that when the domain is fixed (no variation in time), the mixing length and thus the eddy viscosity will be fixed as well, which is not representative for turbulence. To better resolve turbulence, it became more popular to use models that solve transport equations (Wang et al., 2021). This could be done by solving the turbulent dissipation rate (ε) instead of l_m , as done in equation 3. In addition, the mixing length (l_m) can also be calculated using the turbulent dissipation rate (ε) after equation 1 and 3 are combined into equation 4. In equations 3 and 4 , the symbol C_μ represents the turbulence model coefficient for the turbulent viscosity (μ_t) and usually has the value 0.09 [-] (Launder & Sharma, 1974; Launder & Spalding, 1974). Equation 4 is based on the turbulent mixing length (l_m), but now describes the turbulent length scale (l) instead due to the presence of the turbulent dissipation rate (ε) in the equation. The turbulent length scale (l) is therefore closely related to the turbulent mixing length (l_m) and describes the size of the largest eddies in the flow, as these eddies contain the most turbulent kinetic energy.

$$l_m = \kappa y \quad \text{with} \quad \kappa = 0.41 \quad [2] \quad \mu_t = C_\mu \frac{\rho k^2}{\varepsilon} \quad [3] \quad l = \frac{C_\mu k^{3/2}}{\varepsilon} \quad [4]$$

1.1. Reynolds Average Navier Stokes turbulence models

RANS-based models use Reynolds Averaged Navier Stokes equations (equation 5 and 6) to resolve the turbulence in the flow. RANS models use the Reynolds stresses ($u = \bar{u} + u'$) to separate the mean velocity from the turbulent fluctuations in the Navier Stokes equation. In Figure 24 an example is presented of the velocity time series of a turbulence flow structure. The black dotted line in this figure represents the mean velocity, while the red line represents the turbulent fluctuations in the flow.

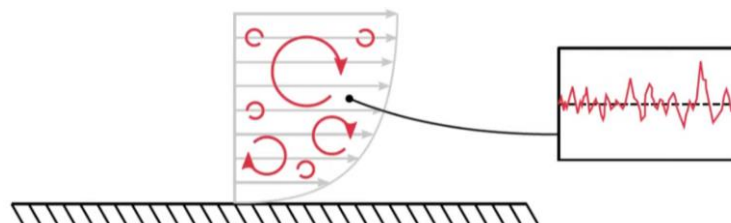


Figure 24 – An example of a velocity time series of a turbulence flow structure. The black dotted line represents the mean velocity and the red line represents the turbulent fluctuations over time. Note: reprinted from Fluid Mechanics (2019)

The standard Reynolds Averaged Navier Stokes equation is presented in equation 5. By rewriting equation 5 the turbulent fluctuations can be obtained. The RANS-based models use this new equation (equation 6) to resolve the averaged turbulence over time. Eventually the eddy viscosity (μ_t) is used to close the momentum equations. In the equations the u -terms represent the velocity, the δ -term represent the Kronecker delta and the f -term represent external forces. These all are denoted in Reynolds-averaged terms ($u(x, t) = \bar{u}(x) + u'(x, t)$) in the i -direction and j -direction. The Reynolds decomposition separates flow variables, such as the velocity, into a mean time-averaged component

($\bar{u}(x)$) and into a component which fluctuates in time and space ($u'(x, t)$). These fluctuating components represent the turbulence ($\overline{\rho u'_i u'_j}$). ρ is the density and μ is viscosity.

$$\rho \bar{u}_j \frac{\partial \bar{u}_i}{\partial x_j} = \rho \bar{f}_i + \frac{\partial}{\partial x_j} \left[-\bar{p} \delta_{ij} + \mu \left(\frac{\partial \bar{u}_i}{\partial x_j} + \frac{\partial \bar{u}_j}{\partial x_i} \right) - \rho \overline{u'_i u'_j} \right] \quad [5]$$

$$\frac{\partial \overline{\rho u'_i u'_j}}{\partial x_j} = -\rho \bar{u}_j \frac{\partial \bar{u}_i}{\partial x_j} + \rho \bar{f}_i + \frac{\partial}{\partial x_j} \left[-\bar{p} \delta_{ij} + \mu \left(\frac{\partial \bar{u}_i}{\partial x_j} + \frac{\partial \bar{u}_j}{\partial x_i} \right) \right] \quad [6]$$

RANS-based models can vary from one equation to four equations needing to be solved. The most popular RANS-based models are the standard k-epsilon (k- ϵ) model, the Wilcox's k-omega (k- ω) model and the k-omega SST model. These models use two equations to resolve the turbulence. For all RANS-based turbulence models many different versions have been developed over time. To gain a better understanding on the approach and differences between RANS-based models, the three most popular models will be explained below.

1.2. K-Epsilon turbulence model

The standard k-epsilon turbulence model was developed in 1973 and is one of the most popular turbulence models. It was one of the first turbulence models available and the first model based on the transport equations (Kok, 2000). The standard k- ϵ model uses two transport equations, which are solved to compute k, the turbulent kinetic energy in m^2/s^2 , and ϵ , the turbulent dissipation rate in m^2/s^3 . The transport equation for k is presented in equation 7, while the transport equation for ϵ is presented in equation 8.

$$\underbrace{\frac{\partial(\rho k)}{\partial t}}_{\text{Time}} + \underbrace{\nabla \cdot (\rho k \mathbf{U})}_{\text{Convection}} = \underbrace{\nabla \cdot \left(\left(\mu + \frac{\mu_t}{\sigma_k} \right) \nabla k \right)}_{\text{Diffusion}} + \underbrace{P_k + P_b - \rho \epsilon + S_k}_{\text{Source + Sinks}} \quad [7]$$

In the diffusion term of equation 7 the parameter μ represents the molecular viscosity, while the parameter σ_k represents a standard k-epsilon model constant, which usually has the value 1.0. The source terms in equation 7 are P_k , which represents the production of turbulent kinetic energy (TKE) caused by the mean velocity shear, P_b , which represents the production of TKE caused by the buoyancy, and S_k , which represents a user-defined source of TKE. On the other hand the sink term is represented by $\rho \epsilon$, which is the density (ρ) multiplied by the turbulent kinetic dissipation rate (ϵ). This can be seen in equation 7, where epsilon (ϵ) is presented in red. If ϵ is large then turbulence dissipation is strong and if ϵ is low turbulent dissipation is small. It is expected that the dissipation (ϵ) becomes higher near walls and shear layers.

$$\underbrace{\frac{\partial(\rho \epsilon)}{\partial t}}_{\text{Time}} + \underbrace{\nabla \cdot (\rho \mathbf{U} \epsilon)}_{\text{Convection}} = \underbrace{\nabla \cdot \left(\left(\mu + \frac{\mu_t}{\sigma_k} \right) \nabla \epsilon \right)}_{\text{Diffusion}} + \underbrace{C_1 \frac{\epsilon}{k} (P_k + C_3 P_b) - C_2 \rho \frac{\epsilon^2}{k} + S_\epsilon}_{\text{Source + Sinks}} \quad [8]$$

The model coefficients C_1, C_2, C_3 & C_n depend on the variant of the chosen model and have evolved in a very short time after the development of the k-epsilon model. In Table 10 some widely used coefficients are presented. The red coefficients are considered to be the most accurate versions, wherein Launder & Sharma (1974) is the most up-to-date version.

Table 10 - Examples of the most popular model coefficient variants used in the transport equation for the turbulent kinetic dissipation rate. The red numbers represents the most accurate coefficient versions, while the boldness indicates which version is most up-to-date (Fluid Mechanics, 2019).

Model	σ_k	σ_ϵ	C_1	C_2	C_3
Jones & Launder (1972)	1.0	1.3	1.55	2.0	0.09
Launder & Spalding (1974)	1.0	1.3	1.44	1.92	0.09
Launder & Sharma (1974)	1.0	1.3	1.44	1.92	0.09

When the transport models have been solved, the kinematic/eddy viscosity (μ_t) can be computed using k and ϵ .

$$\mu_t = C_\mu \frac{\rho k^2}{\epsilon} \quad \text{with} \quad C_\mu = 0.09 \quad [9]$$

The turbulent dissipation rate (ϵ) is the product of kinematic viscosity gradient and velocity gradient of the existing turbulent fluctuations. Therefore, it is possible to mathematically calculate epsilon (ϵ) with use of equation 10 (Launder & Spalding, 1974). However, equation 10 can only be used if the time series for the velocity field and the size of the velocity field is known. When a RANS model is used it is not possible to mathematically calculate epsilon (ϵ), as the turbulent fluctuations in the velocity (U'_i) are unknown. For this reason RANS models will calculate ϵ directly instead, with use of the presented transport equations.

$$\epsilon = \nu \frac{\partial U'_i}{\partial x_j} \frac{\partial U'_i}{\partial x_j} \quad [10]$$

Low-Re formulation

In addition to the model coefficients (C_1, C_2, C_3 & C_n) the k-epsilon model can also take damping effects, caused by the viscous sub-layer, into account. However, instead of using an exponential decay, as is done in the mixing length approach, the k-epsilon model accounts for damping through the use of damping terms (f_1, f_2, f_3 & f_n). This formulation of the k-epsilon model for damping is called the **low-Re formulation** (low-Reynolds number formulation), which is used to calculate the more laminar flow in the viscous sub-layer. The viscous sub-layer can be either laminar or turbulent depending on the local flow conditions. For wave overtopping simulations with the k-epsilon model this low-Re formulation is very important, because the flow in the near-wall region cannot be simulated accurately with the use of the standard k-epsilon model. The standard k-epsilon model is more appropriate for freestream turbulence simulations, because the flow is not damped by the walls and remains highly turbulent (Fluid Mechanics, 2019).

In the low-Re formulation of the k-epsilon model these damping terms (f_1, f_2, f_3 & f_n) are used to damp the model coefficients (C_1, C_2, C_3 & C_n). Herein the damping term f_1 damps the model coefficients C_1 , the damping term f_2 damps coefficients C_2 and so on (f_n damps C_n) (Launder & Sharma, 1974; Launder & Spalding, 1974). By applying these damping functions the k-epsilon model can, in theory, be applied not only in the open stream, but also all the way to the wall. Currently a wide variety of damping functions exist for CFD models, however, the damping functions for the standard k-epsilon model are as follows (Fluid Mechanics, 2019):

$$f_1 = 1 \quad [11] \quad f_2 = 1 - 0.3 \exp(-R_{eT}^2) \quad [12] \quad f_3 = \exp\left(-\frac{3.4}{(1 + (R_{eT}/50))^2}\right) \quad [13]$$

In the equation R_{eT} is the Turbulent Reynolds number, which characterizes the strengths of the near wall turbulence relative to the viscosity. When R_{eT} is small, viscous effects are dominant resulting in

more a laminar flow. Therefore when R_{eT} is higher at a certain location, is it most likely that this location is further away from the wall. The Turbulent Reynolds number can be calculated using equation 14, wherein k is the TKE and ε is the TKE dissipation rate.

$$R_{eT} = \frac{\rho k^{1/2}}{\mu} \left(\frac{k^{3/2}}{\varepsilon} \right) \rightarrow R_{eT} = \frac{\rho k^2}{\mu \varepsilon} \quad [14]$$

The low-Re formulation makes it possible for the model to even solve for the cells closest to the wall that are within the viscous sub-layer. In other words an empirical damping function is used in and close to the wall, in order to reduce the dissipation rate close to the wall. In the low-Re formulation the kinematic/eddy viscosity μ_t can be computed afterwards from k and ε using equation 15.

$$\mu_t = f_\mu C_\mu \frac{\rho k^2}{\varepsilon} \quad [15]$$

At the moment the damping term provided by Launder & Sharma (1974) is the most up-to-date coefficient set. This damping function is presented in equation 16. The damping function reduces the turbulent viscosity (μ_t) in **every cell** in the mesh and not just for wall adjacent cells (Menter, 1992).

$$f_\mu = \exp\left(-\frac{3.4}{(1 + (R_{eT}/50))^2}\right) \quad [16]$$

When a data point is far from the wall the damping function $f_\mu = 1$, meaning a High-Re formulation is used. This indicates that laminar viscosity will dominate the diffusion term in the transport/momentum equations, when further away from the wall. When a data point is far close to the wall the damping function $f_\mu < 1$, meaning a Low-Re formulation is used. This indicates that turbulent viscosity will dominate the diffusion term in the transport/momentum equations, when close to the wall.

This approach indicates that damping function is more a field than a standard value. Low Reynolds number (low-Re) models often provide a very accurate description of the boundary layer, however, require very high mesh resolutions due to the sharp gradients close to walls. This means a trade-off needs to be made between a high accuracy or a high computation time (Fluid Mechanics, 2019).

1.2.1. K-Omega turbulence model

The k-omega turbulence model is also a RANS-based turbulence model and is, compared to the k-epsilon models, better at predicting drag and lift (Kok, 2000). Before the k-omega model came to be, many other turbulence models had been developed in order to reduce the incorrectness of the drag and lift coefficients in the standard k-epsilon models. Models such as the Spalart-Allmaras and Johnson-King models for example. These improved models were all proposed around the same time, to solve the same problem, however, from all these models the k-omega model has become the most popular. Nowadays many different versions of the k-omega model exist, from which most of the modern day versions are based on the Wilcox (1988) model (Kok, 2000). The newest and currently most used version of these k-omega model is the Wilcox (2006) model.

The k- ω model also uses two transport equations, which are solved to compute k , the turbulent kinetic energy, and ω , the specific turbulent dissipation rate. The transport equation for k is the same as used in the k-epsilon model and is presented in equation 7. The transport equation for ω is slightly different from the transport equation for ε and is presented in equation 18. Because ε and ω both describe the dissipation of turbulent kinetic energy, the transport equation can be solved with either one of them using equation 19.

$$\frac{\partial(\rho\omega)}{\partial t} + \nabla \cdot (\rho \mathbf{U} \omega) = \nabla \cdot \left(\left(\mu + \frac{\mu_t}{\sigma_k} \right) \nabla \omega \right) + \frac{\gamma}{v_t} P_k - \beta \rho \omega^2 \quad [18]$$

$$\omega = \frac{\varepsilon}{C_\mu k} \quad \text{with} \quad C_\mu = 0.09 \quad [19]$$

When the transport models have been solved, the kinematic/eddy viscosity (μ_t) can be computed using k and ω .

$$\mu_t = \frac{\rho k}{\omega} \quad [20]$$

In principle the k-epsilon and k-omega models are the same, however, some slight differences do exist between the two models. The main difference between the k-epsilon and k-omega model is that the k-omega model uses different values for the empirical coefficients in the transport equations ($\alpha, \beta, \beta^*, \sigma_k, \sigma_\omega$, etc. depending on the model version). These values can therefore also give an indication on which form of the k-omega model is being used. The reason why the k-omega models are considered to be better than the k-epsilon models, is due to the fact that no damping factors or functions are needed. This makes the k-omega model better in accuracy, as the separation point will be predicted better than with a k-epsilon model. The separation point is the location where flow separation starts to occur.

1.2.2. K-Omega SST turbulence model

The k-omega SST model was introduced in 1994 as an improvement of the k-epsilon and k-omega models. In principle the standard k-omega SST model uses the k- ε model in the freestream and the k- ω model near walls. Both the standard k-epsilon and k-omega model transport equations are used in the k-omega SST model. The transport equation for k is presented in equation 7, the transport equation for ε is presented in equation 8, and the transport equation for ω is presented in equation 18. In the k-omega SST model the switch between the transport equation for epsilon and omega is possible through the use of equation 21 (Menter, 1994).

$$\omega = \frac{\varepsilon}{C_\mu k} \quad \leftrightarrow \quad \varepsilon = C_\mu k \omega \quad \text{with} \quad C_\mu = 0.09 \quad [21]$$

By substituting the second equation in equation 21 ($\varepsilon = C_\mu k \omega$) into equation 18 (the transport equation for ω), the k-epsilon model can be compared to the k-omega model. This new k-omega model equation is presented in equation 22.

$$\frac{\partial(\rho\omega)}{\partial t} + \nabla \cdot (\rho \mathbf{U} \omega) = \nabla \cdot \left(\left(\mu + \frac{\mu_t}{\sigma_k} \right) \nabla \omega \right) + \frac{\gamma}{v_t} P_k - \beta \rho \omega^2 + \underbrace{2 \frac{\rho \sigma_{\omega 2}}{\omega} \nabla k : \nabla \omega}_{\text{Additional term}} \quad [22]$$

Additional term

Doing this shows that an additional term is introduced, which was previously not present in the k-omega model. This additional term is the only difference between the k-epsilon and k-omega model, therefore this term can be modified and used as a 'blending function'. In equation 23 this blending function is presented as F_1 and will have a different value for every cell in the mesh. The tensor in the additional term can look like equation 24 and will give a scalar value.

$$2(1 - F_1) \frac{\rho \sigma_{\omega 2}}{\omega} \nabla k : \nabla \omega \quad [23] \quad \nabla k : \nabla \omega = \frac{\partial k}{\partial x_j} \frac{\partial \omega}{\partial x_j} = \frac{\partial k}{\partial x} \frac{\partial \omega}{\partial x} + \frac{\partial k}{\partial y} \frac{\partial \omega}{\partial y} + \frac{\partial k}{\partial z} \frac{\partial \omega}{\partial z} \quad [24]$$

The blending function F_1 will have a value between 0 and 1, wherein 0 indicates that the k-epsilon model is being used, as $F_1 = 1$ gives $(1-1) = 0$ *additional term, and 1 indicates that the k-omega model is being used, as $F_1 = 0$ gives $(1-0) = 1$ *additional term. This is possible because this additional term only appears in the k-epsilon model and not in the k-omega model. The blending function F_1 can calibrate with the help of equation 25. Herein the term arg_1 depends on the distance to the closest wall (d) and can be calculated using equation 26.

$$F_1 = \tanh(arg_1^4) \quad [25] \quad arg_1 = \min \left[\max \left(\frac{\sqrt{k}}{\beta\omega d}, \frac{500\nu}{\omega d^2} \right), \frac{4\rho\sigma_{\omega_2}k}{CD_{k\omega}d^2} \right] \quad [26]$$

The results of this blending function is a hyperbolic tan-line, which represents a smooth transition between the models as can be seen in Figure 25. In addition, F_1 can also be used to blend between the empirical constants, see for example equation 27. In this equation ϕ_ω is the model constant in k- ω model (e.g. β^*) and ϕ_ϵ is the model constant in k- ϵ model (e.g. C_μ). When only a blending term is used in the k-omega BST model, so when no viscosity limiter is used, the model is called a k-omega BST model instead.

$$\phi = F_1\phi_\omega + (1 - F_1)\phi_\epsilon \quad [27]$$

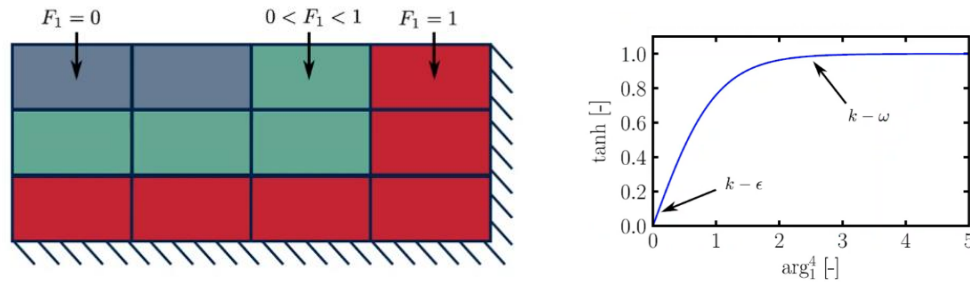


Figure 25 – (left) a visualisation of a step sized blending function in the grid. (right) The resulting hyperbolic tan-line of a smooth the blending function presented above. Note: reprinted from Fluid Mechanics (2019)

In addition to the blending function, the k-omega SST model also uses a viscosity limiter (equation 28). This viscosity limiter is used to obtain results which are in better agreement with experimental measurements of separated flow.

$$\underbrace{\mu_t = \frac{\rho k}{\omega}}_{\text{Original}} \quad \underbrace{\mu_t = \frac{a_1 \rho k}{\max(a_1 \omega, S F_2)}}_{\text{SST model}} \quad [28]$$

In the SST model equation for the kinematic/eddy viscosity (μ_t), F_2 is another blending function similar to F_1 . In this equation the viscosity is limited, or reduced, when F_2 or S is large. The blending function F_2 is empirically calibrated with the help of equation 29. Herein the term arg_1 depends on the distance to the closest wall (d) and can be calculated using equation 30.

$$F_2 = \tanh(arg_2^2) \quad [29] \quad arg_2 = \max \left(\frac{2\sqrt{k}}{\beta\omega d}, \frac{500\nu}{\omega d^2} \right) \quad [30]$$

1.3. Large Eddy Simulation

Turbulent flows contain many eddies. These eddies can take on a range of sizes and energies over time. Large Eddy Simulation or LES uses a part of these present eddies to resolves the turbulence in the flow with the mesh. In other words, the mesh is used to resolve the larger-scale eddies, by simulating a part of the present small-scale eddies. In LES the mesh therefore sets the minimum eddy size that can be

resolved by the model. The mesh can resolve eddies with different sizes, however, to resolve an eddy a minimum of 4 cells is needed (see Figure 26). The mesh of the CFD model cannot resolve eddies smaller than the width of two cells, due to the fact that a minimum of 4 cells is needed to resolve an eddy. In order to simulate eddies that are smaller than the width of two cells, a sub-grid scale model is used. In Figure 26 the principle of LES is presented.

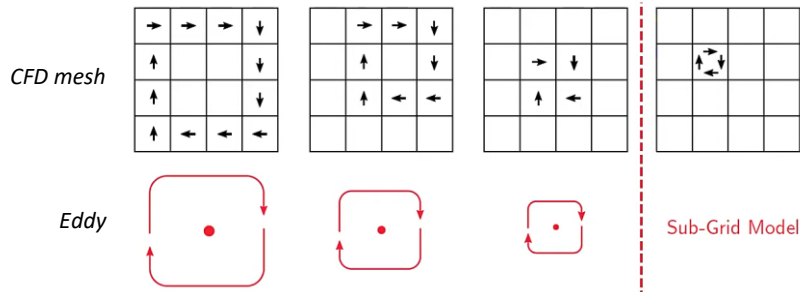


Figure 26 – An example of how eddies are simulated using the CFD mesh. The arrows in the mesh represent the velocity vectors at the cell centroid. A minimum of 4 cells is needed to resolve an eddy in the CFD mesh, smaller eddies are simulated within the sub-grid scale model. Note: reprinted from Fluid Mechanics (2020).

A fine mesh gives more accuracy, because a larger range of eddy sizes and energies can be simulated in the CFD mesh. However, the finer the mesh, the longer it takes to simulate. Therefore it is important to find the most appropriate mesh size for the situation of interest. This can be done by first estimating the required mesh size, with use of the turbulent energy cascade, and afterwards by further refining the mesh. In Figure 27 an example of a turbulent energy cascade is presented.

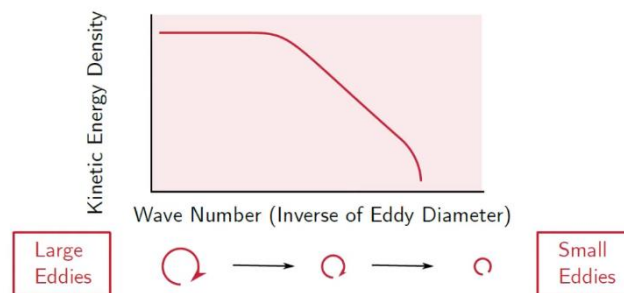


Figure 27 – An example of a turbulent kinetic energy cascade. Note: reprinted from Fluid Mechanics (2020).

The turbulent energy cascade shows how the turbulent kinetic energy, presented on the y-axis, is distributed amongst the eddies. The wavenumber (k) in m^{-1} , presented on the x-axis, represents the spatial frequency of the eddy. Smaller eddies have a larger wavenumber, because smaller eddies occur at a higher frequency than larger-scale eddies. Note that in LES the symbol k stands for the wavenumber, whereas in RANS the symbol k stands for the turbulent kinetic energy. On the y-axis of the turbulent energy cascade the turbulent kinetic energy density is presented. The area underneath the curve (integral) is the turbulent kinetic energy, which is used in RANS. In most cases the mesh does not resolve all eddies. Therefore it will only resolve some of the turbulent kinetic energy. Most researchers state that a good LES will resolve 80% to 90% of the turbulent kinetic energy. This means that at each point in the domain 80% to 90% of the turbulent kinetic energy needs to be resolved, as can be seen Figure 28. The remaining turbulent kinetic energy, the blue part in Figure 28, needs to be resolved within the sub-grid model. The remaining turbulent kinetic energy (the blue part) needs to be resolved within the sub-grid model.

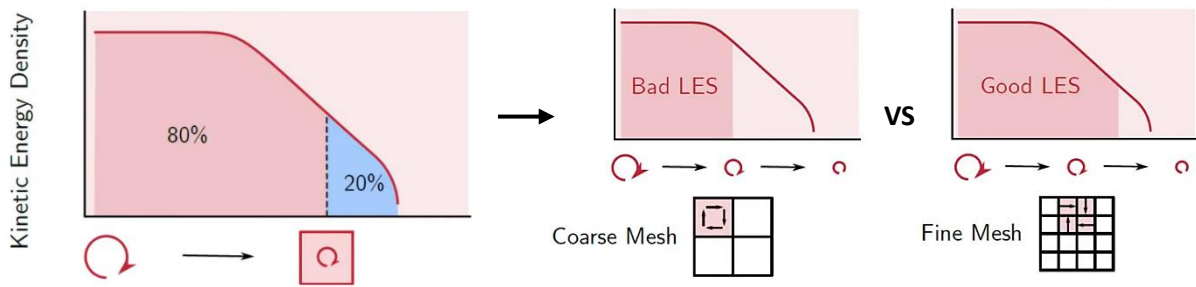


Figure 28 - An example of a good and bad LES-based turbulence model. Note: reprinted from Fluid Mechanics (2020).

To find which mesh size can resolve 80% of the turbulent kinetic energy at each point in the domain, first a rough estimation needs to be made. This estimation becomes more complicated when the domain varies significantly in dimensions. In case the domain dimensions are variable, the eddy sizes and energies and the turbulence energy spectrum will vary far more throughout the domain. An example of this variation is presented in Figure 29.

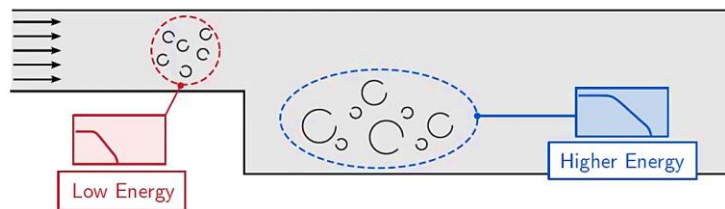


Figure 29 – The variation in eddy size and eddy energy caused by a change in dimensions within the domain. The small blue graph (High energy) and small red graph (low energy) represent the turbulent energy spectrum at that location. Note: reprinted from Fluid Mechanics (2020).

In order to gain a good estimation of the mesh size for domains with dimensional difference, the integral length scale can be used. The integral length scale represents all the eddies at a certain location in the domain. An integral length scale is often used to simplify the data analysis, as analysing single values is easier than looking at a whole spectrum. The integral length scale is denoted by l_0 and is the length of an eddy at the **average** kinetic energy of all eddies, as can be seen in Figure 30.

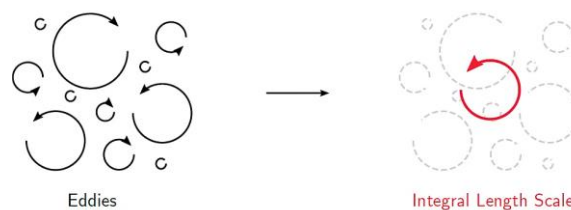


Figure 30 – An example of the integral length scale. Note: reprinted from Fluid Mechanics (2020).

The integral length scale (l_0) can be calculated using equation 31. In the equation k represents the wavenumber, which can be calculated with equation 32, and d represents the diameter/width of the eddy. For smaller eddies the d will also be small, resulting in a larger wavenumber and vice versa.

$$l_0 = \frac{\int_0^\infty k^{-1}E(k)d(k)}{\int_0^\infty E(k)d(k)} \quad [31] \quad \text{with } k = \frac{2\pi}{d} \quad [32]$$

In addition the integral length scale (l_0) can also be calculated using a precursor RANS calculation. This means a RANS simulation would need to be performed before the LES is carried out. This RANS simulation can, however, be performed with either the k-epsilon, k-omega model or k-omega SST. In general, where large length scales are simulated, larger mesh sizes can be used and where small length

scales are simulated, smaller mesh sizes are needed. Using these resulting dissipation rate (epsilon and/or omega), the integral length scale (l_0) can be calculated with equation 33 or equation 34. Where l_0 is small, small cells are needed because the eddies will be smaller and vice versa.

$$l_0 = \frac{k^{3/2}}{\varepsilon} \quad [33] \quad \text{OR} \quad l_0 = \frac{k^{1/2}}{C_\mu \omega} \quad [34]$$

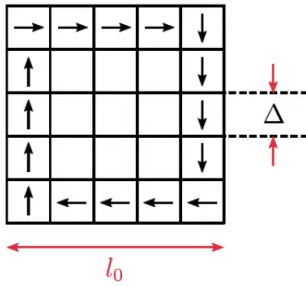


Figure 31 – A mesh with a cell size of at least $1/5^{\text{th}}$ of the obtained integral length scale. Note: reprinted from Fluid Mechanics (2020).

With use of the obtained integral length scales (l_0), a good first estimation of the mesh size can be obtained. In general, 5 cells across the integral length scale is likely to resolve 80% of the turbulent kinetic energy. This means that the cell size is often at least $1/5^{\text{th}}$ of the obtained integral length scale, as can be seen in equation 35 and Figure 31 After using this estimation the mesh can always be further refined by reducing the cell size.

$$\Delta = \frac{l_0}{5} \quad [35]$$

If the mesh is refined, more turbulent kinetic energy can be resolved by the model. An easier way to find which mesh locations need to be refined is by defining a new field. For example a new field called f is defined as equation 36, wherein $\Delta = \text{Cell Volume}^{1/3}$.

$$f = \frac{l_0}{\Delta} = \frac{k^{3/2}}{\varepsilon * \Delta} \quad [36]$$

By plotting this new field (f) in a post-processor, such as was done for the integral length scale, the outcome of the flow field can be compared with the mesh. An example of the resulting plot is presented in Figure 32. At the locations where $f > 5$ the mesh is sufficient enough, while at the locations where $f < 5$ the mesh is too coarse. At these certain locations where the mesh is too course, the grid should be refined.

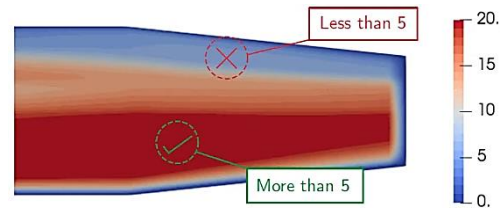


Figure 32 – An example of the comparison between the post-processor results and the mesh flow field outcome. Note: reprinted from Fluid Mechanics (2020).

1.4. Detached Eddy Simulation

DES or Detached Eddy Simulation is a turbulence model which combines the LES-based and RANS-based model approach. DES was developed to overcome the disadvantages of the standard LES models, especially in near-wall regions, by combining the best aspects of LES and RANS models. These disadvantages near the wall are caused by the fact that the near-wall regions contain eddies with smaller turbulent length scales than the rest of the flow. For LES to accurately resolve these small eddies a very small cell size would be needed, causing the computational time to increase significantly. To overcome this problem, a Detached Eddy Simulation uses RANS-like behaviour in near-wall regions and uses LES-like behaviour in the rest of the flow. This means that when the turbulent length scales are larger than the grid dimensions the LES model will be used and vice versa. This application of the LES and RANS models makes DES-based models less demanding in terms of mesh resolution, compared to LES-based models (Nikolaidou, 2019).

Originally the DES model formulation replaced the distance function (d) in the Spalart-Allmaras model, which is a RANS-based one equation model, with a modified distance function. This change in distance function causes the model to behave as a RANS model in regions close to walls. Although DES was originally formulated for the Spalart-Allmaras model, the DES models can also be implemented for

other RANS-based models. One of these more used versions is the DES k-omega SST model, wherein the distance function (d), used in the DES-based models, is modified in the RANS k-omega SST models instead of the one equation Spalart-Allmaras model. These k-omega SST based DES models use the turbulence length scale, obtained from the model's equations, to compare these with the grid length scale in order to switch between LES and RANS models. DES models based on Spalart-Allmaras model will behave like a LES model with a wall model, while DES models based on RANS will behave more like a hybrid of the RANS and LES model. Compared to the RANS and LES models, the grid generation for a DES will be more complicated (Nikolaidou, 2019). This is caused by the fact that the model needs to switch between RANS and LES. Furthermore, more programming is required in practice to appropriately change the calculation of the length scale. DES-based models can provide one single smooth velocity field capturing both the RANS and the LES regions of the turbulence solutions. After the development of the DES models, different DES-like models were developed, such as DDES (Delayed Detached Eddy Simulation) and IDDES (Improved Delayed Detached Eddy Simulation).

1.5. Direct Numerical Simulation

DNS stands for Direct numerical simulation and is used to computationally simulate fluid dynamics in flows (Nikolaidou, 2019). DNS numerically solves the Navier-Stokes equations, presented in equation 1, without the use of a turbulence model. In other words, DNS models will resolve the turbulence in the flow for the whole range of spatial and temporal scales. To do this, all spatial scales of the turbulence are resolved in the computational mesh. This means that the smallest scales (Kolmogorov scales), where kinetic energy is dissipated, up to the integral length scale (l_0), where the most kinetic energy is present, are resolved numerically.

Because all the turbulence is resolved without a turbulence model, the DNS model will require a large number of floating-point operations and a small time step in order to resolve the turbulence for the whole range of spatial and temporal scales. In most cases this means that the number of operations will grow as Re^3 . For example at high Reynolds numbers eddies of 10 μm can occur with a frequency of 20 kHz. This would mean that the DNS model would need 2^{12} points with a time step of 100 μm to resolve the small-scale eddies in the flow. Due to this, the computational cost of DNS becomes very high even at low Reynolds numbers. For most industrial applications the required computational resources for DNS still exceed the capacity of the most powerful computer available. However, in contrast to computational time, the results of DNS are more realistic as can be seen in Figure 33.

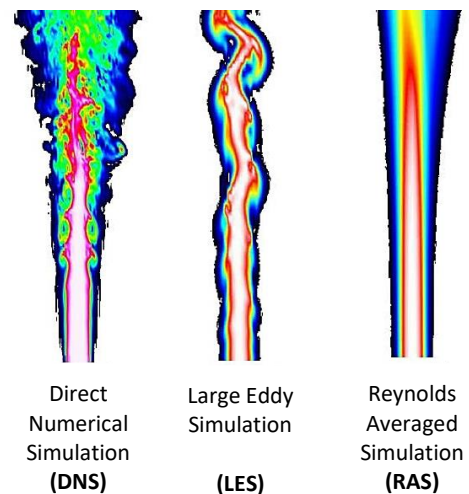


Figure 33 – The visualized difference between DNS, LES and RANS based turbulence modelling. RANS is smoothest due to time averaging. LES shows some of the present eddies over time. DNS gives the most detailed prediction. Note: reprinted from Marisa (2014)

Although DNS is not applicable for most industrial applications, this does not mean that DNS is completely 'useless' at the moment. This is because DNS can still be used as a tool in fundamental research of turbulence, but also as a tool to develop turbulence models for practical application. DNS can be used to perform "numerical experiments" in fundamental research, whereafter information that would be difficult or impossible to obtain in laboratory experiments can be extracted. This can improve the understanding of turbulence.

Limitations of the turbulence models

1.1. Limitations of the k-omega SST model

The k-omega model was developed later in time as an improvement of the k-epsilon model, which was the first RANS-based model. This resulted in different limitations for both the k-epsilon and k-omega models. To overcome the limitations of the k-epsilon and k-omega models, the k-omega SST models were developed (Nikolaidou, 2019; Wang et al., 2021). The k-omega SST models use a k-epsilon model in the freestream, as k-epsilon models struggle to predict the right angle and position of the separation point and become less accurate when predicting the boundary layers with adverse pressure gradients. For this reason the k-epsilon models are usually preferred for high-Re (high Reynolds number) applications, such as the freestream, due to the absence of separation and reattachment of the flow in these cases. The k-omega model, on the other hand, is used in the near-boundary region of the k-omega SST models. This is because the k-omega models are better at predicting boundary layers and flow separation, thus preferred for low-Re (low Reynolds number) applications (Launder & Spalding, 1974).

The limitations of the k-omega models are, however, the sensitivity of the model to initial conditions and the dependence of the model on the freestream turbulence conditions. This dependence and sensitivity is caused by the fact that small changes in the freestream TKE (k_∞) lead to large changes in the turbulent viscosity (μ_t) and the skin friction coefficient (c_f) (Kok, 2000). The skin friction coefficient represents the drag caused by the friction of the fluid against the surface of an object, which is always present in the boundary layer/ viscous sub-layer. When the skin friction coefficient (c_f) changes the forces on the body and the flow separation starting point will be affected. A good example of this dependence and sensitivity is when the freestream turbulence conditions are negligible. In this case k_∞ should be equal to 0, however, because the model input for k_∞ can only be set to a value very close to zero, such as $1e^{-10}$, $1e^{-8}$ or $1e^{-6}$, the model will still take k_∞ into account. Therefore, although the model should be neglecting the effects of k_∞ , in practice the results become very different depending on the value used for k_∞ , even for values in the order of $1e^{-10}$, $1e^{-8}$ or $1e^{-6}$ (Menter, 1994). This means that the k-omega model is very sensitive to small changes in freestream turbulence conditions. The reason for this freestream turbulence dependency is still unknown, however, this limitation of the k-omega model can be fixed by blending the k-omega model with the k-epsilon model. Therefore, the k-omega SST is nowadays preferred for many different applications, as it will switch between the low-Re and high-Re RANS formulation depending on the distance from the wall. Thus, by blending between the two models with a Blending Ratio, the limitations of both models can be reduced. The k-omega SST model is suitable for 1D, 2D and 3D applications and can either be used for steady-state flows or transients.

1.2. Limitations of the LES model

LES-based turbulence models are very useful when simulating thermal fatigue, vibration or buoyant flows used to design ship for example. One of the limitations of LES, however, is that resolving turbulence in near-wall regions can cause difficulties. This is because a very small grid size is required to simulate the many small-scale eddies that are generated in the wall-bounded flows. In addition, 3 dimensional modelling is required to perform a correct LES simulation. This small grid size in the near-wall region combined with the fact that more than two grid cells are needed in the z-direction, causes

the computation time to increase exponentially. It was found that the required grid point in these near-wall regions are often proportional to Re^2 (Nikolaidou, 2019). Therefore, when the flow has a high Reynolds number, the computation time increases even further. Eventually this results in an amount of grid points compatible to DNS.

Another limitation of LES-based turbulence models is how separated flows are treated. When separation occurs the boundary layer becomes a free shear layer, while reattachment causes this free shear layer to become a boundary layer. Because of the gridding and modelling it becomes difficult to track where these boundary layers get attached. Flow separation can occur either abruptly, which is mostly caused by geometry or discontinuity, or slow, caused by the boundary layer being on the edge of separation over a long distance. For LES the slow flow separation is the hardest to simulate. In addition, the model is not very useful in resolving turbulence inside the boundary layer due to the need of a very small cell size. Even when a small cell size is used, the LES model would still experience difficulty in resolving the flow in the near-wall region.

To overcome the limitations of the LES-based turbulence models in the near-wall region, it is possible to use a wall model at the bottom of the boundary. These wall models are similar to the 'law of wall' condition used in RANS-based turbulence models. When using a wall model the computation time can be reduced by a factor of 10 or more. However, when using a wall model a complex wall model is recommended over a simple wall model, as this will give more accurate result. However, when using a wall model a complex wall model is recommended over a simple wall model, as this will give more accurate result (Nikolaidou, 2019). Therefore, the use of wall models in LES models is still very challenging. More development is needed to use LES for complex flows with high Reynolds numbers or in wall-bounded flows. Another way to overcome the limitations of a LES is to create/use a hybrid model, such as DES. In general LES-based models are most suitable for 3D applications and for transients.

1.3. Limitations of the DES model

Just as how the k-omega SST model combines the k-epsilon and k-omega models to overcome the separate limitation of both models, the DES model also combines two turbulence model approaches. DES-based models are a combination of a RANS-based model, either k-epsilon, k-omega, k-omega SST or another RANS model can be used, and a LES-based model (Nikolaidou, 2019). In DES, RANS is used in the boundary layer and LES is used in the freestream. These models are combined to form a Hybrid LES-RANS model, which can be used to overcome the limitations of a RANS and LES model. Often RANS-based models are not accurate enough for many flows and additionally in most cases more than one RANS model is needed to be used to resolve all flows. On the other hand, LES-based models do not carry these kinds of limitations, however, LES is very time expensive compared to RANS. By combining these two models the accuracy of LES and the speed of RANS can be used to resolve the turbulence in the flow.

DES-based models are able to simulate complex flows with high Reynolds numbers and use up less time to resolve turbulence in near-wall regions (Nikolaidou, 2019). DES is good at simulating massively separated flows, but for simpler flows the predictions will be less accurate than when using RANS. To find out if DES is more appropriate to use compared to RANS, the flow characteristics can be used to substantiate the choice. The biggest limitation of DES is the difficulty in simulating transitions. DES-based models are also most suitable for 3D applications and transients, just as LES-based models.

The validation of the OpenFOAM model

To validate the OpenFOAM model, the simulated front velocities are compared with the front velocities measured during the field experiments. If the model results of the original model are in range with the field measurements no changes need to be made, otherwise the model will need to be adjusted. In Figure 34 the front velocity of the field measurement is plotted against the model output of the original model for a volume of 500 l/m, 1500 l/m and 2500 l/m. It can be noted that both the front velocities and the maximum velocity, calculated with the original model, are not in range with the field data. From the three upper subplots of in Figure 34 it stands out that the simulated velocities do not fully match the front velocities measured in the field. However, from the lower three subplots of in Figure 34 it can be noted that the behaviour of the simulated velocities along the dike profile are rather similar, presenting the lower velocities at the crest and the higher velocities at the toe. Only, for the lowest wave overtopping volume (500 l/m) the velocities are underpredicted substantially. To improve the simulated velocities, the model is re-validated for four different validation options from which one option was selected.

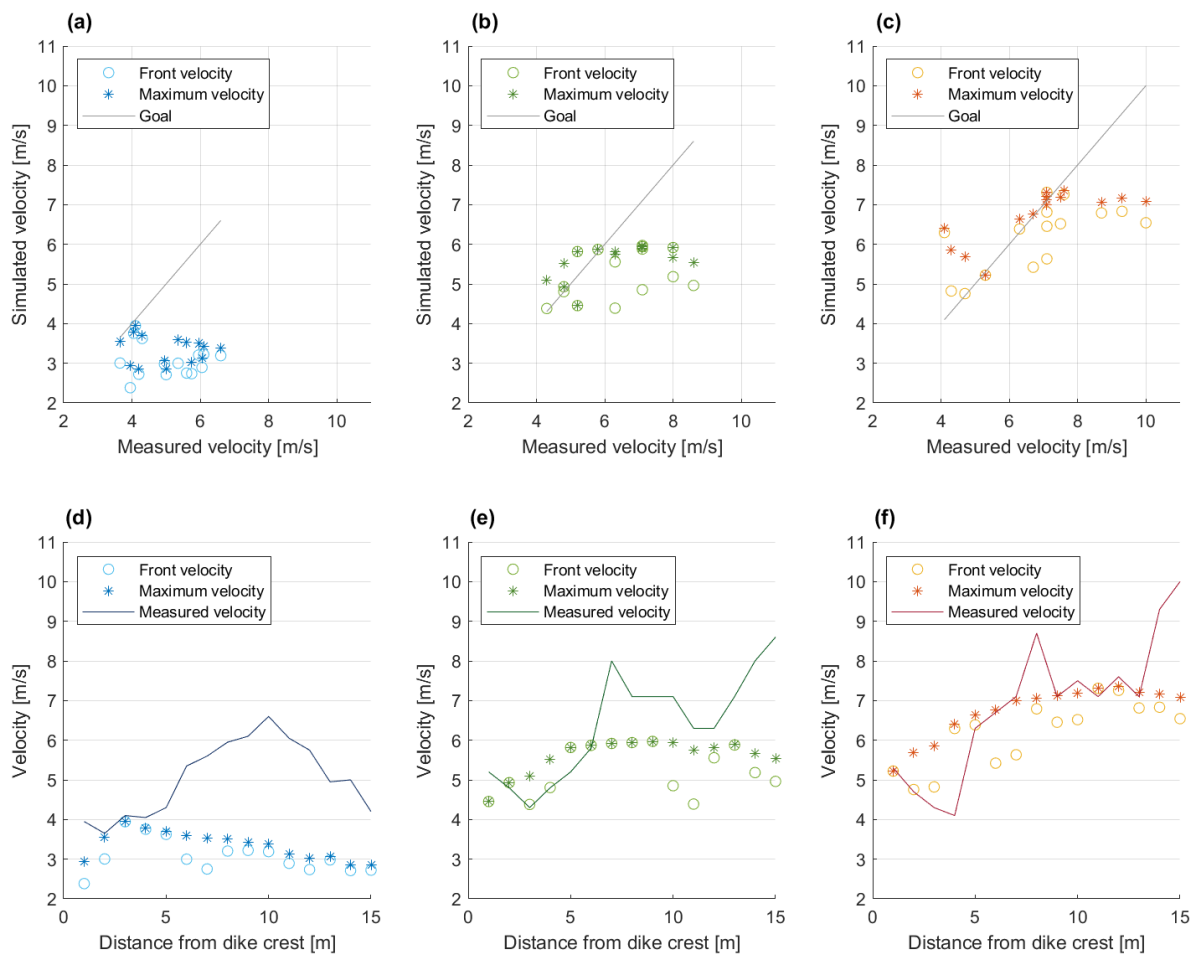


Figure 34 - The value and location of the front velocity and maximum velocity for the wave overtopping volumes of: 500 l/m in blue (a, d), 1500 l/m in green (b, e) and 2500 l/m in orange (c, f). Simulated using the original boundary conditions. The goal-line presents the target range for the velocities. The line of the measured velocities present the target trend along the profile.

1.1. Validation options

The velocity simulated by the model can be improved by adjusting of the boundary conditions for the flow velocity and water layer thickness at the inlet or by adjusting the water-air ratio, which is an initial condition used to adapt the water fraction at the inlet of the model. Four validation options have been simulated for the wave overtopping volumes of 500 l/m, 1500 l/m and 2500 l/m. Three different wave overtopping volumes are compared instead of one, to increase certainty, while limiting the needed runs of the validation. If the model were to be validated using only one volume, the model performance would become less representable for other volume scenarios. Thus, the model predictions would become more questionable. In this section the four validation options are presented. A slightly more detailed version of subsection 1.1.2. and 1.1.3. are presented in the main report (section 4.5.).

1.1.1. Option 1 - Changing the water-air ratio (BC1)

In the original set-up of the wave overtopping model, the water entering the system consists of 80% water and 20% air. This water-air ratio is applied to the inlet, to give a more realistic overtopping simulation as wave overtopping contain a lot of air bubbles. The ratio of 80-20 was implemented by Van Bergeijk et al. (2021) as studies have proven that this water-air ratio is valid for wave overtopping. It is possible for the model to solve the water-air ratio numerically, however, this requires more run-up time, as the model will need to calculate the ratio from scratch. To reduce this run-up time, the water-air ratio at the inlet was adjusted. However, the first version of the wave overtopping model was calibrated and validated using a 100% water and 0% air ratio (Van Bergeijk et al., 2021, 2022). Therefore, this change in water-air ratio between the base and original model could cause the simulated velocities to be underpredicted. To validate whether this water-air ratio could improve the model performance, the water-air ratio is changed again to the 100% water and 0% air ratio.

1.1.2. Option 2 - Changing the maximum flow velocity (BC2)

The original set-up of the wave overtopping model uses empirical equations to compute the boundary condition of the flow velocity. Herein, the maximum flow velocity (u_{max}) determines the maximum velocity at the entrance of the simulation and decreases over time to zero. Thus, the maximum flow velocity functioning as a type of starting condition for the velocity. If the maximum flow velocity is over- or underestimated, the predicted flow velocity will also get over- or underestimated at different locations along the slope. To improve the velocity at the entrance, the u_{max} calculated with the empirical equation is replaced with the flow velocity measured between 0 and 1 meters during field measurements at section 3-2 of the Vecht dike. This means that the front velocity measured at the start of the dike profile is used as input for The maximum flow velocity. In Table 4 the calculated maximum velocities and the measured front velocities can be observed for all the volumes simulated during the field experiments.

Table 11 - Overview of calculated and measured velocity for each measured volume. The volumes 2.5, 1.5 and 0.5 m³/m have been highlighted in green, because these volumes are simulated. In the last column the difference between the velocities is presented by subtracting the calculated from the measured velocity (measured-calculated).

Volume [m ³ /m]	Calculated velocity [m/s]	Measured velocity [m/s]	Difference [m/s]
2.50	5.92	5.30	-0.62
2.25	5.74	5.50	-0.24
2.00	5.54	5.50	-0.04
1.50	5.08	5.20	0.12
1.00	4.50	4.55	0.05
0.50	3.66	3.95	0.29
0.40	3.42	5.20	1.78
0.20	2.78	3.90	1.12

1.1.3. Option 3 - Changing the maximum water layer thickness (BC3)

The maximum water layer thickness (h_{max}) in the wave overtopping model determines the height of the wave at the entrance of the simulation and is also calculated using an empirical equation. Because the water layer thickness was not measured during the field experiments, it is not possible to use field measurements to adjust the maximum water layer thickness. However, it is possible to adjust or replace the equation used in the original wave overtopping model to calculate h_{max} (equation [14]), by incorporate more parameters than the wave overtopping volume. This new equation for the maximum layer thickness (h_{max}) can be obtained by combining equation [21] and equation [22] (Hughes et al., 2012). Equation [21] is used to calculate the overtopping volume in m^3/m and equation [22] is used to the overtopping discharge in m^3/s .

$$V = \int_0^{T_0} q(t) dt \quad [21] \quad q(t) = h_{max} u_{max} \left[1 - \frac{t}{T_0}\right]^m \quad [22] \quad h_{max} = \frac{V(m+1)}{u_{max} T_0} \quad [23]$$

In equation [23] the maximum layer thickness is calculated with help of the maximum flow velocity (U_{max}), the wave overtopping volume (V) and the overtopping period (T_0) that can be obtained through equation [15]. The constant m [-] in equation [23] can be calculated by summing up the constants a and b ($a + b$), as stated in subsubsection 2.5.1.1. Since $a = b = 1$, the constant m has a value of 2. In Table 5 the outcome and difference between the original and adjusted h_{max} can be observed for the volumes 500, 1500 and 2500 l/m, as these will be compared for the validation phase.

Table 12 – The maximum water layer thickness calculated with the original and adjusted equation for the volumes 2.5, 1.5 and 0.5 m³/m. In the last column the difference between the maximum water layer thickness is presented by subtracting the original outcome from the adjusted outcome (adjusted-original).

Volume [m ³ /m]	Original h_{max} [m]	Adjusted h_{max} [m]	Difference [m/s]
2.50	0.210	0.213	0.003
1.50	0.163	0.189	0.026
0.50	0.094	0.145	0.051

1.1.4. Option 4 - Changing the maximum velocity and water layer thickness (BC4)

For the last validation scenario, the changes proposed for the second and the third validation scenarios are combined. This means that the maximum water layer thickness (h_{max}) and the maximum flow velocity (u_{max}) are changed at the same time to explore whether a combination of changes gives the best validation result. For this scenario the maximum water layer thickness (h_{max}) is calculated using the adjusted equation (equation [23]) and that the maximum flow velocity (u_{max}), calculated using equation [13], is substituted with the measured front velocity at the start of the test section. The water-air ratio will remain 80% water and 20% air. This ratio is not changed for this scenario, as the water-air ratio is more an starting condition which influences the ratio between the two phased flow at the inlet, while the maximum velocity and layer thickness directly influences the discharge rate at the inlet.

1.2. Selection of the validation option

When the water-air ratio is changed to 100-0% (BC1), the maximum and front velocity at the start of the dike profile increases for all wave overtopping volumes. However, along the profile the rest of the profile the maximum velocity remains equal in range, while the front velocity decreased compared to the original simulation, especially between 5 and 10 meter. When a measured velocity is used as input for u_{max} (BC2), the maximum velocity at the start of the dike profile become almost equal to the measured velocities, while the difference between the front and maximum velocities become larger for all wave overtopping volumes. Furthermore, the maximum velocity along the rest of the profile

decreases, especially for a wave overtopping volume of 2500 l/m. This is most likely caused by the fact that the measured front velocity is lower than the calculated velocity (Table 4). The velocities at the end of the profile also decrease significantly. Overall the velocities become lower and more deviated.

When an adjusted equation is used as input for h_{max} (BC3), the maximum velocities along the dike profile increases for all simulated volumes. Especially the velocities at the end of the dike profile increased, while the velocities at the start remained unchanged. The front velocity increased at most the positions along the profile for a wave overtopping volume of 2500 l/m, but decreased at some positions for a wave overtopping volume of 500 l/m and 1500 l/m. Due to these changes the front velocities for all simulated volumes present a more comparable trend than the original front velocities. When a measured velocity is used as input for u_{max} and an adjusted equation is used as input for h_{max} (BC4), both the maximum and front velocities along the dike profile increase for a wave overtopping volume of 500 l/m and 1500 l/m. However, a larger deviation between the maximum and front velocities can be observed for a volume of 1500 l/m. In addition, a more comparable trend along the profile can be observed for these two wave overtopping volumes. For a wave overtopping volume of 2500 l/m the maximum velocities present an very small decreases compared to original velocities. However, a smaller deviation between the maximum and front velocities can be observed.

From the four analysed boundary condition changes it can be noted that two validation scenarios presented an overall decrease in velocities (BC1 & BC2). Therefore, these two validation scenarios are not used for the further simulations. On the other hand, two validation scenarios presented an overall and comparable increase in velocities (BC3 & BC4). When these validation scenarios are compared with one another, it can be noted that the fourth validation scenario presents comparable estimations for the wave overtopping volumes of 500 l/m, better estimations for 1500 l/m and slightly less estimations for 2500 l/m. Although the performance of the fourth validation scenario seems slightly better than the third validation scenario, the choice was still made to continue the research with the use of BC3. This is because only wave overtopping volumes up to 2500 l/m have been used during the field experiments, which means that a new equation for u_{max} would be needed to predicts the front velocities of unmeasured wave overtopping volumes.

Appendix D

The modelled turbulence results

1.1. The sensitivity towards the volume

The sensitivity of wave overtopping turbulence towards the wave overtopping volume (V) is analysed by comparing seven different wave overtopping volumes, described in more detail in subsection 4.7.1. Figure 35 the value and location turbulence maxima and Figure 36 the turbulence maxima along the dike profile.

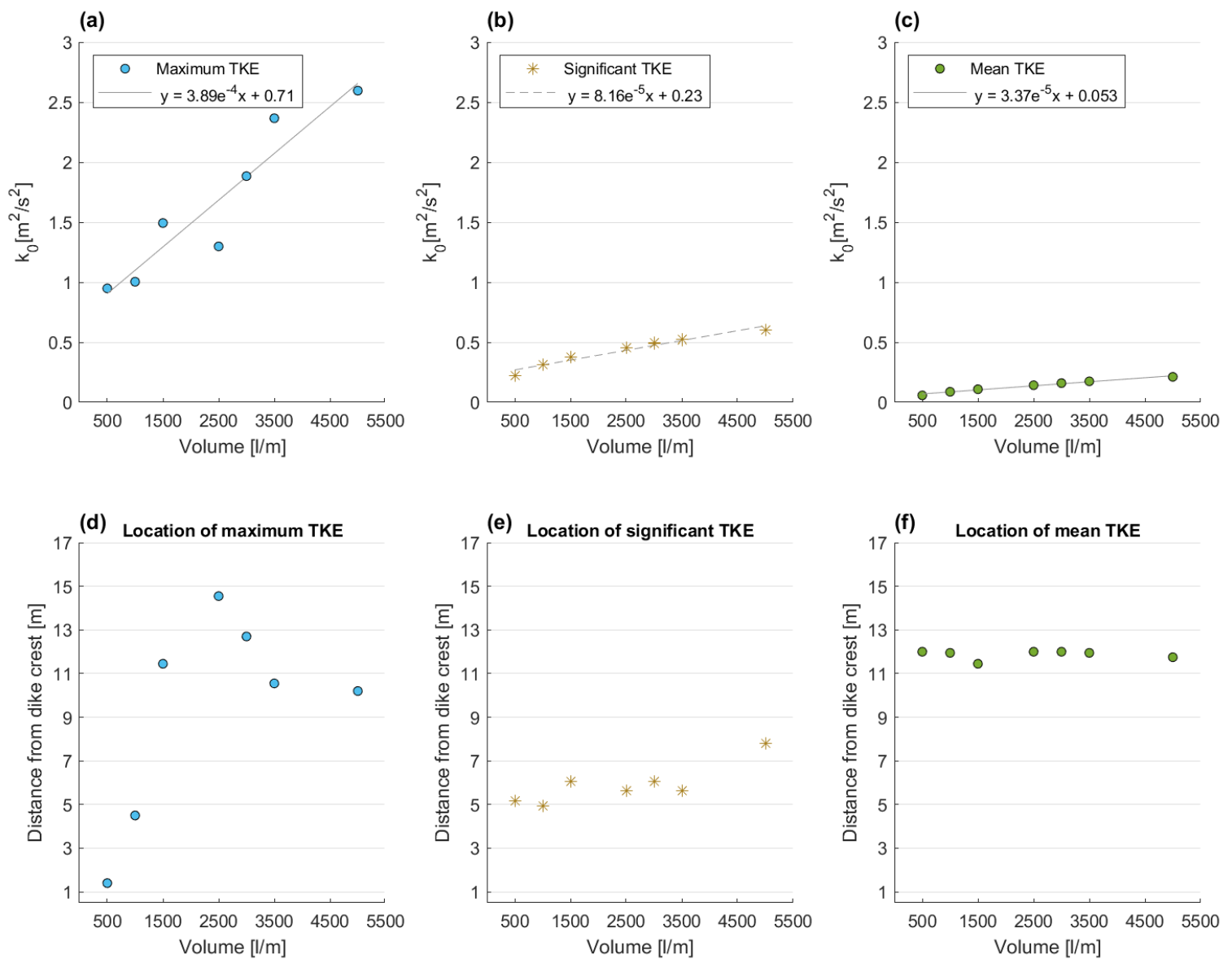


Figure 35 – Value and location of the turbulence maxima of: the maximum TKE (a, d), the maximum significant TKE (b, e) and the maximum mean TKE (c, f). The crest starts at 0.5 m, the slope at 2 m and the toe at 15 m.

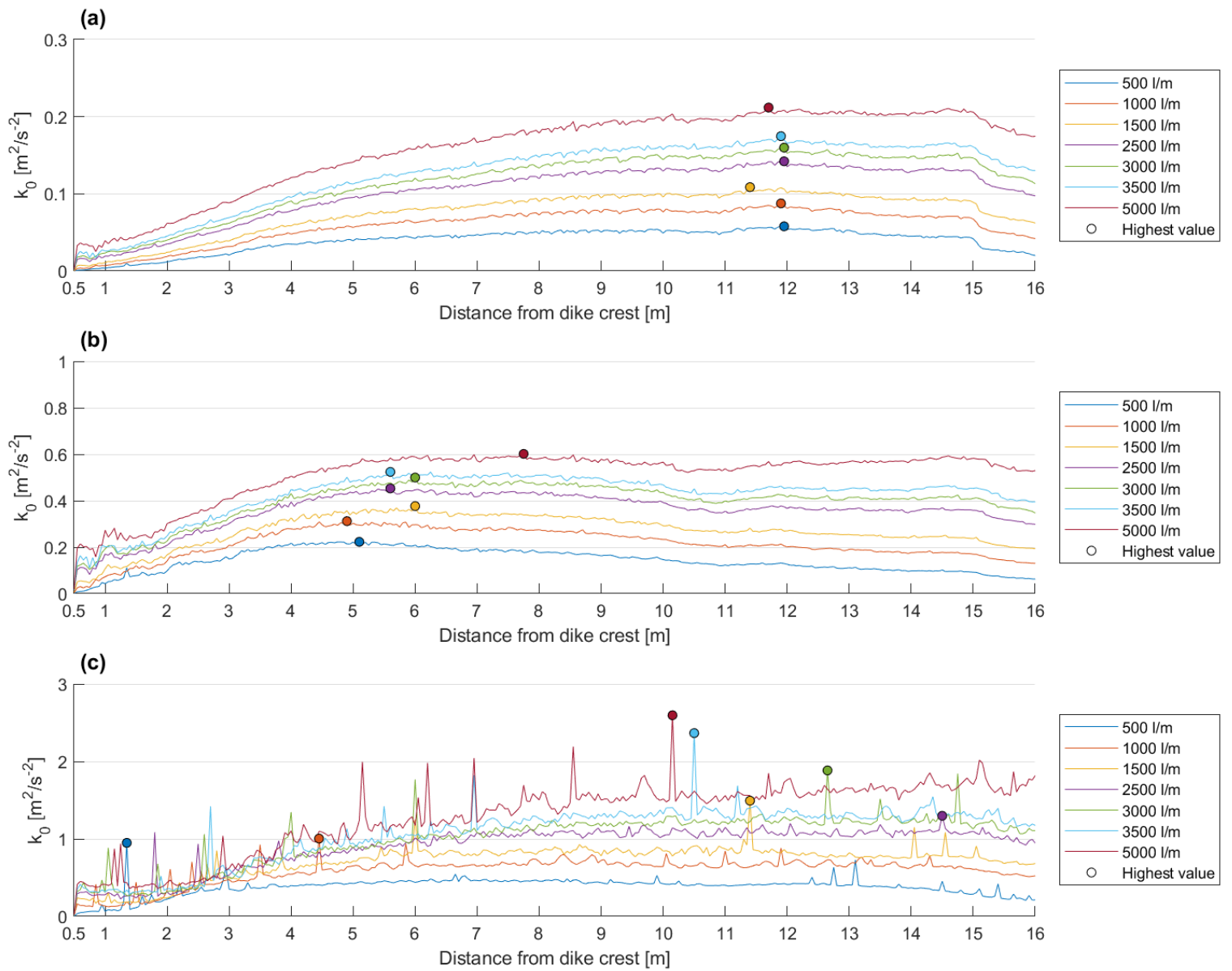


Figure 36 – The depth-averaged turbulence maxima plotted against the dike profile. The maximum mean depth-averaged TKE (a), the maximum mean significant depth-averaged TKE (b) and the maximum depth-averaged TKE (c). The crest starts at 0.5 m, the slope at 2 m and the toe at 15 m. Note: The y-axis use different scaling.

1.2. The sensitivity towards the roughness height

The sensitivity of wave overtopping turbulence towards the roughness height (k_s) is analysed by comparing four different roughness heights, described in more detail in subsection 4.7.2. Figure 37 the value and location turbulence maxima and Figure 38 the turbulence maxima along the dike profile.

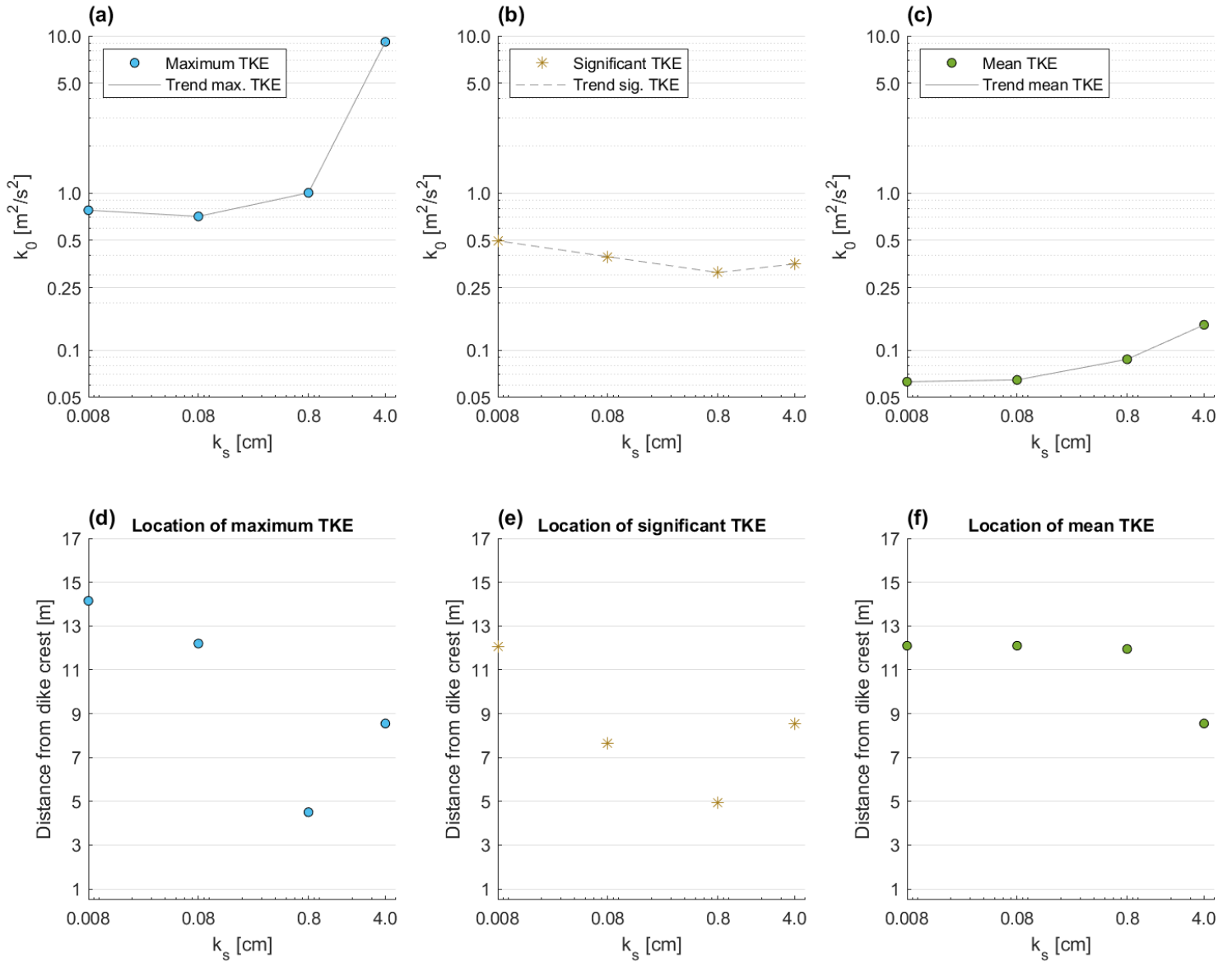


Figure 37 - Value and location of the turbulence maxima of: the maximum TKE (a, d), the maximum significant TKE (b, e) and the maximum mean TKE (c, f). The crest starts at 0.5 m, the slope at 2 m and the toe at 15 m. Note: The y-axis in sub-plots (a, b, c) use a logarithmic-scale.

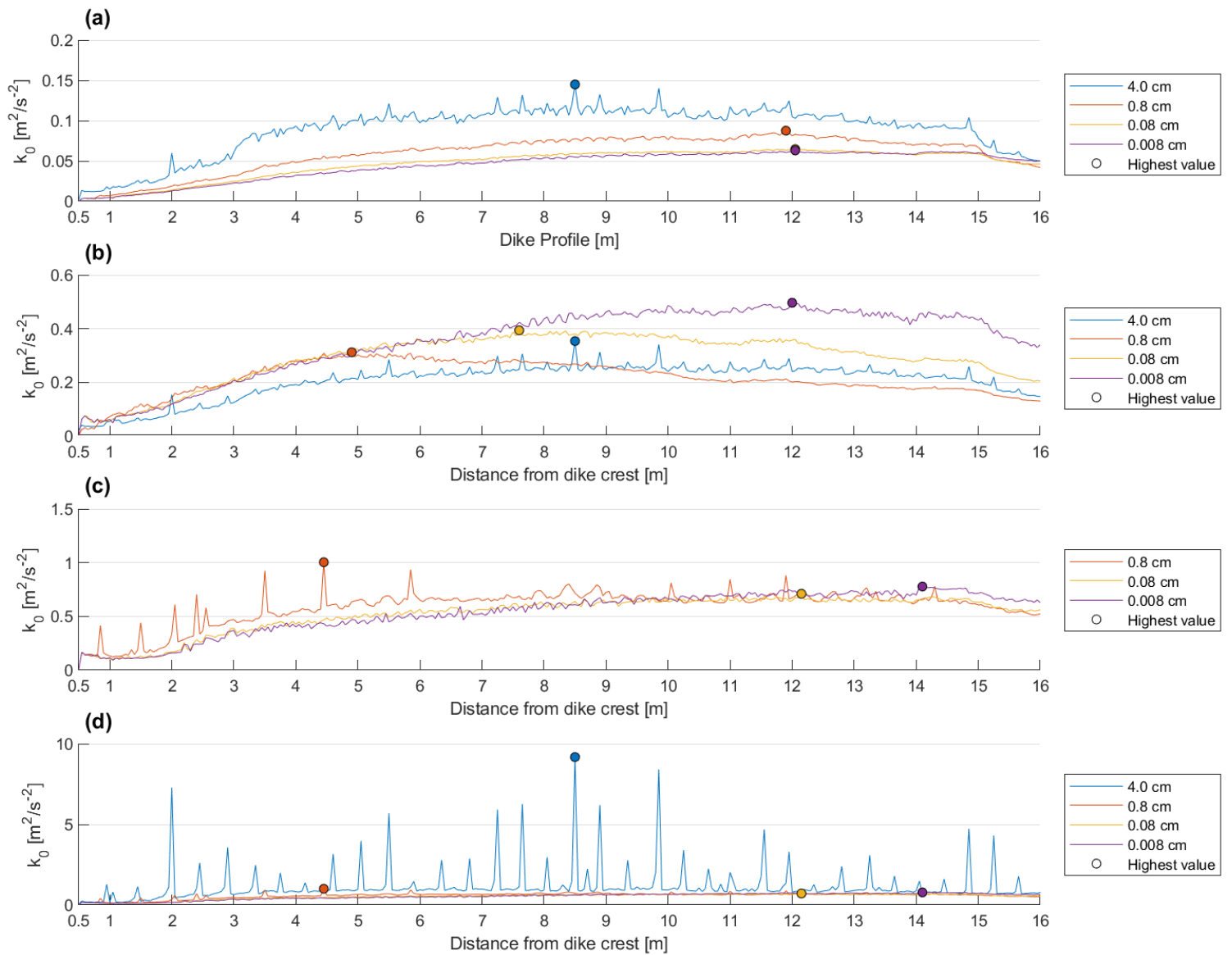


Figure 38 – The depth-averaged turbulence maxima plotted against the dike profile. The maximum mean depth-averaged TKE (a), the maximum mean significant depth-averaged TKE (b) and the maximum depth-averaged TKE (c, d). The crest starts at 0.5 m, the slope at 2 m and the toe at 15 m. Note: The y-axis use different scaling.

1.3. The sensitivity towards the volume and roughness height

The sensitivity of wave overtopping turbulence the wave overtopping volume (V) and roughness height (k_s) is analysed by comparing four different wave overtopping volumes for four different roughness scenarios. These sixteen combination scenarios are introduced in subsection 4.7.3.

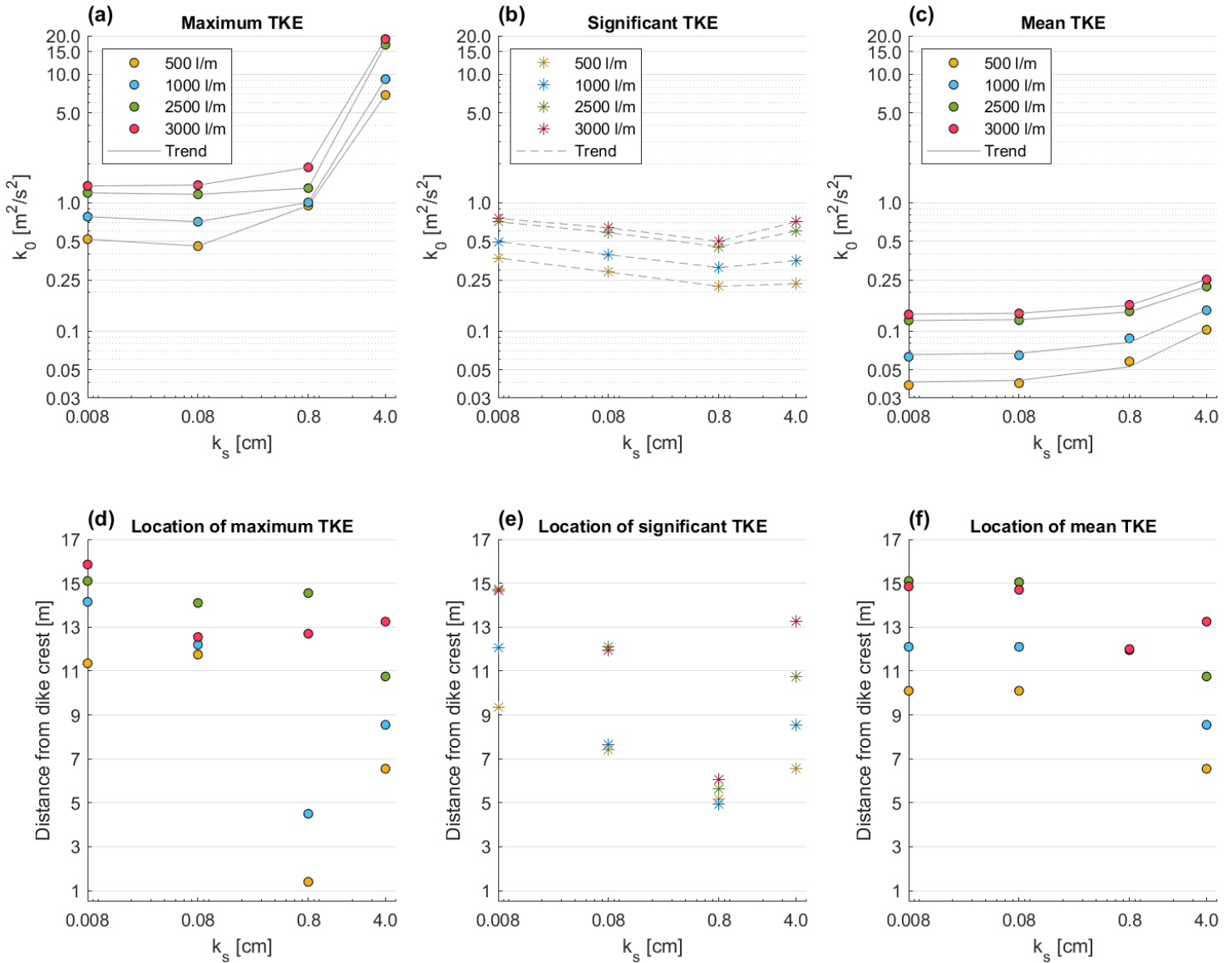


Figure 39 – Value and location of the turbulence maxima for the wave overtopping volumes of 500 l/m (yellow), 1000 l/m (blue), 2500 l/m (green) and 3000 l/m (red): The maximum depth-averaged TKE (a, d), the maximum mean significant depth-averaged TKE (b, f) and the maximum mean depth-averaged TKE (c, e). The crest starts at 0.5 m, the slope at 2 m and the toe at 15 m. Note: The y-axis in sub-plots (a, b, c) use a logarithmic-scale.

| Appendix references

- Fluid Mechanics (Producer). (2019). [CFD] The k - epsilon Turbulence Model. Retrieved from <https://www.youtube.com/watch?v=fOB91zQ7HJU&list=PLVKU8cvQithfqvjusvDzgmRTCdNdWB4sL&index=2&t=5s>
- Fluid Mechanics (Producer). (2020). [CFD] Large Eddy Simulation (LES). Retrieved from https://www.youtube.com/watch?v=r5vP45_6fB4&list=PLVKU8cvQithfqvjusvDzgmRTCdNdWB4sL&index=6&t=29s
- Hughes, S. A., Thornton, C. I., Van der Meer, J. W., & Scholl, B. N. (2012). IMPROVEMENTS IN DESCRIBING WAVE OVERTOPPING PROCESSES. *Coastal Engineering Proceedings*, 1(33). doi:10.9753/icce.v33.waves.35
- Kok, J. (2000). Resolving the dependence on freestream values for the k-omega turbulence model. *AIAA journal*, 38. doi:10.2514/3.14547
- Launder, B., & Sharma, B. I. (1974). Application of the energy-dissipation model of flow near a spinning disc. *Lett. Heat Mass Transfer*, 131-138.
- Launder, B., & Spalding, D. B. (1974). The numerical computation of turbulent flows. *Comput. Methods Appl. Mech. Eng.*, 103, 456-460.
- Marisa, N. (2014). APPLICATION OF RANS/PDF & LES/FDF METHODS TO PREDICTION OF PREMIXED TURBULENT FLAMES. Retrieved from <https://www.slideserve.com/marisa/application-of-rans-pdf-les-fdf-methods-to-prediction-of-premixed-turbulent-flames>
- Menter, F. R. (1992). Influence of freestream values on k-omega turbulence model predictions. *AIAA journal*, 30(6), 1657-1659. doi:10.2514/3.11115
- Menter, F. R. (1994). Two-equation eddy-viscosity turbulence models for engineering applications. *AIAA journal*, 32(8), 1598-1605. doi:10.2514/3.12149
- Nikolaidou, L. (2019). *Wall-Modelled Large Eddy Simulation of fully rough non-uniform flow for the purpose of predicting stone stability*
- (MSc). Delft University of Technology,
- Van Bergeijk, V. M., Warmink, J. J., & Hulscher, S. J. M. H. (2021). *Experimental set-up and modelling tools for the load by overtopping waves in erosion models*. Retrieved from
- Van Bergeijk, V. M., Warmink, J. J., & Hulscher, S. J. M. H. (2022). The wave overtopping load on landward slopes of grass-covered flood defences: Deriving practical formulations using a numerical model. *Coastal Engineering*, 171, 104047. doi:<https://doi.org/10.1016/j.coastaleng.2021.104047>
- Wang, G., Yang, F., Wu, K., Ma, Y., Peng, C., Liu, T., & Wang, L.-P. (2021). Estimation of the dissipation rate of turbulent kinetic energy: A review. *Chemical Engineering Science*, 229. doi:10.1016/j.ces.2020.116133

